Institute for Polar Ecology
of the Christian-Albrechts-Universität Kiel

GEOMAR
Helmholtz-Zentrum für Ozeanforschung Kiel

MASTER'S THESIS

Activity of methanotrophic microorganisms in sediments from a methane blow-out in the northern North Sea

Master of Science Programme:

Biological Oceanography

GEOMAR Helmholtz Centre for Ocean Research Kiel

Submitted by

Philipp Wilfert

November 2012

1st Reviewer:	**Professor Dr. Tina Treude** Department of Biogeochemistry GEOMAR Helmholtz Centre for Ocean Research Kiel
2nd Reviewer	**Professor Dr. Manfred Bölter** Institute for Polar Ecology University of Kiel
Project Initiation:	Dr. Peter Linke Department of Biogeochemistry GEOMAR Helmholtz Centre for Ocean Research Kiel
Practical Supervisor:	Dr. Stefan Krause Department of Biogeochemistry GEOMAR Helmholtz Centre for Ocean Research Kiel

Summary

Due to global warming, large volumes of methane may get released from marine sediments by melting gas hydrates, enhancing ocean acidification, bottom water hypoxia and global warming. In anoxic marine sediments, microbial induced anaerobic oxidation of methane provides a long- term sink for methane via the formation of methane derived authigenic carbonates (MDAC). In the view of destabilizing gas hydrates it is mandatory to understand, how fast AOM communities can adapt to an onset of methane flux. So far, the response of AOM consortia has been studied in theoretical models only. In laboratory experiments it was shown that AOM organisms showed extremely slow growth rates (doubling time: 4-7 months).

In 1990 an oil rig caused a blow-out in the northern North Sea and formed a 20 m deep crater at the seafloor. More than 20 years later, the blow-out still releases significant amounts of methane. The site provides a unique natural laboratory to study the adaption of AOM communities in a newly formed methane-seep. A sediment core was recovered from in-side the blow-out crater, a reference core 50 m away from the crater. Both cores were sliced into three horizons (0-6, 6-12 and 12-18 cm bsf). Methane dependent sulphate reduction, which is equivalent to AOM activity, was determined by measuring total alkalinity and sulphide over 47 days in samples from the blow-out sediments incubated at 4, 13, 20, 37 and 60 °C. These long-term measurements revealed high potential rates of methane-dependent sulfate reduction in all horizons (1.5 - 3.5 µmol SO_4^{2-} cm^{-3} sediment d^{-1}). Potential AOM rates determined by radiotracer measurements in short-term incubations (24 h, 13 °C) showed similar patterns but slightly lower rates (0.6 - 2.4 µmol CH_4 cm^{-3} sediment d^{-1}). The temperature optimum of AOM was between 13 and 20 °C indicating the presence of psychrophilic to mesophilic microorganisms, adapted to the relatively constant in-situ temperature (7 °C). No AOM activity was detected in incubations at 37 and 60 °C, indicating sensitivity of the AOM organisms against higher temperatures. Highest AOM activity was found in the deepest horizon. Both, long and short-term measurements of potential AOM rates show, the vast majority of sulphate reduction in the core was coupled to AOM. Neither an increase of total alkalinity nor of sulphide concentrations was detected in the sediments from the reference core incubated at 13 °C for 21 days.

Samples from sediments of the blow-out crater were analyzed for their mineral composition using X-ray powder diffraction (XRD). Three out of six samples were composed of brucite ($Mg(OH)_2$), mainly. Overall, different polymorphs of calcium carbonate such as aragonite, calcite, magnesium calcite and vaterite were the dominant minerals. Aragonite and magnesian calcite have been related to AOM. However, no indications for MDAC formation were found by stable isotope analyzes. Typically, MDAC show distinct stable isotope values ($\delta^{13}C$ <-20 and $\delta^{18}O$ > 0), if formed under present day conditions in the marine environment. Some samples show negative $\delta^{13}C$ values (-7.3 to -17.6 ‰) indicating that carbonates were, at least partly, derived from AOM. Corresponding $\delta^{18}O$ values (between -12 and -3), clearly argue against a recent MDAC formation. All other samples showed positive $\delta^{13}C$ which argue against microbial induced carbonate formation.

Unspecific cell staining using DAPI revealed cell aggregates, which are typical for AOM consortia, in high numbers in all horizons ($2.5*10^{12}$ aggregates m^{-2}). Total cell counts were one order of magnitude higher in the blow-out core (23 – $68*10^8$ cells mL^{-1}), compared to the reference core (3.9-$7.3*10^8$ cells mL^{-1}).

Methane turnover and AOM aggregate density were similar to very active cold seep environments. Pore water profiles measured in a replicate core, show sufficient sulphate supply throughout the sandy and porous sediments. Therefore, it is likely that the extreme broad AOM zone exceeded the sampling depth of 18 cm.

This study demonstrates that the AOM community at the North Sea blow-out is extremely active; suggesting that adaptation to strongly increasing methane fluxes might take less than 20 years. The question, whether or not, the AOM community has established within the last 20 years, cannot be answered finally. To gain certainness, it is necessary to analyze the sediment layers at reference sites 20 m bsf. It needs to be analyzed whether or not AOM activity is there as well.

Table of contents

List of abbreviations

AOM	Anaerobic Oxidation of Methane
ANME	ANaerobic MEthanotrophs
bsf	below seafloor
CH_4	chemical formula for methane
cpm	counts per minute
CARD-FISH	CAtalyzed Reported Deposition-FISH
DAPI	4´, 6-DiAmidino-2-PhenylIndole-phydrochloride
DNA	DeoxyriboNucleic Acid
dw	dry weight
EtOH	ETanOHl
FISH	Fluorescence In-Situ Hybridization
H_2O	chemical formula of water / in this study: ultrapure water
H_2S	chemical formula for hydrogen sulphide
HCl	chemical formula of hydrochloric acid
HRP	HorseRadish Peroxidase
IAPSO	International Association for the Physical Sciences of the Oceans
IPCC	Intergovernmental Panel on Climate Change
MDAC	Methane-Derived Authigenic Carbonates
Mg	Magnesium
Milli-Q	Ultra purified water type 1 (Milli-Q)
MOx	aerobic Methane Oxidation
N_2	chemical formula for molecular Nitrogen gas
PDB	Pee Dee Belemnite
PES	PolyEtherSulfone
PBS	Phosphate Buffered Saline
PSU	Practical Salinity Units
ROV	Remotely Operated Vehicle
rRNA	ribosomal RiboNucleic Acid
SMT	Sulphate Methane Transition Zone
SRB	Sulphate Reducing Bacteria

SR	Sulphate Reduction
T1	Sediment horizon between 0-6 cm bsf in the reference core
T2	Sediment horizon between 6-12 cm bsf in the reference core
T3	Sediment horizon between 12-18 cm bsf in the reference core
XRD	X-Ray Diffraction
ZnAc	Zinc Acetate

1 Introduction

1.1 General Introduction

Methane (CH_4) is the simplest, perhaps most abundant hydrocarbon molecule on earth and main component of natural gas (URL 1). It is a very potent greenhouse gas, with a global warming potential that is 25 times higher than the one of carbon dioxide (Lelieveld et al. 1993; IPPC 2007; URL 2). In the marine realm, methane can be formed in anoxic sediments during geological processes (pyrolysis) from organic matter (thermogenic methane), during the degradation of organic matter by methanogenic archaea (biogenic methane) or by geological processes without any organic matter involvement (abiogenic methane) (Judd, Hovland 2007).

Although 7-25 % of total methane production takes place in the marine realm, the oceans contribute about 2 % to the total global methane emissions only (Reeburgh 2007). This gap in the methane budget is caused mainly, by the consumption of methane by microbes during the anaerobic oxidation of methane (AOM) in marine sediments (Treude et al. 2003; Reeburgh 2007).

Methane, which is not captured by the biological filter (AOM) within sediments, seeps into the water column. This methane gets partly or fully oxidized to CO_2 by aerobic methanotrophic bacteria in the oxygenated seawater (Valentine et al. 2001; Schubert et al. 2006). At high methane fluxes from the seafloor, specifically at shallow water depths, methane can partly escape both, anaerobic and aerobic oxidation. Thus, rising methane bubbles emanated from the sediment reach the sea surface and get released into the atmosphere (e.g. Rehder et al. 1998).

Usually, methane forms in deeper sediment layers. This methane may get released later on at active plate margins (Wefer 2003; Figure 4). Such settings explain the discharge of gaseous or dissolved methane at cold seeps and mud volcanoes (Kulm et al. 1986; Vogt et al. 1997).

Methane can stay within sediments in the form of methane clathrates (=methane hydrate). Methane clathrates consist of methane molecules that are surrounded by a crystal structure

of water molecules (Kvenvolden 1993). Methane clathrates are stable under low temperature and high pressure conditions only (e.g. Buffett, Archer 2004). Large methane hydrate reservoirs have been discovered globally, at continental margins, and represent a gigantic potential energy reservoir (Kvenvolden 1993; Buffett 2000).

Ongoing global warming may trigger the release of large quantities of methane from sediments due to the destabilization of methane clathrates (Kvenvolden 1993; Biastoch et al. 2011). For climate research it is necessary to understand how much methane can be captured by AOM within marine sediments when methane clathrates destabilize. However, by now, grow kinetics of methane consuming microorganisms have been studied in laboratory experiments only (Nauhaus et al. 2002; Nauhaus et al. 2007; Wegener, Boetius 2009). The reaction of AOM to newly emerged methane fluxes has been investigated in a theoretical model. The model predicts, that it takes about 60 years to establish a steady state biomass in response to an onset of methane flux (Dale et al. 2008).

This study investigates the adaption of the AOM community to a newly emerged methane source. Namely, at a blow-out site that has been caused by drilling operations in the northern North Sea, 21 years ago.

1.2 Synoptic view on the anaerobic oxidation of methane (AOM)

Biogeochemical zonation in sediments

AOM takes place in distinct zones within sediments, were growth factors for reproduction, gaining energy and growing are available to AOM organisms. In general, all microorganisms require a variety of nutrients (such as nitrogen, carbon, phosphorus, sulfur, vitamins, and minerals) for the maintenance of growth and reproduction. However, zonation of sediments is usually defined according to the available energy sources which also determine the zone of AOM. The microbes gain energy by transferring electrons from electron donors (organic molecules, hydrogen etc.) to electron acceptors (oxygen, sulphate, nitrate etc.). Thereby, the electron acceptors become reduced and form characteristic end products of metabolic pathways (carbon dioxide, hydrogen sulphide, molecular nitrogen etc.). Sediments can be separated into different biogeochemical horizons. In each of these horizons, distinct

microbial processes with specific electron acceptors and donators (=redox couples) and reduced end products dominate (Figure 1).

During aerobic respiration, organic matter is degraded using oxygen as final electron acceptor. Aerobic respiration is energetically the most favorable of all metabolic pathways. In fine-grained sediments, with high organic matter input, oxygen is depleted rapidly due to high aerobic respiration rates and slow replenishment of oxygen. In some coastal areas oxygen penetrates a few millimeters into the sediment only (Jørgensen 1982). Thus, below the oxygenated zone, microbes that use electron acceptors other than oxygen take over. In general, the energy yield of a reaction depends on the type of the involved redox couples. Inevitably, redox couples which are generating high energy yield dominate the upper sediment. Low energy yielding processes occur in deeper sediment layer. This results in a redox cascade with increasing sediment depth (Figure 1).

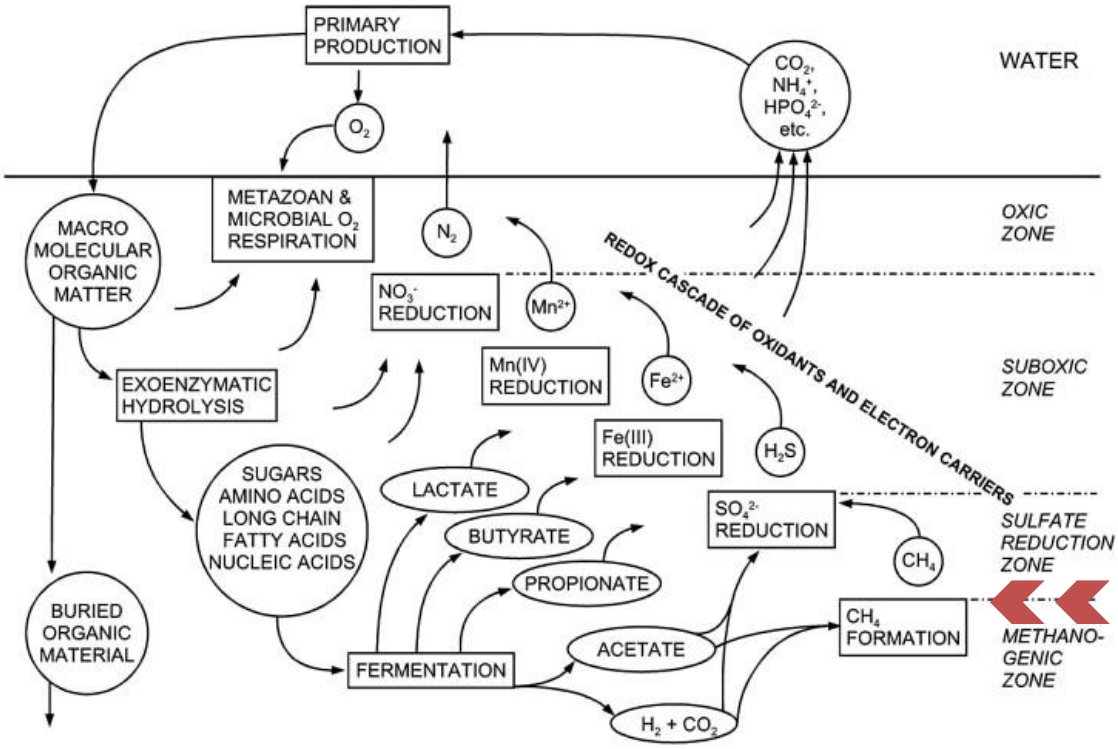

Figure 1: Zonation of marine sediments according to the dominating microbial processes in diffusive systems. The chevrons indicate the AOM zone where both methane and sulphate are available to AOM organisms (modified from Schulz, Zabel 2006).

Stoichiometry of AOM

AOM refers to a process where methane is oxidized in the absence of oxygen to bicarbonate (HCO_3^-) by a syntrophic consortium of anaerobic methanotrophic archaea (ANME) and sulphate reducing bacteria (SRB) (Boetius et al. 2000; reviewed by Knittel, Boetius 2009; Figure 6). AOM involves two reactions. In the first reaction, the unreactive methane molecule is activated and metabolized during reverse methanogenesis by archaea. The second reaction is carried out by the syntrophic sulphate reducing bacterial (SRB) partner of the archaea. A still unknown intermediate metabolite, which is generated during reverse methanogenesis, is used as electron donor by SRB. Overall, sulphate (SO_4^{2-}) is the final electron acceptor and is reduced to sulphide (HS^-). Water (H_2O) and bicarbonate are, besides HS^-, end products of AOM (Orphan et al. 2001; Equation 1). During AOM, one sulphide molecule is formed from the reduction of one sulphate molecule (Nauhaus et al. 2002). Simultaneously, total alkalinity increases by one unit due to the formation of one mole of bicarbonate (Dickens, Snyder 2009; Equation 1).

Under standard conditions, the free energy change of AOM is ΔG°=-16.6 kJ mol^{-1}. However, standard conditions are found in-situ rarely. The energy change varies with differences in-situ conditions between ΔG°= -10 and -40 kJ mol^{-1}. The energy yield increases at high methane concentrations (Nauhaus et al. 2002) and possibly decreases at sulphate concentrations below 0.5 mmol L^{-1} (Knittel, Boetius 2009).

Equation 1

$$CH_4 + SO_4^{2-} \rightarrow HCO_3^- + HS^- + H_2O$$

Sulphate reduction and AOM

Quantitatively, sulphate reduction is the most important anaerobic mineralization process, since sulphate is the most abundant electron acceptor in anoxic sediment pore water (Jørgensen 1982; Henrichs, Reeburgh 1987). Reactions involving other redox couples, such as nitrate, manganese and iron, yield more energy. However, these electron acceptors are usually available in comparatively low concentrations only, and therefore, play a minor role as electron acceptor in microbial processes.

In diffusive systems, AOM occurs, in anoxic sediments, below the zone of organoclastic sulphate reduction and above the zone of methanogenesis (Figure 1). Here, both sulphate

and methane are available to the microorganisms. This zone is termed sulphate methane transition zone (SMTZ). Here, methane and sulphate are usually consumed completely (Figure 2). At continental margins, the SMTZ is usually found, one to several meters below the seafloor (Jørgensen et al. 1990). In sediments on the continental shelves the SMTZ may be located narrower below the seafloor. In shelf areas, such as Eckernförde Bay, the organic matter content of the sediments and sedimentation rates are relatively high. At Eckernförde Bay, maximum AOM rates were detected between 20 and 60 cm bsf (e.g. Bussmann et al. 1999). Here, AOM activity was found in horizons between 0-5 cm bsf as well (Treude et al. 2005b).

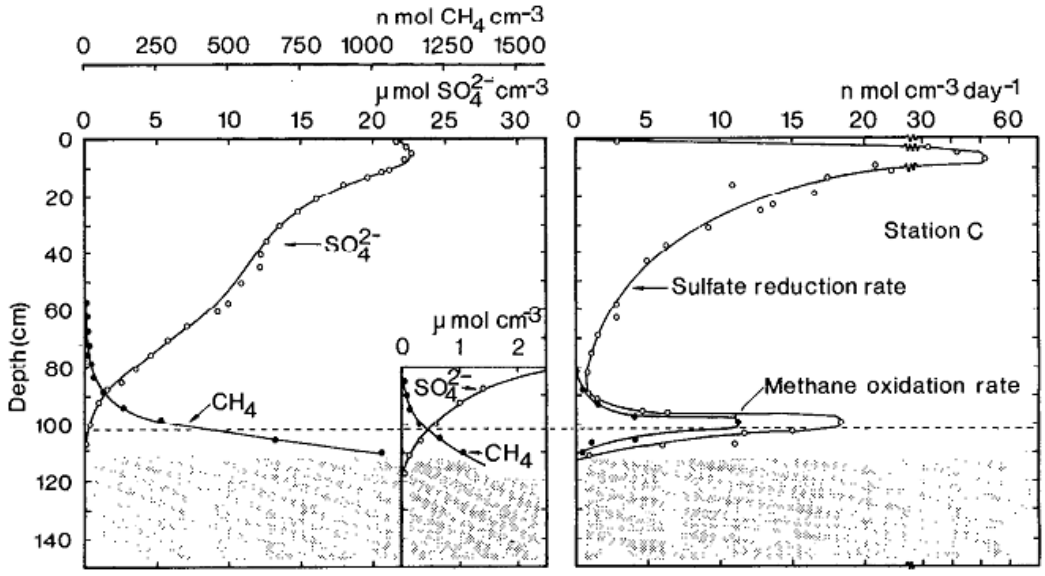

Figure 2: Profiles of methane and sulphate concentrations in marine sediments in 200 m water depth at Skagerrak (left). The small diagram shows the concentration profiles within the SMTZ. Rates of AOM and sulphate reduction are shown on the right. Note that the highest AOM rate coincidences with the depth where methane and sulphate occurred at a molar ratio of 1:1 (Iversen, Jorgensen 1985).

Dense AOM communities and high AOM rates are reported from cold seeps (Treude et al. 2003; Krüger et al. 2005; Treude, Ziebis 2010). These systems can be found at active and passive continental margins, where methane rich but sulphate depleted fluids, are literally squeezed through sediments into the water column, due to tectonic activities. Sulphate, from the oxygenated seawater, diffuses into the sediment and fuels AOM just below the seafloor (Treude et al. 2003). At high fluid flow rates, sulphate becomes the limiting factor at cold seeps (Niemann et al. 2006). The sulphate reduction zone is confined to a narrow horizon in these advective systems in contrast to the “usual” diffusive settings in marine sediments. In advective systems a large part of the sulphate reduction is coupled to methane

oxidation. AOM may become the dominant microbial pathway at cold seeps (Boetius et al. 2000; Treude et al. 2003; Boetius, Suess 2004; Figure 3).

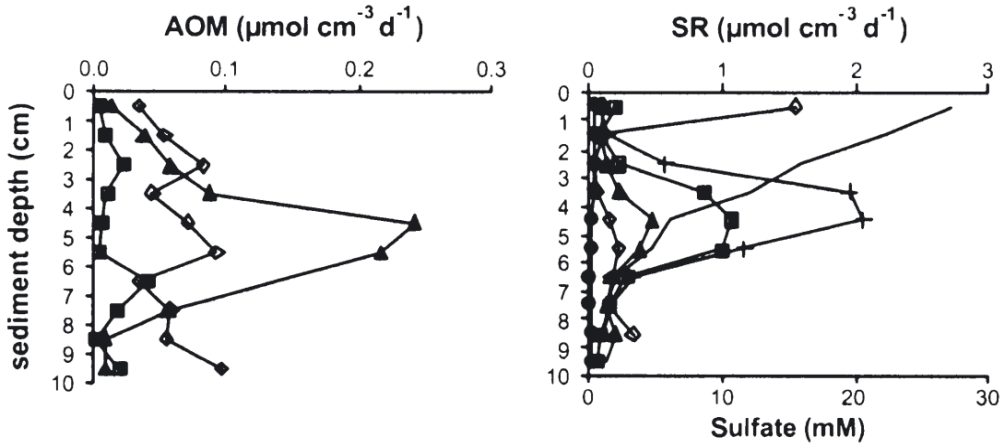

Figure 3: Profiles of AOM and sulphate reduction rates above gas hydrates at a cold seep where methane rich fluids seep through sediments. Zones of highest AOM and sulphate reduction rates overlap. Each replicate core is represented by a different symbol (Treude et al. 2003).

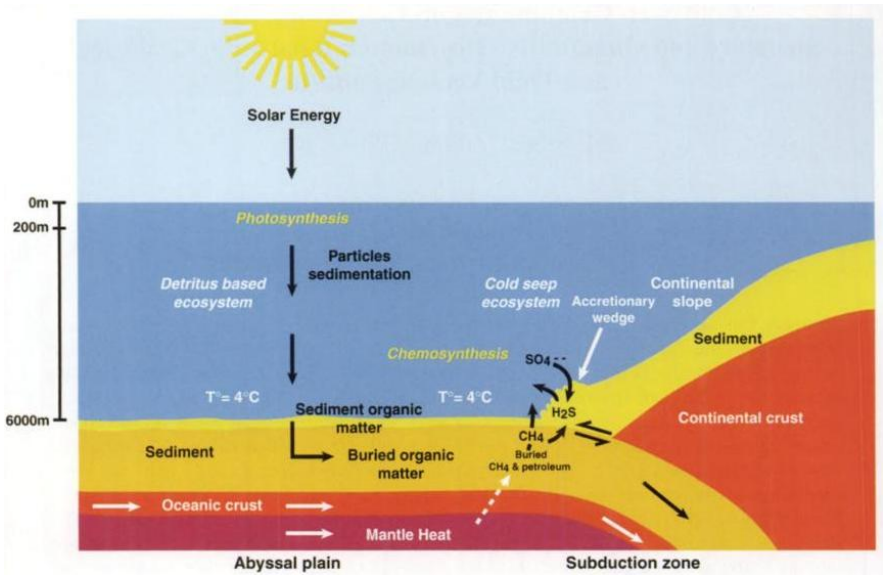

Figure 4: Schematic overview on geology settings and biogeochemical processes at cold seeps (Wefer 2003).

AOM consortia and carbonates

Besides dissolved hydrogen sulphide, AOM leaves solid marks also. Microbial formed bicarbonate ions (Equation 1) increase alkalinity. Due to the increase of alkalinity, the precipitation of carbonates is promoted in sediments with high AOM rates. Increasing alkalinity can result in the precipitation of bicarbonate with calcium ions to form calcium carbonate minerals ($CaCO_3$). These carbonates are called methane-derived authigenic carbonates (MDAC) with respect to their in-situ formation from methane oxidation.

Accordingly, carbonates related to AOM are reported from numerous cold seeps (e.g. Ritger et al. 1987; Bohrmann et al. 1998; Peckmann et al. 1999; Aloisi et al. 2002).

Carbon has several stable isotopes. The heavy ^{13}C and the lighter ^{12}C isotopes are, geochemical, the most important ones. Biogenic methane is generally depleted in ^{13}C (Figure 5). Microbes utilize methane during AOM and form ^{13}C depleted bicarbonate due to kinetic isotopic fractionation. The subsequently precipitated MDAC are enriched in isotopic light carbon (^{12}C). MDAC can be distinguished from carbonates, that have been formed without involvement of methane, by the ratio of heavy to light carbon isotopes (Pierre et al. 2012; Figure 5).

The isotopic ratio of MDAC provides information about the of source methane (thermogenic, biogenic or abiogenic methane), involved in the carbonate formation (Judd, Hovland 2007, Figure 5). The carbon isotopic composition of methane may vary, due to isotopic fractionation, during formation (Judd, Hovland 2007). However, interpretations of isotopic analyzes are not straight forward, since the formation process of authigenic carbonates often includes a mixture of carbon sources (e.g. Magalhães et al. 2012).

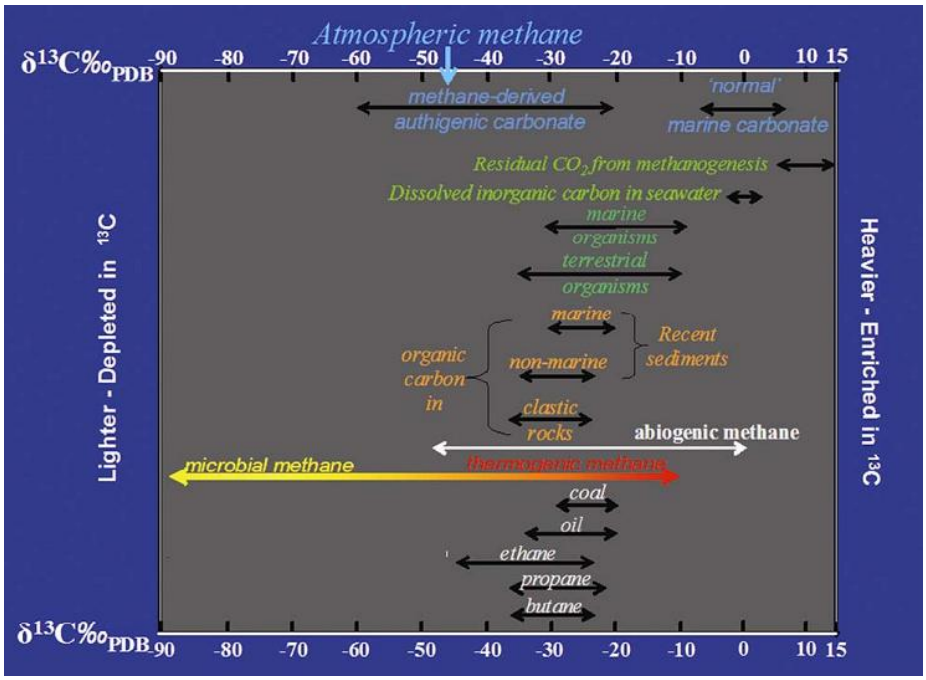

Figure 5: The use of carbon isotope ratios to discriminate between methane of different origins (Judd, Hovland 2007).

Similar to carbon, oxygen has three stable isotopes with different mass numbers (^{16}O, ^{17}O and ^{18}O). Isotopic oxygen composition of authigenic carbonate depends on the temperature at the time of precipitation, the carbonate chemistry/mineralogy and on the isotopic composition of the formation fluid (Stakes et al. 1999). The carbonate mineral dolomite ($CaMg(CO_3)_2$) for instance, has a higher content of ^{18}O than the carbonate mineral calcite ($CaCO_3$). Contrary, high temperatures, at the time of formation or precipitation of carbonates from fresh water, decrease the content of the heavy oxygen isotope ^{18}O (Urey 1947).

Phylogeny

Archeal diversity in sediments, dominated by AOM, is low, with the presence of a few phylogenetic groups only (Knittel et al. 2005; Knittel, Boetius 2009). Three main groups of anaerobic methanotrophic archaea are known (ANME 1, 2 and 3). All ANME are closely related to methanogenic archaea. ANME 1 archaea are closely related to the order Methanosarcinales and Methanomicrobiales. Archaea of the groups ANME 2 and 3 belong to the order Methanosarcinales.

ANME 1 and 2 are typically found in syntrophy with sulphate-reducing bacteria of the genera *Desulfosarcina*/*Desulfococcus*. ANME 3 exists as single cells or in consortia associated with sulphate-reducing bacteria of the *Desulfobulbus* group.

ANME 1 and 2 are ubiquitous in sediments all over the world. By now, ANME 3 has been found at mud volcanoes mainly (Knittel, Boetius 2009). ANME 1 and 2 often co-occur. However, usually one of the groups is dominating (Knittel et al. 2005; Figure 6).

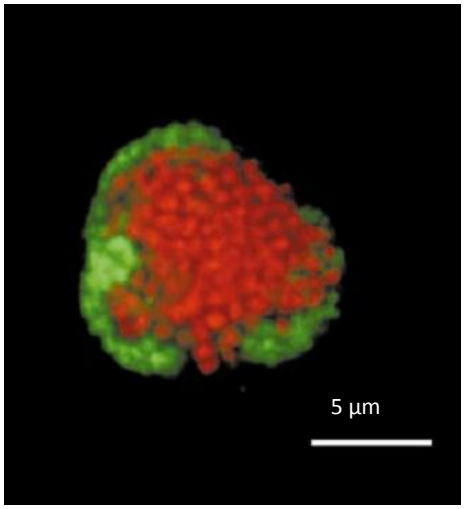

Figure 6: Microscopic image of a consortium of sulphate-reducing bacteria (stained green) and methanogenic archaea (stained red) mediating anaerobic oxidation of methane (Boetius et al. 2000)

Most studies indicate that cold seeps are dominated by ANME 2 (reviewed by Knittel, Boetius 2009). Which environmental factors select for presence, absence and dominance of an ANME group, is presently not known.

AOM consortia are generally found in a wide variety of marine sediments, at different temperature regimes (Krüger et al. 2005; Knittel, Boetius 2009). Active ANME have been reported from Antarctic sediments, with ice-cold water (Niemann et al. 2009), but also in sediments with boiling hot water (100 °C), at active hydrothermal vents (Teske et al. 2002). AOM rates however are temperature dependent (Nauhaus et al. 2002; Krüger et al. 2005). In vitro experiments indicate, that the optimum temperature for AOM organisms is 5-10 ° C above their in-situ temperature (Krüger et al. 2005; Boetius et al. 2009).

AOM and global warming

Gigantic temporary methane reservoirs are methane clathrates (methane hydrates), along continental margins (Klauda, Sandler 2005). These clathrates are stable under specific temperature and pressure conditions only (Tishchenko et al. 2005). When clathrates destabilize, due to rising water temperatures caused by global warming (Krey et al. 2009) or shifts in ocean currents (Phrampus, Hornbach 2012), oceanic methane emissions may increase in the future. This increased methane release could accelerate global warming.
Also, aerobic oxidation of methane could potentially be stimulated by higher methane concentrations in bottom waters. Carbon dioxide is one metabolic end product of aerobic oxidation of methane and has the potential to amplify ocean acidification. The consumption of oxygen during aerobic oxidation of methane may result in oxygen depleted bottom waters (Biastoch et al. 2011).

Higher methane release from the ocean may trigger a positive feedback by accelerating global warming, which again increases methane emission. It has been suggested, that melting methane hydrates contributed to the “Latest Paleocene Temperature Maximum” (Dickens et al. 1995). During that period, atmospheric and bottom water temperatures raised by about 5 °C within a few thousand years (Kennett, Stott 1991).

A young blow-out - a natural laboratory

In 1991 an oil rig accidently hit a shallow methane pocket and caused a blow-out in the northern North Sea. After more than 20 years the blow-out still releases methane (Pfannkuche 2006; Linke et al. 2011). Assuming, that the age of the methane blow-out is

dated back exactly, it offers a unique chance to observe and measure the development time of AOM communities in a young methane habitat.

The biogeochemical conditions at the young blow-out site in the North Sea and at cold seeps are similar, in terms of continuous and excess input of methane. However, microbial communities had little time to establish, in the relatively young system at the blow-out site. This scenario may be analogous to a situation when methane clathrates destabilize and high amounts of methane are released into marine sediments.

1.3 Aim of this study

It is crucial to better understand how much methane can be captured by AOM within sediments (Knittel, Boetius 2009). This information could help to predict future climate and ocean scenarios more precisely. So far, the onset of growth of AOM consortia, exposed to a newly emerged influx of dissolved methane, has been modeled only. It is estimated that it takes 60 years to establish a steady state AOM biomass (Dale et al. 2008). The doubling time of ANME has been studied during in-vitro incubations and was estimated to be approximately 4-7 months (Nauhaus et al. 2007). Presumably, these slow growth rates can be attributed to the low energy yield during AOM (Boetius et al. 2009).

Numerous studies have been conducted in a wide variety of AOM habitats (Knittel, Boetius 2009). The investigated blow-out site in the North Sea represents a relatively young habitat for methanotrophic microorganisms. The start of continuous methane input is known exactly. Thus, this offers a unique chance to observe the progression and to measure the development time of AOM communities.

It is important to know how fast AOM communities develop at in-situ conditions, to estimate the potential impact future of methane release from methane hydrates. The central question is how much of the methane from destabilizing methane clathrates can be captured by methanotrophs before it reaches the water column or atmosphere. Solving this task allows to predict effects of melting methane hydrates on ocean acidification, on oxygen depletion of the ocean and on global warming, much better.

This study investigates the methanotrophic activity in a sediment core from relatively young methane blow-out site in the northern North Sea.

<u>The hypotheses underlying this work are:</u>

1. **The activity and abundance of consortia, mediating anaerobic oxidation of methane, at the particular blow-out site is lower, compared to established methane habitats (Dale et al. 2008).**

2. **The microbial turnover rate of methane is temperature dependent. The optimum temperature of AOM organisms is 5-10 °C above the in-situ temperature (Krüger et al. 2005).**

3. **The sediment at the blow-out harbors consortia of anaerobic methanotrophic archaea and sulphate reducing bacteria that are already known from other methane habitats.**

4. **MDAC have not precipitated at the blow-out site, since AOM organisms have not fully established within 20 years.**

2 Material and methods

2.1 Study area

In November 1991 an oil rig accidently hit a shallow base-Quaternary methane pocket and caused a methane blow-out in the northern North Sea off Scotland (~57°55'N; 1°37'E; Well Site 22/B-4; Figure 7; Rehder et al. 1998; Judd, Hovland 2007). The blow-out site is located within a major gas area of the North Sea. Natural methane leaks from oil and gas reservoirs are omnipresent in this part of the North Sea (Judd, Hovland 2007). After more than 20 years the blow-out still releases methane, bubbles can be detected at the sea surface, even visually (Figure 8).

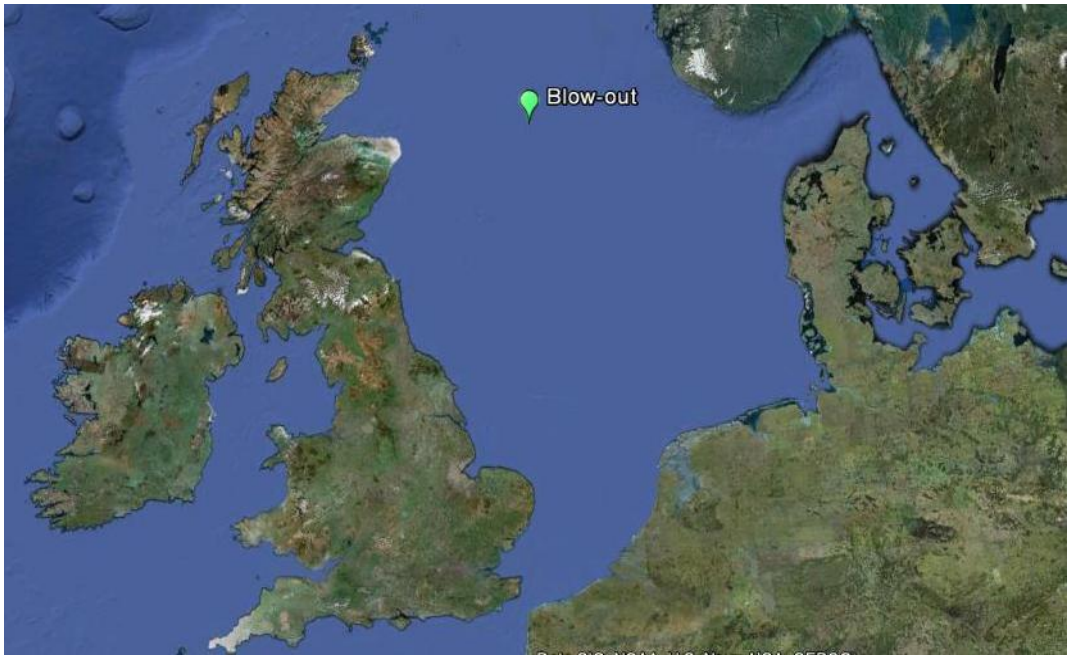

Figure 7: Position of the blowout in the northern North Sea (map: Google Earth)

Figure 8: Gas bubbles at the sea surface observed at the methane blow-out site (Linke et al. 2011).

The blow-out formed a 20 m deep crater, with a diameter of 75 m at the seafloor, in 98 m water depth. The base of the crater in about 120 m water depth is divided into two basins by a sediment ridge (Figure 9). Both, the crater and the ridge are densely covered with shells of the clam *Arctica islandica* (Pfannkuche et al. 2006).

The methane, released from the blow-out, is strongly depleted in heavy carbon isotopes ($\delta^{13}C$ = -70; P. Linke, unpubl. data), which indicates a biological origin of the gas (Whiticar et al. 1986).

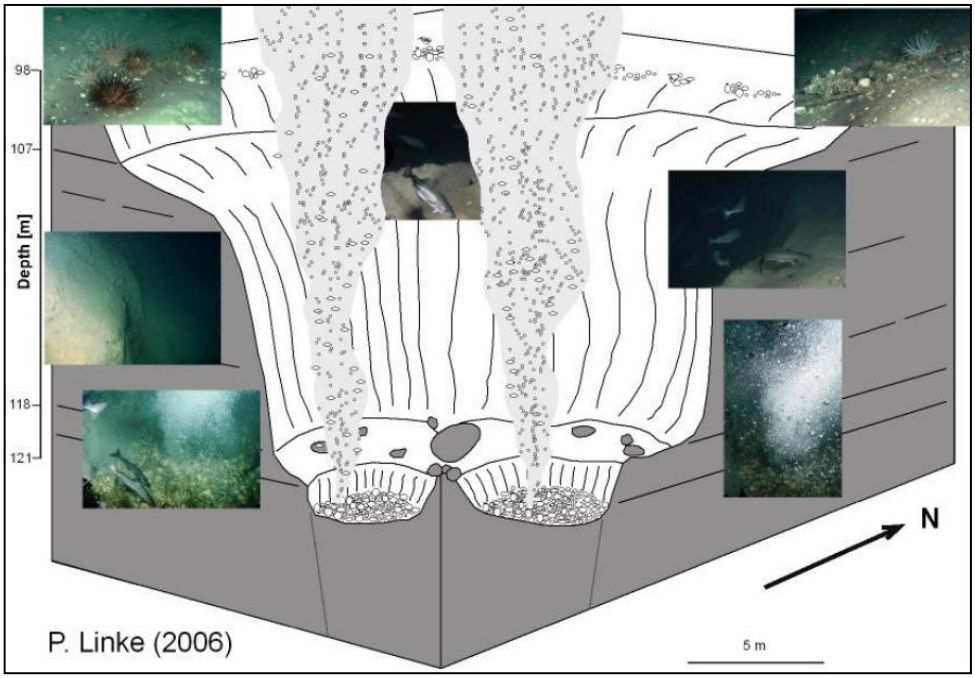

Figure 9: Schematic drawing of the crater at the blow-out site by Peter Linke (Pfannkuche 2006).

Three undisturbed sediment push cores (length: 18 cm; diameter: 7.4 cm) were taken from the sediment ridge (57°55.36'N; 1°37.86'E) within the crater, at 118 m water depth. Cores were taken by a Triton XLS working class Remotely Operated Vehicle (ROV) during a cruise with the survey vessel Noordhoek Pathfinder, on the 9th of September 2011. Two of the cores were used to study pore water chemistry (referred to as “pore water core” in the following) and foraminifera, respectively. Analyzes, conducted in the present study, were done using material from the third core. This core, from inside the crater, will be referred to as “blow-out core” in the following.

In July 2012 three reference cores were taken using the ROV KIEL 6000 during Celtic Explorer Cruise 12010. The undisturbed cores (length: 15 cm; inside diameter: 7.4 cm) were taken 50 m south-east of the blow-out crater in 99 m water depth (57°55.27‘N; 01°37.88‘E) using a push corer. Two of the cores were used to study foraminifera and pore water chemistry respectively. The third core was used as reference core and will be referred to as “reference core” in the following.

2.2 Storing, visual examining and processing the cores

Core description

Blow-out core

The sediment core was dark grey with some black spots, presumably caused by organic matter enrichments. The core had a 2 to 15 mm wide oxidized layer on top, where the sediment was in contact with oxygenized seawater (Figure 10). In the first (T1; 0-6 cm bsf) and in the second horizon (T2; 6-12 cm bsf) the sediment was “crunchy”, and contained shell fragments. The upper horizon (T1) was classified as sediment consisting of fine sand with clay. The intermediate horizon (T2) was classified as transition between fine sand and clay and the third horizon (T3; 12-18 cm bsf) as pure clay sediment. A strong sulphide odour was noticed in all horizons.

Figure 10: Undisturbed sediment core from the blow-out site in the North Sea. The top of the core was covered with clam shells (bottom right). One can clearly see a distinct oxidized layer where the sediment was in contact with oxygenated seawater (top right). The sediment color below the oxygenated layer was dark grey with some black dots (left).

Pore water core

A pore water core was taken in-side the blow-out crater next to the blow-out core. It was analyzed for chloride, total alkalinity, sulphate and bromide (data provided by P. Linke; February 2012; Figure 11).

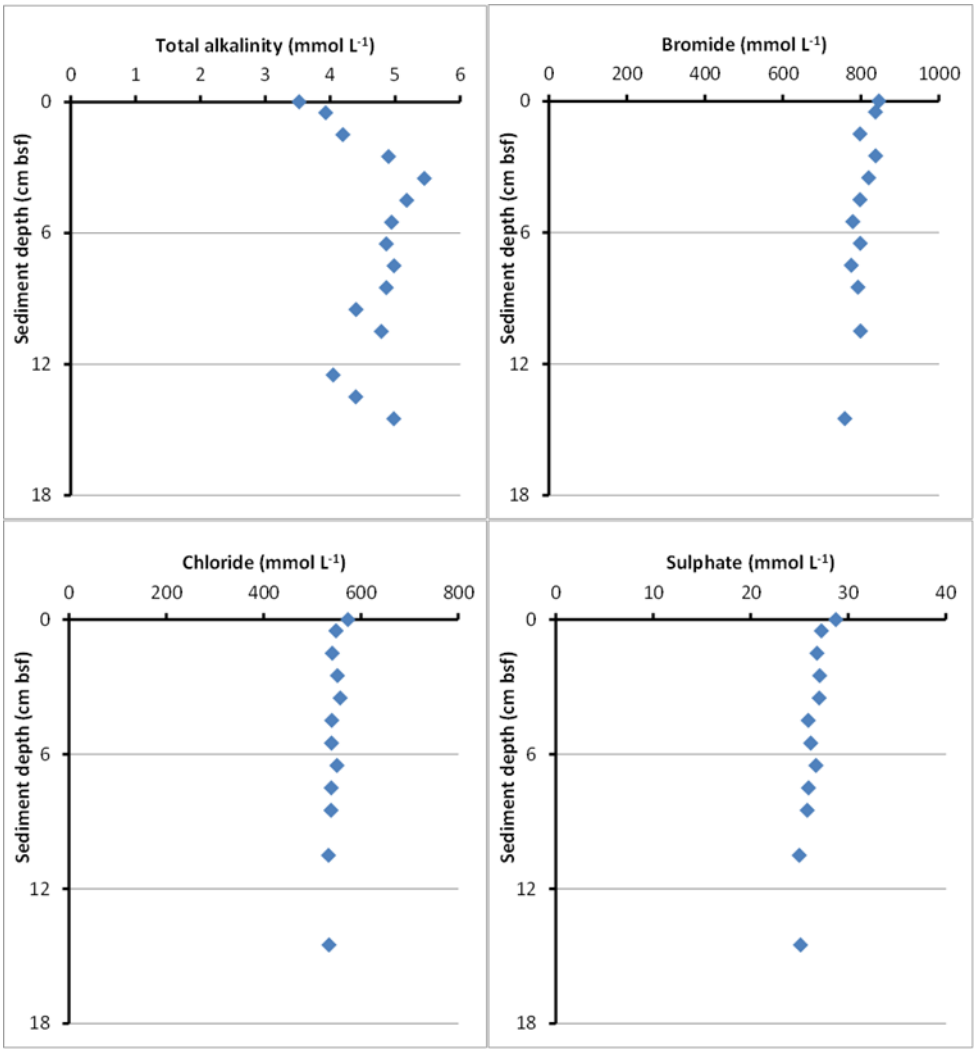

Figure 11: Pore water profiles of total alkalinity, bromide, chloride and sulphate. These measurements were done in a core that has been sampled next to the blow-out core used in this study (data provided by P. Linke).

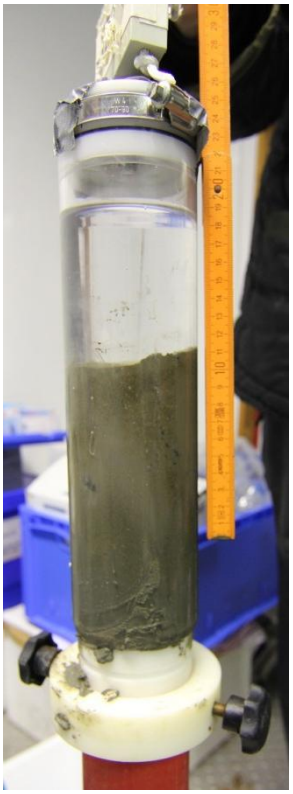

Figure 12: Profile of the reference core.

Reference core

This core was entirely light brown and showed some few black spots (Figure 12). The black spots were located in the second horizon between 6-12 cm bsf mainly. No distinct layering was detectable in the core. Rather a smooth transition from light brown on top of the core to a darker brown at 18 cm bsf was visible. A high density of clam shells was found in the upper and especially in the intermediate horizon. Almost no clam shells were found in the deepest horizon. Sediment from all horizons was classified as sandy. A light sulphide odor was noticed in the second horizon only.

Storing & processing

The blow-out core was stored after sampling in the airtight core liner in the dark (4 °C), until further processing in December 2011. Then, after visual inspection and photo documentation, the core was pushed out of the core liner using a piston with an O-ring gasket (Schönfeld et al. 2012). The core was sectioned into three depth layers-0-5, 6-11 and 12-18 cm below seafloor (bsf).

Each depth layer was sampled by the same scheme (summarized in Figure 13). First, one sample (3 mL) was taken for the determination of porosity and density using a cut off plastic syringe. Samples were filled into pre-weighted vials. The samples were then weighted before and after drying (48 h, 60 °C) to determine the water content (porosity) of each sediment horizon (Appendix, Table 16).

Second, the remaining sediment was homogenized using a metal spoon.

Subsamples (≈20 mL) for biomarker and DNA/RNA analyzes were taken from the homogenized sediment using a metal spoon. Biomarker samples were wrapped in aluminium foil and got frozen (-20 °C). DNA/RNA samples were filled into sterile Whirl-Bags

and got frozen (-80 °C). The analyzes of biomarker will be carried out at partner institutes and are not included in the present study. DNA/RNA samples are routinely stored for phylogenetic analyzes (not conducted in this study).
For microbial community analyzes, by catalysed reporter deposition fluorescence in situ hybridization (CARD-FISH), duplicate 0.5 mL samples from each of the homogenized sediment horizons were filled with cut off syringes into tubes containing 1.5 mL fixation buffer (4 % formol in 1xPBS, all reagents are listed in the attachment: A.3) and stored (2.5 hours, 4 °C) for further processing (section 2.4).

Always, after taking sub-samples from one horizon, the core was pushed one additional centimetre out of the sampling tube due to technical reasons. The remaining sediment from each horizon (width: 6 cm) was filled into pre-weighted, nitrogen (N_2) flushed glass-bottles for the preparation of sediment slurries (section 2.3). Thus, sediment slurries were made from sediment horizons which were 1 cm longer (surface-6, 6-12 and 12-18 cm bsf) compared to the horizons of the sub-samples.

The horizons from the blow-out core are referred to as T1 (surface-6 cm bsf), T2 (6-12 cm bsf) and T3 (12-18 cm bsf) in the following.

All subsequent steps and analyzes of the blow-out core were done in an anoxic environment using the Hungate method (Hungate 1950).

The reference core was stored and processed similarly. But processing was done within 10 days. However, samples for CARD-FISH, DNA/RNA and biomarker analyzes were taken from horizons that were 0-6, 6-12 and 12-15 cm bsf. The preparation of sediment slurries from the reference core were done under the exclusion of oxygen likewise. But sediment slurries were prepared in a glove box with a nitrogen atmosphere at very low oxygen levels (between 0.2–2 ppm).

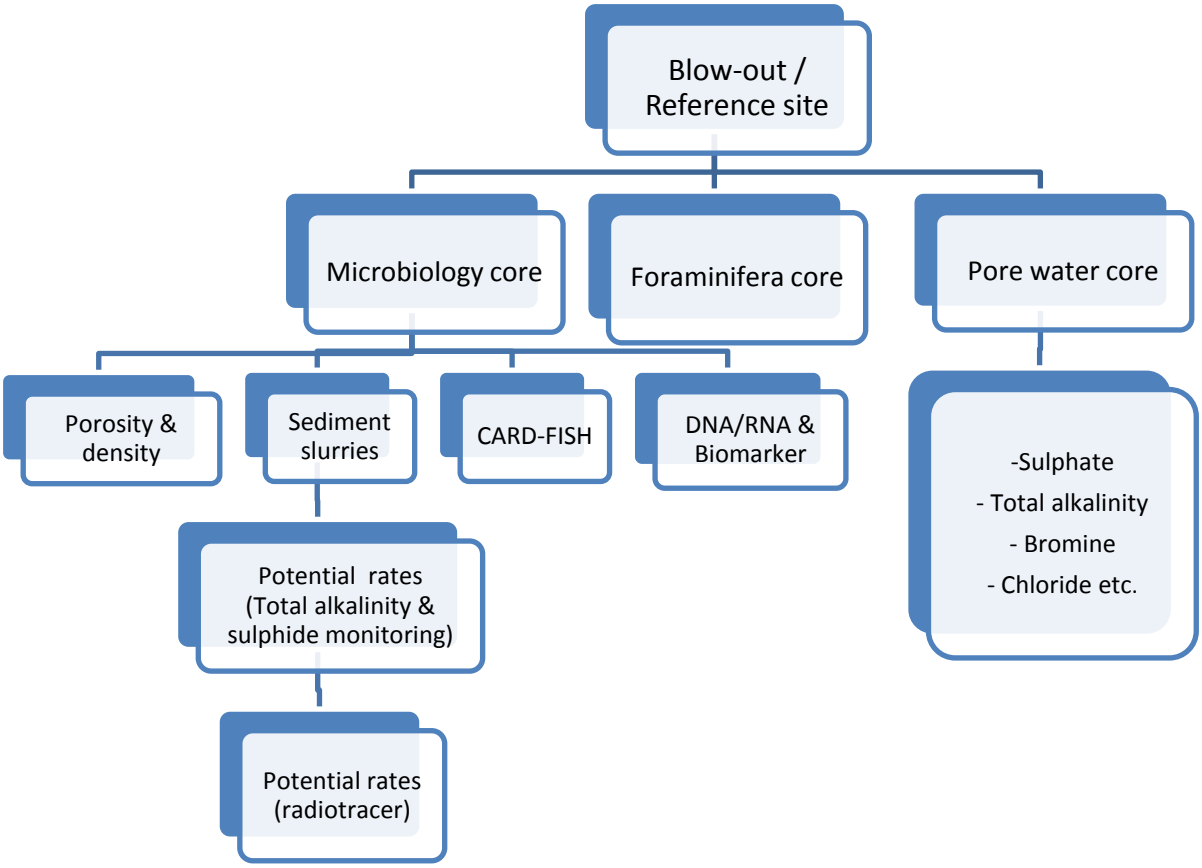

Figure 13: Sampling scheme at the blow-out and reference site.

2.3 Potential rates of sulphate reduction and AOM

2.3.1 Sediment slurries and sample preparation

Sulphate reduction rates can be determined by measuring the metabolic end products of sulphate-reducing bacteria directly (hydrogen sulphide) or indirectly (bicarbonate via total alkalinity) over time.

Potential rates of methane dependent sulphate reduction were determined through long-term in vitro experiments (set-up according to Nauhaus et al. 2002), by measuring total alkalinity and sulphide concentrations over 47 days (stoichiometry according to Equation 1).

In addition, AOM and sulphate reduction were determined by short term measurements using radiotracers.

For both, monitoring and radiotracer analyzes, sediment stock slurries (1:2, v:v) were prepared to facilitate handling of sediment samples. Slurries were prepared separately for

each depth horizon (T1, T2 and T3), for the reference and the blow-out core and then filled into N_2 flushed glass bottles (section 2.2). After transfer, bottles were again flushed with N_2 for 5 minutes. Then, artificial seawater medium for sulphate-reducing bacteria (Widdel, Bak 1992; Appendix A.1) was added (final dilution: 1:2, v:v) using N_2-rinsed syringes through a septum. Bottles were again flushed with N_2 (5 minutes) and after this, flushed with CH_4 (5 minutes). Finally, the bottles were stored with an excess CH_4 pressure (0.1 bar) in a horizontal position in the dark at 13 °C. The seawater medium in the bottles was changed once during storage (3 months) to supply microorganisms with nutrients and electron acceptors. For this purpose, bottles were put into a vertical position (12 hours) to obtain a clear supernatant. The supernatant was then replaced with fresh seawater medium using N_2 rinsed syringes trough the septum. Resazurin in the seawater media served as an indicator for O_2 contamination of the slurries. Over the full time of storage (91 days) and incubation in the Hungate tubes (up to 85 days), no indication of O_2 penetration into the vessels was observed.

In March 2012 (after 91 days pre-incubation) triplicate samples and controls were prepared in N_2 flushed Hungate tubes (17 mL, Figure 14) from the stock slurries (1:2, v:v), using the Hungate technique (modified from Hungate 1950). For each sample and control 20 mL of stock slurry were transferred into an autoclaved and N_2 flushed glass bottle and diluted with seawater to the final dilution of the slurries (1:8, v:v). Then, 11.3 mL of the 1:8 diluted sediment slurries were filled into Hungate tubes using N_2 -flushed pipettes, i.e. filling height of Hungate tubes was 2/3. Tubes were sealed with butyl rubber stoppers and screw caps. The samples in the tubes were flushed for 10 minutes with CH_4 and then incubated with a CH_4 excess pressure of 0.1 bar, at different temperatures (4, 13, 20, 37 and 60 °C; Table 1). Controls were treated analogue to the samples, however, N_2 was used instead of CH_4. The excess pressures of CH_4 or N_2 respectively was re-established weekly. Samples and controls were stored horizontally to enhance gas exchange between the sediment slurries and the N_2 or CH_4 headspace respectively. During the entire course of the experiment, O_2 contamination was not detected. Samples and controls were shaken carefully, twice a week, to improve diffusion of gases.

The slurries prepared from the reference core were processed similarly but with the following exceptions: Slurries were prepared in a N_2 atmosphere within a glove box at low oxygen levels (between 0.2-2 ppm). Additionally, samples and controls from all horizons were incubated at one temperature regime only (13 °C).

Table 1: Calculated concentrations of dissolved methane in samples (in mmol per liter seawater) incubated at different temperatures. The last row shows the in-situ concentration of methane assuming fully methane saturated water. Methane concentrations were calculated using experimentally derived Bunsen solubility coefficients (Yamamoto et al. 1976).

Temperature (°C)	Partial Pressure CH_4 (atm)	Dissolved CH_4 (mmol L_{sw}^{-1})
4	1.1	2.0
13	1.1	1.6
20	1.1	1.4
37	1.1	1.1
60	1.1	0.9
7 (in-situ)	2.3	3.9

2.3.2 Monitoring hydrogen sulphide and alkalinity

Hungate tubes were brought into vertical position to allow the settlement of suspended sediment 12 h hours before measurements. Subsequently, water samples (200 µL) of the clear supernatants were taken using N_2 flushed syringes, to determine total dissolved sulphide concentration and total alkalinity.

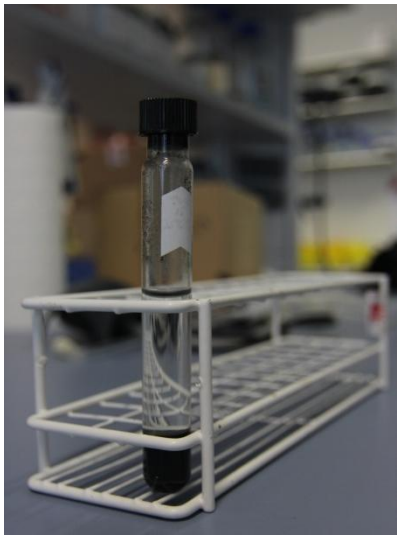

Figure 14: Hungate tube for the cultivation of anaerobic micro-organism. This sample has already been stored in a horizontal position for 24 h. Suspended sediment has settled. Samples for measuring total alkalinity and hydrogen sulphide concentrations were taken from the clear supernatant.

Sulphide concentrations were measured immediately after sampling (according to Cord-Ruwisch 1985). Therefore, 100 µL of the sample were directly injected from the syringe into reaction tubes containing 4 mL copper sulphate solution. This solution was transferred rapidly into a quartz cuvette. The formation of colloidal copper sulphide (CuS) was quantified spectrophotometrical at 480 nm. Hydrogen sulphide concentrations were calculated using a calibration curve, generated with sulphide standards, ranging from 0-20 mmol L^{-1} (Appendix A.1; Figure 26). The photometer was set to zero before measurements, with a blank reading of pure copper sulphate solution.

The remaining sample in the syringes was filled into Eppendorf tubes and stored for subsequent total alkalinity measurements (according to URL 4; Ivanenkov, Lyakhin 1978). For this purpose, 50 µL sample, 20 µL indicator solution (Appendix, A.1) and 1000 µL H_2O were pipetted into a titration vessel after G. Pavlova. The solution was titrated, under continuous N_2 bubbling with hydrochloric acid (HCl, 0.01 M), until a stable pink color occurred. Calibration was done by three measurements of IAPSO standard seawater with a known alkalinity (2.325 mmol L^{-1}): 500 µL standard seawater, 1000 µL H_2O and 20 µL indicator solution.

During AOM and dissimilatory sulphate reduction one molecule of sulphide is formed from the reduction of one molecule of sulphate (Equation 2). In AOM the reduction of one sulphate molecule causes a simultaneous increase of total alkalinity by one unit (Equation 1). But during dissimilatory sulphate reduction the reduction of one sulphate molecule

corresponds to an increase of the total alkalinity of two units (Equation 2). Thus monitoring alkalinity in controls is very sensitive to detect dissimilatory sulphate reduction that is not coupled to AOM.

Equation 2

$$2[CH_2O] + SO_4^{2-} \rightarrow 2HCO_3^- + H_2S$$

Sulphate reduction rates were calculated using the slope of the trend line (increase of total alkalinity or sulphide over time), calculated by linear regression analysis. At least four points in a row were included in these calculations. Control incubations with nitrogen instead of methane headspace allow the calculation of sulphate reduction rates that are not coupled to AOM. Thus, AOM coupled (methane dependent) sulphate reduction rates were calculated by subtracting control rates from the total sulphate reduction rate determined in the samples with methane headspace. However, controls rates were subtracted only when the linear regression analyzes was significant ($p \leq 0.05$). Rates are given in µmol SO_4^{2-} cm^{-3} undiluted sediment d^{-1}.

Total alkalinity and hydrogen sulphide in the incubations at 4 °C were measured for 41 days only. Due to malfunctioning of the cooling system all samples got frozen after that day.

Measurements of sulphide concentrations and total alkalinity were continued in samples and in controls which were incubated at 13 °C. This was done to find out, whether or not AOM rates slow down over a larger period of time. Measurements were continued until all media in the Hungate tubes was used up (85 days).

To examine the stoichiometric relationship between total alkalinity and hydrogen sulphide concentrations a linear regression analysis was performed. Only data from the incubations that showed a significant increase of both, alkalinity and hydrogen sulphide, over time (incubations at 4, 13 and 20 °C) were included in the model. Furthermore, all values from the first measurement day were excluded.

2.3.3 Radiotracer measurements

2.3.3.1 General introduction & preparations

In general, radioactive labeled molecules, so called radiotracers, can be used to track and quantify biochemical pathways with high resolution in short-time incubations. Radioactive labeled substrates (in this study: $^{35}SO_4^{2}$- and $^{14}CH_4$) are injected into samples and incubated. After a certain time the reaction is stopped. Formed products (in this study: $H^{35}S^-$ and $H^{14}CO^-_3$) and remaining substrates are chemically fixed. The ratio of radioactive products/substrates can be quantified using a scintillation counter which allows a subsequent calculation of turnover rates (in this study: based on Equation 1).

After finishing the in-vitro experiments on monitoring sulphide and total alkalinity, radiotracer experiments were conducted with slurries from Hungate tubes, incubated at 13 °C (section 2.3.2). These incubations were chosen since they showed the highest AOM rates. Before the injection of radiotracers, seawater media was exchanged in the tubes. The final dilution in the sediment slurries for the radiotracer experiments ranged between 1:10 and 1:18 (v:v). One week later, triplicate samples were prepared by transferring 5 mL sediment slurry with CH_4 flushed pipettes, into small, CH_4 flushed Hungate tubes (5 mL). Samples were prepared without headspace to prevent the diffusion of radioactive tracers into the headspace. Hungate tubes were closed with butyl rubber stoppers. Then radiotracers were injected through the stoppers using microsyringes ($^{14}CH_4$ or $^{35}SO_4^{2-}$ respectively) and tubes were incubated in the dark (13 °C). After incubation, the reaction was stopped and samples were prepared to determine the ratio of radioactive labeled remaining educts and microbial formed products respectively.

Technical difficulties during the filling process of small Hungate tubes (5 mL) resulted in dilution factors (between 1:10 and 1:18.5; Appendix, Table 14).

2.3.3.2 Sulphate reduction rate

Radioactive labeled sulphate ($^{35}SO_4^{2}$-) is used to determine rates of sulphate reduction in sediments (Jørgensen 1978; Fossing, Jorgensen 1989). Potential sulphate reduction rates were determined by the cold chromium distillation method (Kallmeyer et al. 2004, Figure 15). Besides the dilution factor of slurries, required parameters for the calculation of sulphate reduction rates are: total sulphate concentration ($[SO_4^{2-}]$), activity of total reduced

inorganic sulfur (a_{TRIS}), porosity ($m_{SEDIMENT}$), total activity in the sample (a_{TOTAL}) and the incubation time (t) (Equation 3).

Total sulphate concentration ($[SO_4^{2-}]$) in the water phase of the slurries was determined using an ion chromatograph (Metrohm ion-chromatograph), equipped with an anion exchange column. For these measurements samples (1 mL) were taken from clear supernatants in the large Hungate tubes (12 mL, section 2.3.1) before transferring samples into the small Hungate tubes. N_2 flushed microsyringes were used to transfer sediment slurries into small Hungate tubes (5 mL), for subsequent radiotracer measurements (section 2.3.3.1).

After the injection of $^{35}SO_4^{2-}$ (30 µL, 220 kBq, 22 kBq μL^{-1}) and incubation in the dark (13 °C, 24 hours), samples were transferred into centrifuge vials (50 mL) containing 20 mL zinc acetate (ZnAc, 20 %, w:v). ZnAc fixes all sulphide, resulting in the precipitation of zinc sulphide (ZnS), and thereby prevents the oxidation of sulphide to sulphate. After centrifuging (1100 g, 5 minutes, 20 °C), samples were weighted and 100 µL of the supernatant were pipetted into scintillation vials (6 mL) for subsequent counting of the total amount of radioactivity (^{35}S) in the samples (a_{TOTAL}) using a scintillation counter (TRI-CARB 2100 TR Liquid Scintillation Counter, Packard). These vials contained 1 mL H_20 and 3 mL Ultima Gold (Ultima Gold XR, Perkin Elmer). Blanks were prepared by filling 1 mL H_2O and 3 mL Ultima Gold in scintillation vials without adding supernatant.

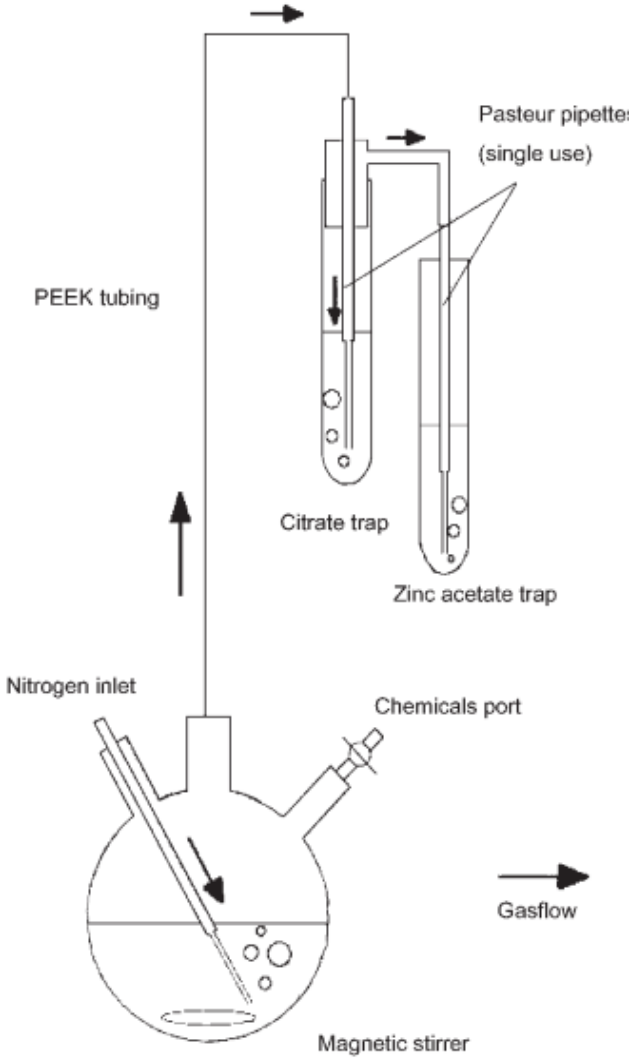

Figure 15: Set up for the cold chromium distillation to trap radioactive labeled reduced inorganic sulfur from sediment samples, in a zinc acetate solution, for the subsequent determination of sulphate reduction rates (Kallmeyer et al. 2004).

Subsequently, the supernatant in the vials was discarded and centrifuge vials were weighted again to determine the net weight of the sediment sample. The sediment was transferred from the centrifuge vials into triple-necked round bottom flasks (100 mL), containing a drop of antifoam (silicone emulsion) and a magnetic stir bar for subsequent determination of the total activity of inorganic reduced sulfur (a_{TRIS}). Centrifuge vials were rinsed twice with 5 mL Dimethylformamid. During AOM, sulphate is reduced to sulphide which precipitates or stays in solution. a_{TRIS} comprises dissolved sulphide species (S^{2-}, HS^- and H_2S), precipitated metal sulphides like iron sulphide (FeS) or pyrite (FeS_2) and elemental sulfur (S^o).

Then the sediment sample was acidified within the flask with 8 mL hydrochloride acid (HCl, 6 M) to protonate acid volatile sulfur (hydrogen sulphide and ferrous sulphide) to H_2S. To retrieve the chromium reducible sulfur species as well (pyrite and elemental sulfur), 16 mL of reduced chromium chloride solution was added into the flask. Consequently, H_2S is released from the sediment and transported with a stream of nitrogen (N_2) via a trap for aerosols, containing citrate acid, into a tube containing 9 mL zinc acetate (20 %) to precipitate H_2S as ZnS. After 1 hour and 45 minutes, the nitrogen stream was slightly increased and distillation was continued for 15 minutes. The obtained ZnAc solution was stirred, transferred into a 20 mL scintillation vial and then 10 mL Ultima Gold were added. Radioactivity was determined using a scintillation counter (TRI-CARB 2100 TR Liquid Scintillation Counter, Packard). Solutions, containing 9 mL ZnAc (5 %), 10 mL Ultima Gold and 1 drop of antifoam, served as blanks.

Due to the large dilutions of the slurries with seawater medium (between 1:10 and 1:18) porosity of slurries ($m_{SEDIMENT}$) was set to one (water content equals 100 %).

The activity (number of decays) of the solutions, to determine a_{TRIS} and a_{TOTAL}, was measured (in counts per minute, cpm) with a scintillation counter (TRI-CARB 2100 TR Liquid Scintillation Counter, Packard) to calculate rates of sulphate reduction rates (Equation 3).

Equation 3

$$Sulphate\ Reduction\ Rate\ (\mu mol\ mL^{-1}\ Sediment\ d^{-1}) = \frac{[SO_4^{2-}] \cdot a_{TRIS}}{t\ \cdot\ a_{TOTAL}\ \cdot\ m_{SEDIMENT}} \cdot 1.06$$

$[SO_4^{2-}]$	Sulphate concentration (µmol L^{-1})
a_{TRIS}	Activity of total reduced inorganic sulfur (cpm)
t	Incubation time (d)
a_{TOTAL}	Total activity in the sample (cpm)
$m_{SEDIMENT}$	Porosity of sediment (= 1 mL pore water cm^{-3} sediment)
1.06	Correction factor for discrimination of bacteria to the heavier sulfur isotope (Jørgensen, Fenchel 1974)

2.3.3.3 AOM rate

Radioactive labeled methane ($^{14}CH_4$) was used to determine rates AOM (modified from Iversen, Blackburn 1981; Treude et al. 2003).

The calculation of AOM rates by radiotracers requires, besides the dilution factor, the determination of 3 parameters (Equation 4): the initial methane concentration in the samples (CH_4), the initial total activity in the sample ($^{14}CH_4$) and the amount of radiolabelled carbon dioxide ($^{14}CO_2$).

After injecting of $^{14}CH_4$ (30 µL, 15 kBq) into small Hungate tubes and shaking, samples were incubated in the dark (13 °C, 24 hours). The incubation was stopped by transferring sediment slurries from Hungate tubes into glass vials, containing 20 mL NaOH (2.5 %). Glass vials were closed with butyl rubber stoppers.

One sample from each horizon (2 mL) was filled into a serum vial containing 5 mL NaOH (final concentration: 5 %). The vials were closed with a butyl rubber stopper and sealed using an aluminum seal. No radiotracers were injected into the sediment. These samples were used for the subsequent measurement of the initial methane concentration in the samples ([CH_4]).

After 48 hours, gas samples (100 µL) from the headspace of the serum vials was taken with microsyringes to determine initial methane concentrations ([CH_4]) using a gas chromatograph (Hewlett Packard Series II). The gas chromatograph was equipped with a packed column (Haye SepT, 6 feet, inner diameter: 3.1 mm, 100/120 mesh, Resteck, temperature setting: 75 °C) and a flame ionization detector (temperature setting of injector and detector: 160 °C). The carrier gas was helium (20 mL min^{-1}). Combustion gases were synthetic air (240 mL min^{-1}) and hydrogen (20 mL min^{-1}). Standard measurements for the calculation of methane concentrations were done using a 100 ppm methane standard (Scotty analyzed gases).

Within one week, the CH_4 in the solutions of the glass vials (containing the samples and 20 mL NaOH (2.5 %)), was combusted to CO_2 for the subsequent determination of $^{14}CH_4$. The complete gas phase of the glass vials was transported with a stream of artificial air (20 minutes, 20 mL $minute^{-1}$) through a quartz tube filled with Cu(II)-oxide in a combustion

oven (850 °C). Formed CO_2 was trapped in scintillation vials (20 mL) containing 10 mL of a mixture (1:7) of phenylethylamine and ethylenglycolmonomethylether. 10 mL Ultima Gold were added before measuring the activity with a scintillation counter.

Afterwards, samples were filled from the glass vials into Erlenmeyer flasks (250 mL) containing a drop of antifoam, for the following quantification of $^{14}CO_2$. Glass vials were rinsed twice with NaOH (2.5 %). Then 6 mL HCl (6 M) were filled into flasks which were quickly closed with a butyl rubber stopper. Acidification of the sample resulted in the outgassing of all CO_2 from the liquid phase into the gas headspace. The rubber stopper was equipped with a clamp holding a scintillation vial (10 mL), which contained 6 mL phenylethylamine and 1 mL NaOH (2.5 %) to trap gaseous CO_2. Then the glass vials were placed on a shaking table (4 hours, 60 rounds minute^{-1}). Three mL Ultima Gold were added into the scintillation vial before measuring the activity in a scintillation counter.

Five sediment samples were fixed within glass vials containing 5 mL NaOH (final concentration 5 %) before the injection of radiotracers and served as controls. Samples were considered "active" when the difference in $^{14}CO_2$ activity between a sample and a control was larger than three times the standard deviation of the control mean. The mean activity of 5 controls was subtracted from sample activity.
Combustion blank activities (containing 10 mL Ultima Gold and 10 mL of the (1:7) mixture of phenylethylamine and ethylenglycolmonomethylether) was doubled and subtracted from the activity of methane in the sample.

The radioactivity in the samples ($^{14}CH_4$ and $H^{14}CO_3^-$) was determined using a scintillation counter (TRI-CARB 2100 TR Liquid Scintillation Counter, Packard) which allows the subsequent calculation of AOM rates (Equation 4).

Equation 4

$$\boldsymbol{AOM\ rate\ (\mu mol\ CH_4\ cm^{-3}\ sediment\ d^{-1}) = \frac{^{14}CO_2 \cdot [CH_4]}{^{14}CO_2 +\ ^{14}CH_4} / t}$$

$^{14}CO_2$	Activity of microbial formed bicarbonate (cpm)
$[CH_4]$	Initial methane concentration (µmol cm^{-3} sediment)
$^{14}CH_4$	Initial activity of methane (cpm)
t	Incubation time (d)

2.4 Microbial community analyzes

2.4.1 CARD-FISH

Ribonucleic acid 16S rRNA is a molecule with an atomic weight of 16 Svedberg (16S). It is found in Ribosomes (r) of all bacterial and archaeal cells. The ribosomal ribonucleic acid (RNA) mediates the synthesis of proteins within cells. The single-stranded 16S rRNA harbors highly conserved and variable nucleic acid sequences.

Fluorescence in situ hybridization (FISH) allows the quantitative detection of different phylogenetic groups of uncultured cells in environmental samples (Amann et al. 1995). Some nucleotide sequences are consistent throughout phylogenetic groups and can be targeted by specific oligonucleotides (probes). In FISH fluorescent labeled probes are brought into permeabilized cells and bind (hybridize) to distinct rRNA regions. Excess fluorescent probes are removed afterwards by several washing steps. Subsequently all cells in the samples are stained with 4´, 6-DiAmidino-2-PhenylIndolephydrochloride (DAPI). Stained cells are counted using a fluorescence microscope. Switching between two types of filters during microscopic analyzes allows differentiating between unspecific stained cells using DAPI and specific stained cells (FISH) to determine relative cell numbers of microorganisms targeted by the probe.

However, environmental samples from marine sediments may contain slow growing bacteria that contain low numbers of rRNA molecules. Applying conventional FISH to tag these kinds of microorganisms may result in low signal intensities below, detection limit (Ravenschlag et al. 2000). Extending the common FISH protocol by Catalyzed Reporter Deposition (CARD) increases its sensitivity. For CARD-FISH, the probe is labeled with the enzyme horseradish

peroxidase (HRP) and fluorochrome labeled tyramide is added (Figure 16). Each enzyme catalyzes the activation of many tyramide molecules, which subsequently bind to cellular proteins and thereby increase the brightness of the fluorochrome signal (Bobrow et al. 1989).

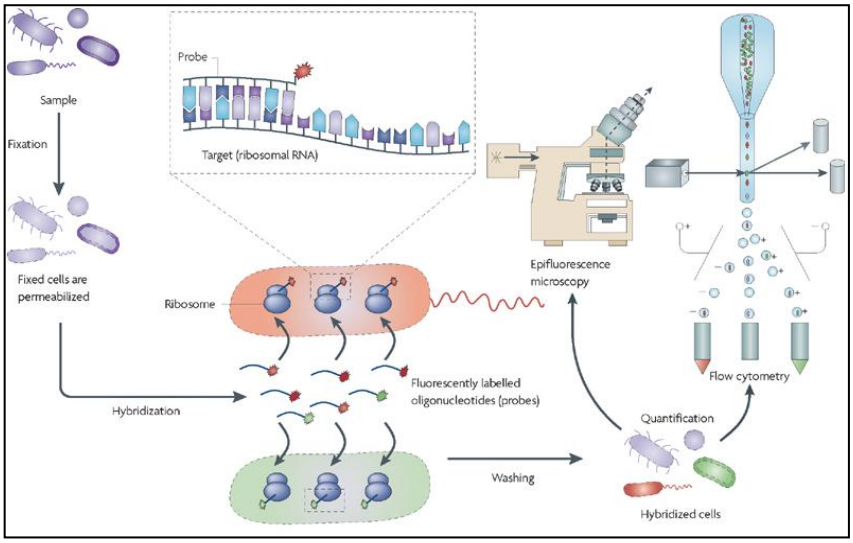

Figure 16: Schematic overview of the CARD-FISH protocol to identify specific cells in environmental samples (Amann et al. 1995).

CARD-FISH was applied to quantify groups of anaerobic methanotrophic archaea and associated sulphate reducing bacterial partners in the sediment samples from the blow-out (modified from Pernthaler et al. 2002; Ishii et al. 2004). All reagents needed for CARD-FISH are listed in the appendix.

Note, the CARD-FISH protocol described in the following never worked for sediments at the blow-out site. It is the final protocol which was used to detect microorganisms in the sediments (successful DAPI staining, clear view, no CARD-FISH signal).

Fixation

First, sediment samples from the core were fixed (0.5 mL sample in 1.5 mL fixation buffer) and stored (2.5 hours, 4 °C; section: 2.2). Fixed sediment samples were centrifuged (10 minutes, 4 °C, 1400 g), the clear supernatant was discarded. 1.5 mL sterile 1xPBS was added to re-suspend pellets with a spatula while vortexing it. The sediment was spined down again (10 minutes, 4 °C, 1400 g) and the supernatant was discarded. This procedure was repeated once to get rid of the formaldehyde. Finally the pellets were re-suspended in

1.5 mL 1xPBS/EtOH (1:2, v:v) to the final dilution (1:4, v:v), transferred into cryo vials and stored (-20 °C).

Preparation of filters

Stock solutions (final dilution: 1:40) were prepared from the fixed sediment samples (dilution: 1:4) by diluting the samples 1:10 with 1xPBS/EtOH. The samples were then 6 times sonicated with an ultrasonic probe on ice (20 seconds, cycle: 20, intensity: 40 W, Bandelin Sonoplus GM 200) to separate cells from sediment particles. Working solutions were prepared by diluting samples with 1xPBS. Trail DAPI runs showed that the best dilution (between 1-5 cells per grid, low sediment coverage) for the horizons T1; T2 and T3 were: 1:6000, 1:5500 and 1:6000 respectively. The working solutions were let stand for 10 seconds to allow sedimentation of larger sand grains. Then 1 mL supernatant from the working solutions were added to 5 mL 1xPBS in a filtration tower and filtered (0.5 mbar) on white polycarbonate filters (25 mm, 0.2 µm pore size; Whatman). Cellulose nitrate filters (25 mm, 0.45 µm pore size, Sartorius) were used as supporting filters below the polycarbonate filters. After air drying, polycarbonate filters were shortly dipped face down into agarose (0.2 %, 40 °C) to prevent cells loss during the following processing. Then the agarose embedded filters where dried (46 °C, ~30 minutes) and dehydrated with EtOH (96 %).

1/8 of the agarose embedded filter is usually sufficient for the application of one CARD-FISH probe, i.e. for the detection of one specific type of microorganisms (here: ANME 1/2/3, Desulfococcus/Desulfosarcina (DSS), Desulfobulbus (DBB) and probes for Eubacteria). Polycarbonate filter were therefore excised into eight pieces using an ethanol-sterilized scalpel.

Trail runs to optimize the CARD-FISH protocol for sediment samples should be performed with unspecific probes for eubacteria (EUB 338; Amann et al. 1990).

Permeabilization

Cell walls of microorganisms have to be permeabilized to allow the intrusion of probes, horseradish peroxidase and tyramide into the cells. However, different groups of microorganisms have distinct types of cell walls. Thus permeabilization procedures are depended on the target organisms:

<u>ANME-1</u>

Filters were incubated in proteinase K solution (3 minutes), and rinsed in H_2O.

ANME-2

Filters were incubated in 1xPBS containing SDS (0.5 %) for 10 minutes and rinsed in H_2O.

ANME-3

Filters were incubated in 0.1 M HCl for 1 minutes or 0.01 M HCl for 10 minutes, transferred to 1xPBS and rinsed in H_2O.

SRB and Eubacteria

Filters were incubated (37 °C, 60 minutes) in lysozyme in a petri dish and rinsed in H_2O water.

Inactivation of endogenous peroxidase

Active endogenous peroxidase may activate tyramide and may thereby produce a fluorescence signal. Thus, endogenous peroxidase has to be inactivated to reduce background fluorescence signals. For this reason, moist filters from the permeabilization step were incubated in 10 mL 0.15 % Methanol/H_2O_2 solution (20 °C, 30 minutes), shortly washed in H_2O, in EtOH and then air dried.

Hybridization

Hybridization buffer (Formamide concentration: ANME1/2: 40 %, ANME 3: 20 %, Desulfococcus/Desulfosarcina: 50 %, Desulfobulbus: 60 %) was used to prepare working solutions for the probes. Therefore 1 µL probe working solution (50 ng µL; ANME 1-350: Boetius et al. 2000; ANME 2-538: Treude et al. 2005a; ANME 3-1249: Niemann et al. 2006; DSS-658: Manz et al. 1998; DBB-660: Devereux et al. 1992) was mixed with 300 µL hybridization buffer. Up to 4 filters were incubated in one Eppendorf tube (46 °C, 2.5 hours). After hybridization filters were incubated in washing buffer in a water bath (48 °C, 30 minutes) and afterwards washed in 1xPBS (20 °, 30 minutes).

Coupling of HRP to the probes

After incubation, samples filters were washed in 2x saline-sodium citrate (2xSSC) and incubated in a drop (150 µL) of blocking reagent in 1xPBS (45 minutes, 20 °C). Filters were then incubated in streptavidin-HRP (20 °C, 30 minutes).

Washing

After coupling of HRP, filters were washed in 1xPBS (20 °C, 15 minutes). Excess liquid was removed but it was avoided to let filters run dry since this will reduce the activity of HRP.

CARD (Catalyzed Reporter Deposition)

All following steps were done under low light condition since fluorescing dyes (like dyes coupled to tyramide) are light sensitive. For CARD, 2000 µl amplification buffer with 1 µl 0.5 % H_2O_2 and 1 µl fluorescent-labeled tyramide (Alexa 488) were mixed in Eppendorf tubes. Filters were incubated in the tubes (46 °C, 15 minutes) and then washed in 1xPBS (20 °C, 10 minutes).

Inactivation of HRP

To inactivate HRP, filters were washed in 0.01 M Tris HCl (20 °C, 10 minutes). Finally, filters were washed in 1xPBS (20 °C, 5 minutes), rinsed in H_2O and in EtOH and air dried.

Counter staining and microscopy

DAPI is a blue fluorescent dye that unspecifically binds to DNA (Porter, Feig 1980). It was used for counterstaining during CARD-FISH since it stands in clear contrast to, the other applied fluorescence dye, Alexa 488. Filters were dipped, upside down, in a drop of DAPI (50 µL) and incubated in a petri dish, cell side up, in the dark (20 °C, 10 minutes). After incubation filters were first washed in a large volume of H_2O (20 °C, 10 minutes), then washed in EtOH (20 °C, 5 minutes) and finally air dried. Then filters were put on glass slides with 4 µL Cittifluor and covered with a cover slip. At least 800 DAPI stained cells or a maximum of 70 views per filter were counted with an epifluorescence microscope (x1000, Leitz Aristoplan). Filters cube of type A and L were used for counting DAPI or Alexa 488 labeled cells respectively (specifications of filter cubes: URL 3).

2.4.2 Density of AOM consortia and total cell numbers (DAPI staining)

AOM consortia have a distinct, round morphology. This characteristic appearance allows an easy identification using fluorescent staining methods, such as DAPI (Boetius et al. 2000). In-situ, the average diameter of AOM consortia ranges usually between 3-5 µm (Boetius et al. 2000; Knittel, Boetius 2009). Cells from all depth horizons of both, the blow-out and the reference core, were stained using DAPI. Cell aggregates that resemble AOM consortia were counted and the density of AOM consortia was calculated. The total cell number was calculated, including the cells of the AOM consortia (Equation 5). Cell numbers of consortia were calculated assuming spherical shape of the consortia and an average cell volume of

0.065 µm^3 (Boetius et al. 2000). The average volume of consortia for each horizon was calculated using the mean diameter of 25 consortia in the respective horizon.

Samples were diluted, sonicated and embedded in agarose as described before (section 2.4.1, preparation of filters for CARD-FISH) with the exception that the dilution factor was 1:2500 (15-20 cells/view). The CARD-FISH samples were higher diluted to reduce background fluorescence. This was not necessary for the DAPI staining protocol, since DAPI stained cells were clearly visible despite of higher background fluorescence.
DAPI staining of filters was done as described above for the counter staining of the CARD-FISH filters (section 2.4.1, Counter staining and microscopy).

Equation 5

$$Cell\ number\ (cells\ mL^{-1}) = \left[(CC - BC) * \frac{FF}{GF} * DF\right]$$

CC	Mean cell number per view
BC	Mean cell number per view (blank filter)
FF	Filter area (318.9 mm^2)
GF	Counting grid area (0.0121 mm^2)
DF	Dilution factor (2500)

2.5 Carbonate analyzes

2.5.1 Origin of samples and their visual observation

Carbonates may precipitate in forms of white, crystalline layers on a wide variety of substrates like sediment surfaces, clam shells, or rocks. These carbonates can be detected by optical microscopy (e.g. Magalhães et al. 2012). Under the microscope these layers appear as white crystalline spheres.
Clam shells, rocks and cemented sediment from the blow-out were visually examined for signs of carbonate formation using a stereo light microscope. Material showing evidence of carbonate precipitation on the surface was further analyzed for mineralogy and isotopic composition of the carbonate crust.

Material from different origins was examined for precipitation of crystalline structures on its surface. Cemented sediment and clam shell were extracted from the sediment slurries (2.3.1). Furthermore, clam shells, cemented sediment and rocks were extracted from samples that have been taken from inside the blow-out crater, using the submersible JAGO and a van Veen grab during ALKOR cruise 290, in 2006 (Pfannkuche et al. 2006).

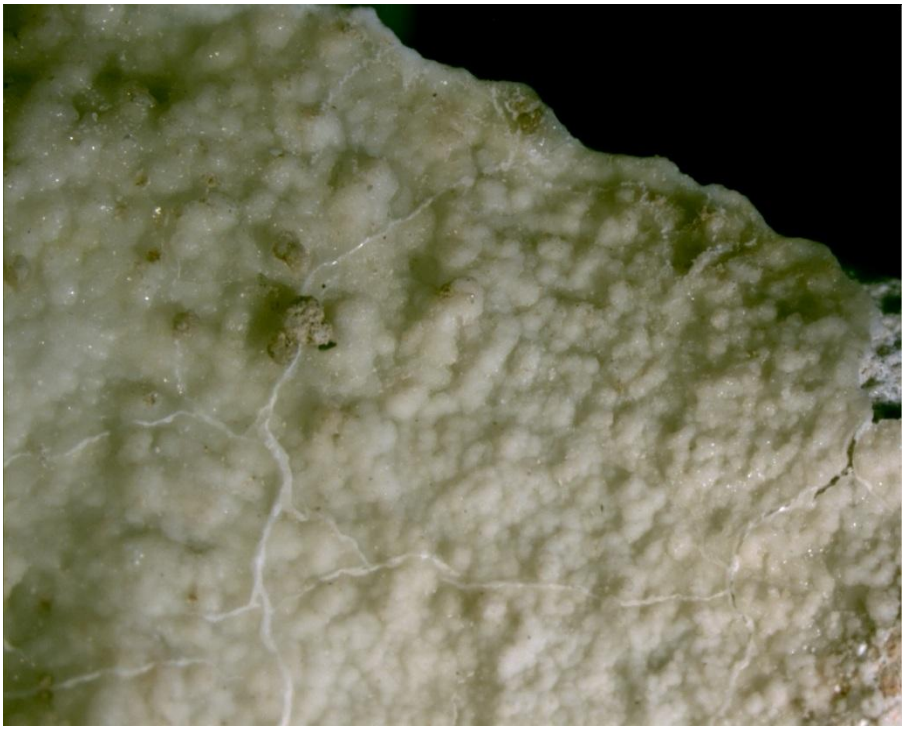

Figure 17: Crystalline layer (size: 2x2 cm, sample: BL1Crys) as an example for structures that have been classified as carbonate crust during microscopic observation.

2.5.2 Preparation for isotope analyzes and XRD

A powder was prepared for subsequent analyzes of isotopic and mineralogical composition. For this purpose, a hand held rotary tool equipped with a diamond wheel point was used. The powder was produced by carefully milling off material from the respective samples using the wheel point.

Only a small amount of powder could be extracted from some samples (BL1Res and T2Bulk, Table 8). These samples were analyzed for their isotopic composition only.

2.5.3 Analyzes

X-ray powder diffraction

Powder from the samples was analyzed for its crystalline structure using X-ray powder diffraction (Philips X-ray diffractometer PW 1710 with monochromatic CuKα) between 2 and 70 2θ. Spectra were analyzed using the software XPowder (Version: 2010.01.09 Pro). Minerals with a quantitative mass portion below 5 % and the percentage of global amorphous stuff are not stated.

Stable isotope analyzes

Powder samples (1 mg) were analyzed for carbon ($\delta^{13}C$) and for oxygen ($\delta^{18}O$) stable isotopes, separately. The powder was dissolved by water-free phosphoric acid (73 °C) in a "Carbo-Kiel" (Thermo Fischer Scientific Inc.) online carbonate preparation line and measured for carbon and oxygen stable isotope ratios using a MAT 253 mass spectrometer (Thermo-Fischer Scientific Inc.). The $\delta^{13}C$ and $\delta^{18}O$ values are reported in per mil (‰) deviation from laboratory standard referred to the Pee Dee Belemnite (PDB) scale (Equation 6).

Equation 6

$$ä\ (‰) = \left(\frac{R_{sample-}\ R_{standard}}{R_{standard}}\right) x\ 1000$$

ä (‰)	Stable isotope ratio of carbon ($ä^{13}C$) or oxygen ($ä^{18}O$), reported relative to PDB (per mil)
R_{sample}	Isotope ratio sample ($^{13}C/^{12}C$) or ($^{18}O/^{16}O$)
$R_{standard}$	Isotope ratio standard ($^{13}C/^{12}C$) or ($^{18}O/^{16}O$)

2.6 Statistical analyzes

Statistics were done using the software package RStudio (Version: 0.96.316). Significance level for all analyzes was 5 %. For normal distributed data arithmetic mean and confidence interval (95 %) are given, as measure of location and parameter of spread respectively.

Significant differences between mean values were analyzed using a one-way ANOVA and Tukey's post hoc test. Normality of the data was checked using the Shapiro-Wilks test. Homogeneity of variances were tested using Cochran's Test.

3 Results

3.1 Turnover rates

3.1.1 Monitoring sulphide and alkalinity

General pattern

Sediment slurries in Hungate tubes were incubated with methane headspace (samples) or with nitrogen headspace (controls). Hydrogen sulphide concentrations and total alkalinity were measured in Hungate tubes as indicators for sulphate reduction over 47 days in three horizons (Figure 18, Figure 19).

All samples incubated at 4, 13 and 20 °C revealed a clear linear increase of hydrogen sulphide and total alkalinity over time. In general, the steepest increase was found in samples incubated at 13 °C, followed by the incubations at 20 and 4 °C. The deepest horizon (T3, 12-18 cm bsf) showed the steepest increase of total alkalinity and sulphide concentrations over time, whereas the intermediate horizon (T2, 6-12 cm bsf) showed the slightest increase.

Neither an increase of total alkalinity nor of sulphide concentrations was detected in samples and controls from sediments of the reference core (13°C; 21 days).

Hydrogen sulphide over time

The highest increase of hydrogen sulphide concentrations were measured in the deepest horizon at 13 °C. Here, mean hydrogen sulphide concentrations increased from around 1 up to 19 mmol L^{-1} within 47 days. The lowest significant increase of sulphide was detected in the incubations at 37 °C. In these incubations, sulphide concentrations increased by factors of about 2 (6-12 cm bsf, T2), 2.5 (0-6 cm bsf, T1) and 2.8 (12-18 cm bsf, T3) within 47 days only. Neither in samples nor in controls, incubated at 60 °C, was a significant increase of sulphide detectable (Appendix, Table 12).

In some controls the increase of sulphide was significant. However, the sulphide production in the controls at 4, 13 and 20 °C was still low compared to the samples with methane headspace. At 37 °C the increase of sulphide in all controls and samples was significant and in a similar magnitude (Figure 18).

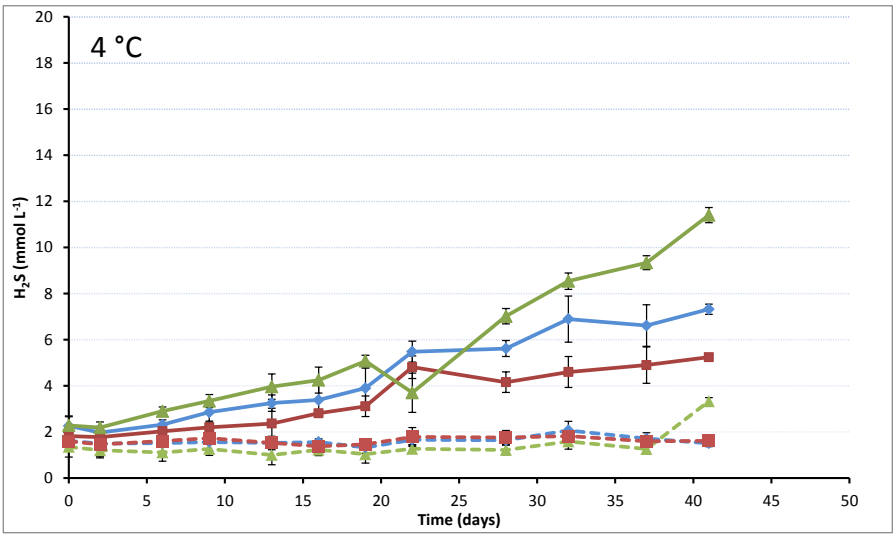
4 °C
H2S (mmol L-1)
Time (days)

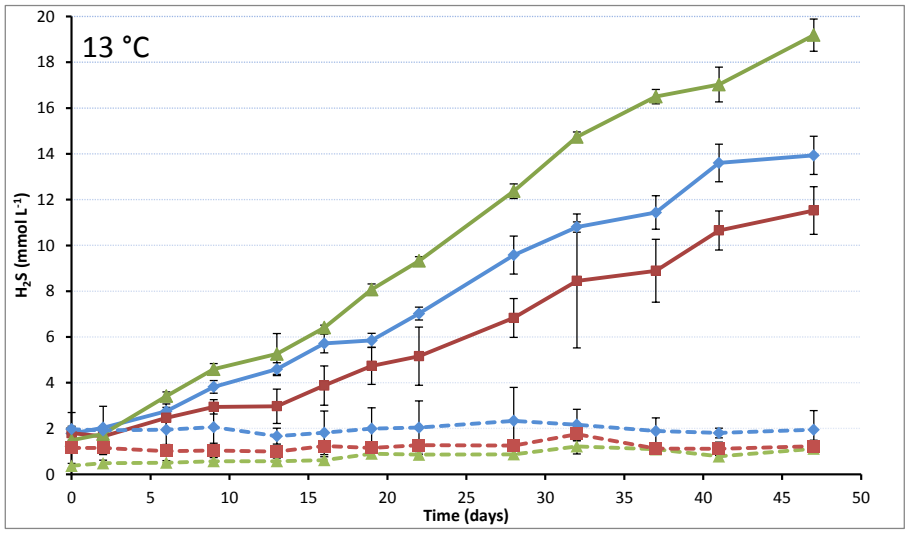
13 °C
H2S (mmol L-1)
Time (days)

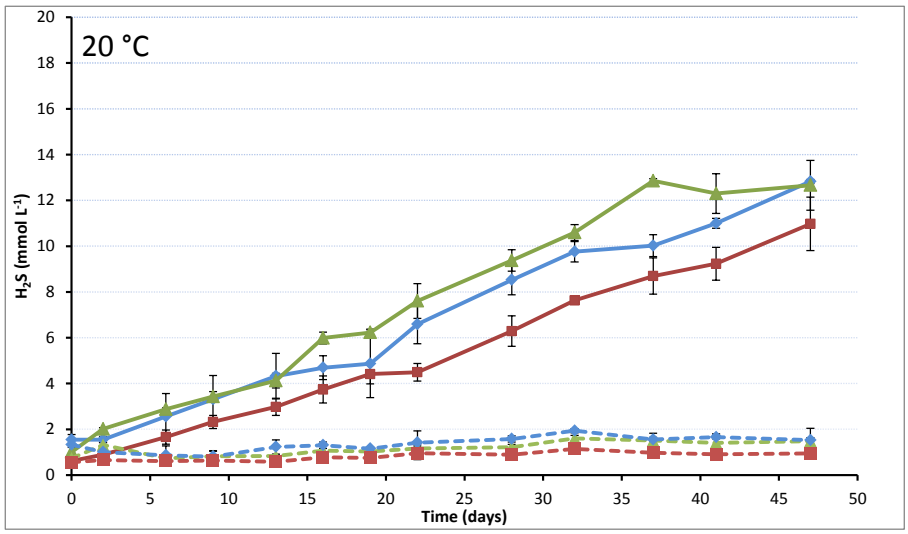
20 °C
H2S (mmol L-1)
Time (days)

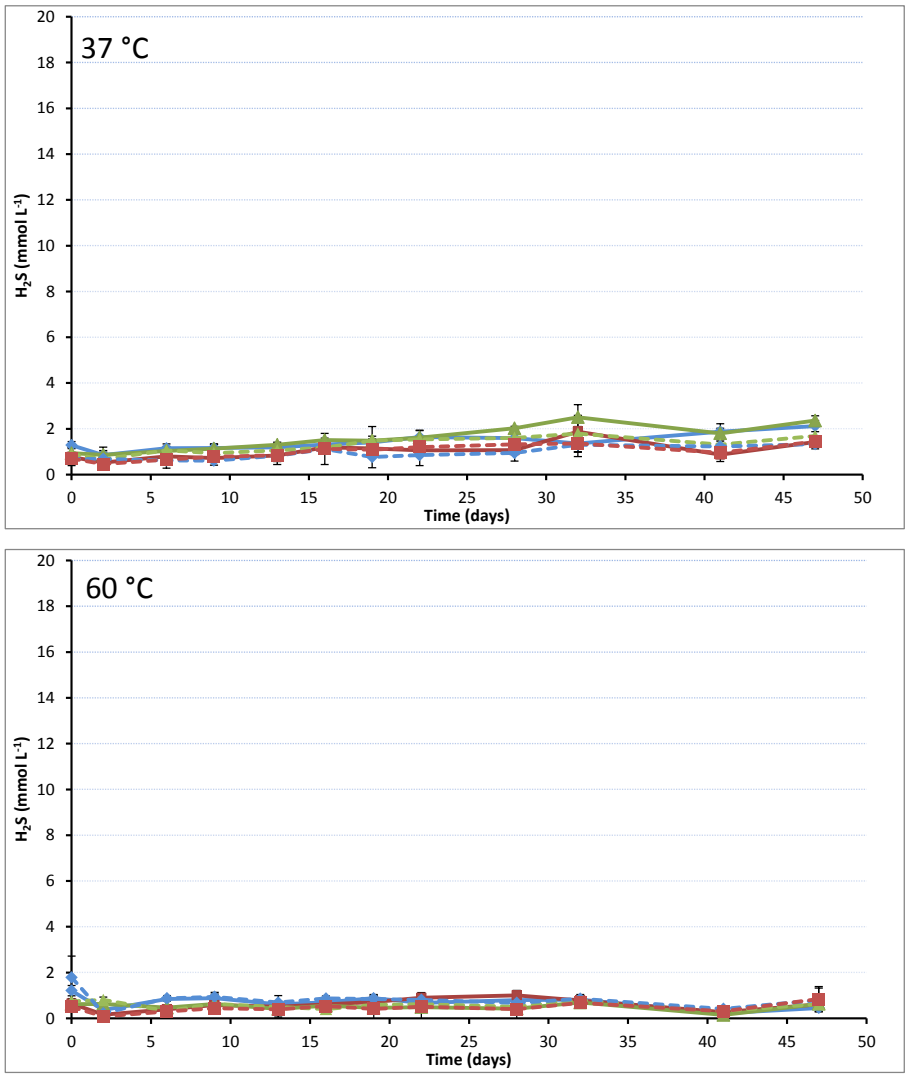

Figure 18: Mean hydrogen sulphide concentrations (n=3, error bars indicate 95 % confidence intervals) measured in three depth horizons over 47 days in samples with methane headspace (solid lines) and control incubations with nitrogen headspace (dashed lines) Different colors represent replicate samples or controls respectively.

Total alkalinity over time

Highest total alkalinity was measured in incubations at 13 °C in horizon T3. Here alkalinity increased from initial values of around 30 mmol L^{-1} up to 55 mmol L^{-1} within 47 days.

In general, the increase of total alkalinity was positively correlated with time in the incubations at 4, 13 and 20 °C. The increase of alkalinity over time in samples incubated at 37 °C was very low. Linear regression analysis for these incubations was not significant for all replicates in horizons T1 and T2, but statistically significant for two replicates in horizon T3 (Appendix, Table 12).

Total alkalinity decreased in all samples and controls incubated at 60 °C in a similar way. Within 47 days, alkalinity decreased (linear) on average by 4.5 mmol L^{-1} (n=18, 95%

Confidence interval: 0.85). In some controls incubated at 4, 13 and 20 °C, linear regression analysis was significant (Appendix, Table 12). However, the increase of total alkalinity over time was very low compared to samples with methane headspace (Figure 19).

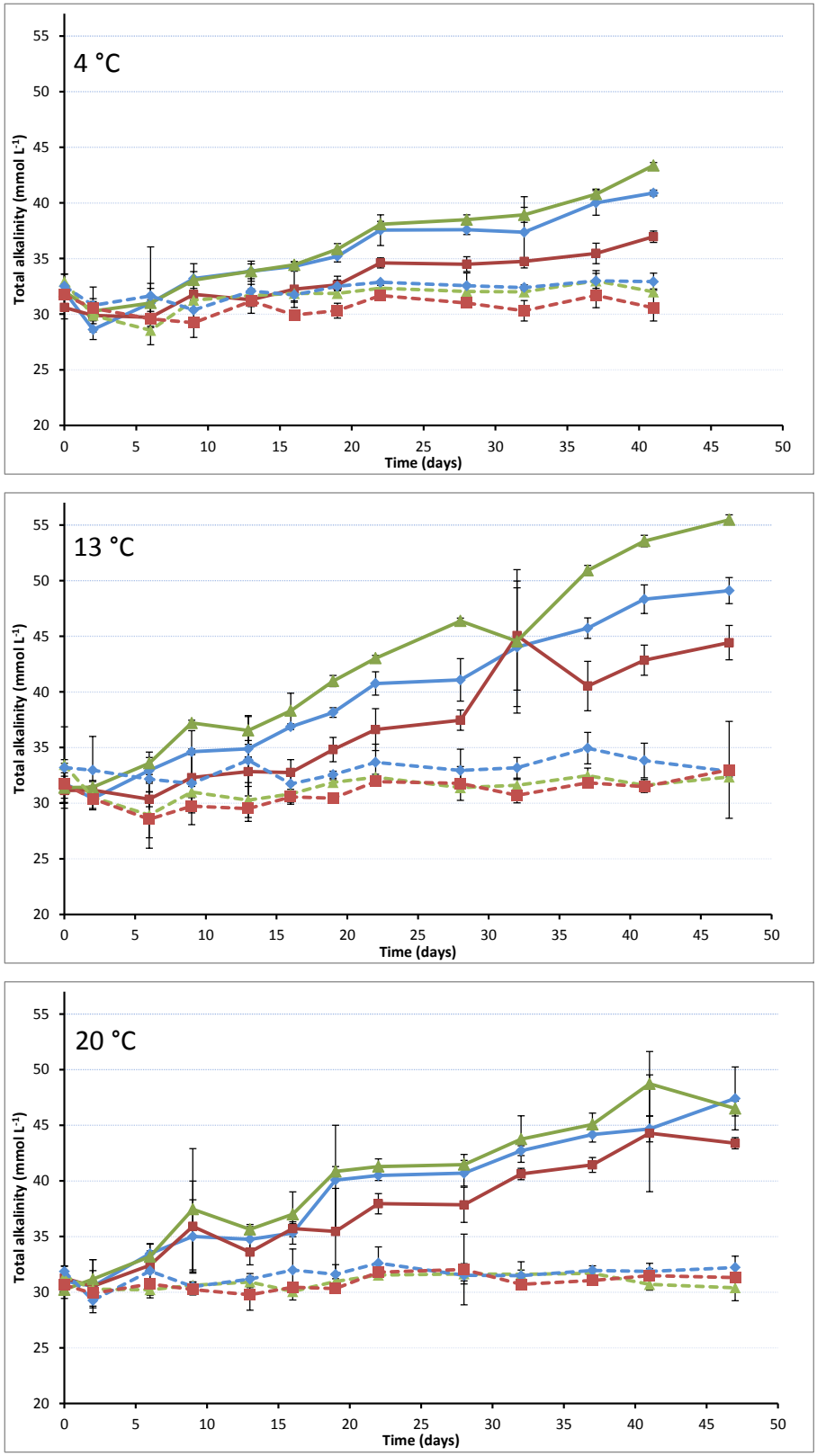

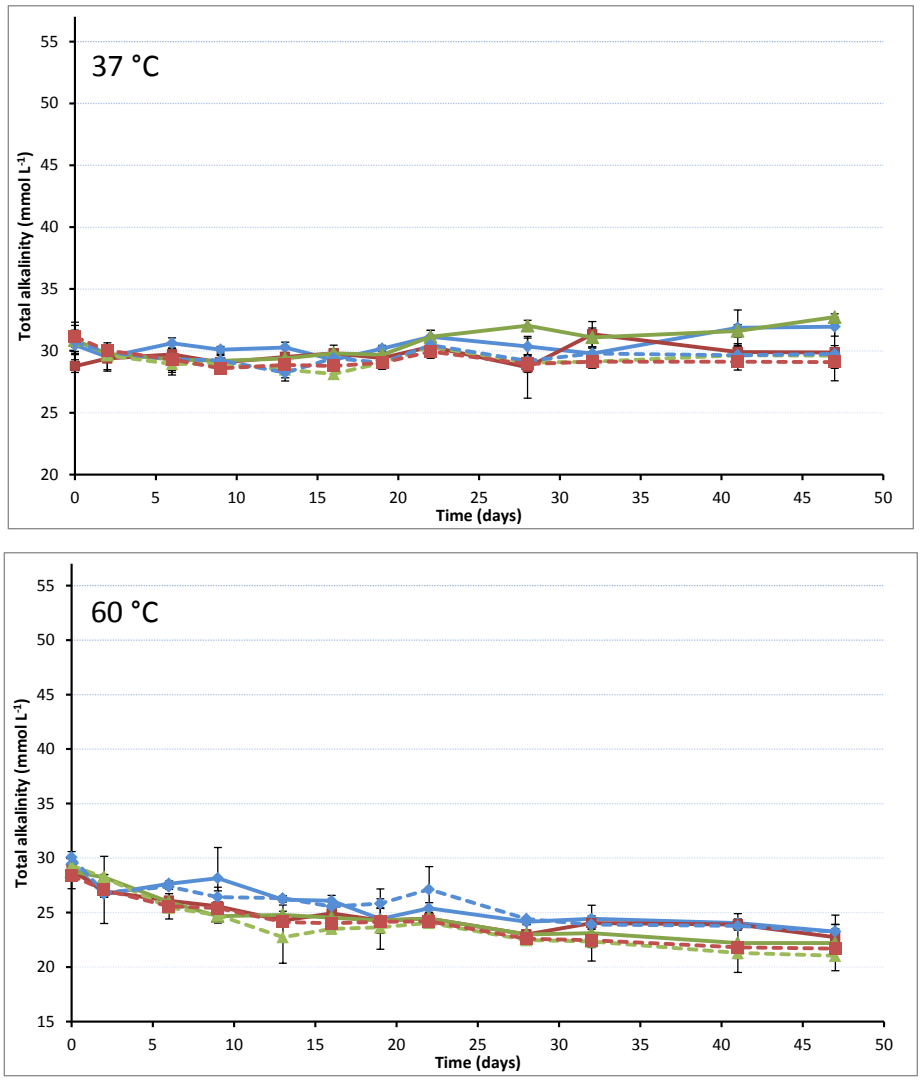

Figure 19: Mean total alkalinity (n=3, error bars indicate 95 % confidence intervals) measured in three depth horizons over 47 days in samples with methane headspace (solid lines) and control incubations with nitrogen headspace (dashed lines). Different colors represent replicate samples or controls respectively.

Rates of methane dependent sulphate reduction

The slope of the trend line, for increasing/decreasing sulphide concentrations and total alkalinity over time, was determined by linear regression analysis for all samples and controls. Total sulphate reduction rates were calculated using the slope of the incubations with methane headspace. Subsequently, methane dependent sulphate reduction rates were calculated by subtracting control rates from total sulphate reduction rates. All stated rates refer to undiluted sediment.

Rates, calculated by measuring alkalinity or sulphide over time, showed similar patterns (Figure 20, Figure 21). The highest rates were measured in the incubations at 13 °C followed

by the incubations at 20 and 4 °C respectively. Rates differed clearly between the different horizons in incubations at 4 and 13 °C (Table 3).

At 20 °C rates between the horizons did not vary as clear as between incubations at 4 and 13 °C. Rates in the different horizons were almost identical when incubated at 37 or 60 °C respectively. The deepest horizon (T3) showed the highest sulphate reduction rates as compared to horizons T1 and T2. The lowest rates were determined in the intermediate horizon (T2).

The increase of sulphide, in all samples and almost all controls (1 exception), incubated at 37 °C, was significant. This could indicate that sulphate reduction in sediments from the blow-out site, at 37 °C, is not methane dependent. However, the picture looks different for the measurements of total alkalinity in the same samples. Two samples and one control showed a significant increase of total alkalinity over time (horizon T3, Appendix, Table 12).

Potential sulphate reduction rates, at 60 °C, were slightly negative when calculating it, based on alkalinity measurements (Figure 21).

Total alkalinity decreased in a similar magnitude in controls and samples incubated at 60 °C. For the calculation of methane dependent sulphate reduction, control rates were subtracted from sample rates. Thus, in this case, control and sample rates almost offset each other.

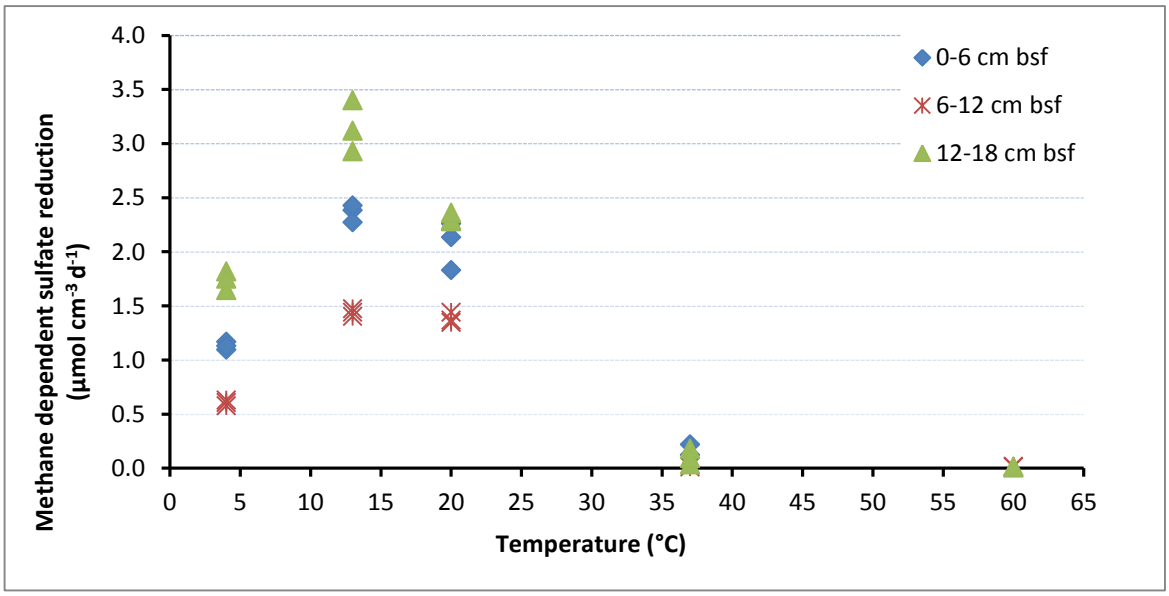

Figure 20: Sulphate reduction rates determined in vitro by monitoring the increase of sulphide over time, in Hungate tubes, with methane headspace (in µmol SO_4^{2-} cm^{-3} sediment d^{-1}).

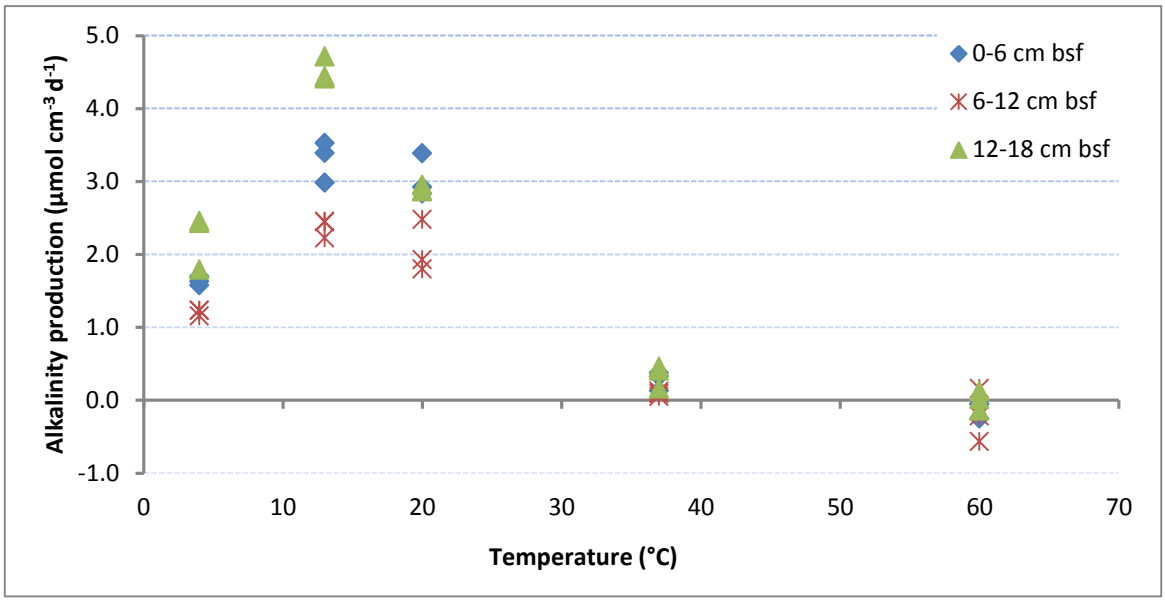

Figure 21: Sulphate reduction rate determined in vitro by monitoring increase of total alkalinity over time, in Hungate tubes, with methane headspace (in µmol SO_4^{2-} cm^{-3} d^{-1}).

Temperature coefficients (Q_{10}) were calculated for methane dependent sulphate reduction rates between 4 and 13 °C, 13 and 20 °C and between 20 and 37 °C (Table 2). Between 4 and 13 °C, Q_{10} values were slightly above two, indicating that an increase in temperature of 10 °C results in a doubling of microbial activity. Between 13 and 20 °C the AOM activity slightly decreases, indicated by Q_{10} values below 1. Beyond 20 °C, rates sharply decrease as indicated by Q_{10} values around 0.

Table 2: Temperature coefficients (Q_{10}) calculated from potential methane dependent sulphate reduction rates at 4, 13, 20 and 37 °C. Rates were determined by measuring total alkalinity and sulphide over 47 days.

	Total alkalinity			
Temperature range	**Q_{10} (0-6 cm bsf)**	**Q_{10} (6-12 cm bsf)**	**Q_{10} (12-18 cm bsf)**	**Mean Q_{10}**
4-13°C	2.2	2.1	2.3	**2.2**
13-20°C	0.9	0.9	0.6	**0.8**
20-37°C	0.1	0.1	0.1	**0.1**
	Sulphide			
Temperature range	**Q_{10} (0-6 cm bsf)**	**Q_{10} (6-12 cm bsf)**	**Q_{10} (12-18 cm bsf)**	**Mean Q_{10}**
4-13°C	2.3	2.6	1.9	**2.3**
13-20°C	0.9	1.0	0.7	**0.9**
20-37°C	0.0	-	0.0	**0.0**

Table 3: Mean methane dependent sulphate reduction rates (µmol SO_4^{2-} cm^{-3} sediment), calculated from the increase for total alkalinity or hydrogen sulphide over 47 days (n=3, 95 % confidence interval in brackets). Symbols: † or ^{I} indicate that the increase/decrease of all (†) or one (^{I}) replicate respectively was not significant. Rates, marked with different letters, show significant differences between incubations of the same incubation temperatures but different horizons (p≤5 %).
Rates marked with different numbers (superscript) indicate significant differences between samples incubated at different temperatures but originate from the same horizons (p≤5 %).

Methane dependent sulphate reduction rates (µmol cm^{-3} d^{-1})						
	Total alkalinity			Hydrogen sulphide		
cm bsf	0-6	6-12	12-18	0-6	6-12	12-18
4 °C	$^{a/1}$1.63 (+/- 0.19)	$^{b/1}$1.12 (+/- 0.05)	$^{c/1}$2.10 (+/- 0.03)	$^{A/1}$1.11 (+/- 0.02)	$^{B/1}$0.73 (+/- 0.04)	$^{C/1}$1.74 (+/- 0.12)
13 °C	$^{a/2}$3.29 (+/- 0.11)	$^{b/2}$2.23 (+/- 0.06)	$^{c/2}$4.49 (+/- 0.19)	$^{A/2}$2.37 (+/- 0.06)	$^{B/2}$1.75 (+/- 0.05)	$^{C/2}$3.15 (+/- 0.24)
20 °C	$^{a/2}$2.94 (+/- 0.37)	$^{b/2}$2.07 (+/- 0.23)	$^{a,b/3}$2.75 (+/- 0.06)	$^{A/2}$2.08 (+/- 0.02)	$^{B/2}$1.73 (+/- 0.07)	$^{A/3}$2.28 (+/- 0.12)
37 °C	0.29† (+/- 0.05)	0.24† (+/- 0.04)	0.31^{I} (+/- 0.05)	$^{A/3}$0.07 (+/- 0.05)	$^{A/3}$-0.01 (+/- 0.03)	$^{A/3}$0.10 (+/- 0.03)
60 °C	$^{a/3}$-0.12 (+/- 0.11)	$^{a/3}$-0.21 (+/- 0.36)	$^{a/4}$0.00 (+/- 0.07)	-0.03† (+/- 0.02)	0.00† (+/- 0.03)	0.00† (+/- 0.02)

The increase of alkalinity over time was, on average, about 1.4 times higher than the increase of hydrogen sulphide in the incubations at 4, 13 and 20 °C (Figure 22). Thus, corresponding rates of methane dependent sulphate reduction were on average 1.4 times higher when calculated from the change of total alkalinity over time (Table 3).

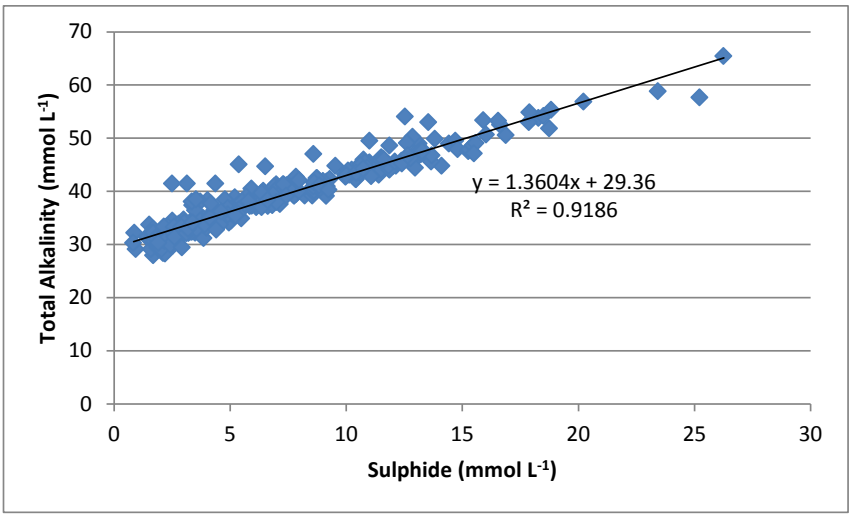

Figure 22: Linear regression analysis of sulphate concentrations and total alkalinity in the samples at 4, 13 and 20 °C.

Integrated sulphate reduction rates

Sulphate reduction rates, determined for horizons T1-3 in the blow-out core, were used to calculate integrated rates. Note, the rates were calculated from the surface to 18 cm sediment depth only (equals the length of the core).

Table 4: Sulphate reduction rates integrated over 18 cm.

	Integrated sulphate reduction rates			
	Derived from H_2S monitoring		Derived from TA monitoring	
Temperature (°C)	mmol m^{-2} d^{-1}	mmol m^{-2} y^{-1}	mmol m^{-2} d^{-1}	mmol m^{-2} y^{-1}
4	215	78406	346	126408
13	436	159106	629	229767
20	365	133353	493	180006
37	10	3657	46	16834
60	-2	-666	-168	-61151

Inhibition of sulphate reduction due to end product accumulation

Experiments, for the determination of methane dependent sulphate reduction, by monitoring total alkalinity and hydrogen sulphide, ended after 47 days. However, measurements in samples and controls incubated at 13 °C were carried on. Measurements were continued to find out if high sulphide concentrations slow down or stop sulphate reduction.

After 61 days, sulphide had reached concentrations around 25 mmol L^{-1} in horizon T3. After 85 days, mean sulphide concentration had slightly increased to 26 mmol L^{-1} in this horizon (Appendix, Figure 27).

In horizons T1 and T2 a slightly slower increase of sulphide over time, from day 61 on, was visible (Appendix, Figure 27). Sulphide concentrations rose to about 20 and 17 mmol L^{-1} respectively, after 85 days. All media in the Hungate tubes was used up until then, measurements could not be continued, after 85 days.

Likewise, total alkalinity measured in the same samples, over 85 days, showed a similar pattern (Appendix, Figure 28). In horizon T3, total alkalinity further increased to about

60 mmol L^{-1} within 61 days. After 85 days total alkalinity had decreased to an average of 58 mmol L^{-1} in these samples.

In horizons T1 and T2, total alkalinity rose to 50 and 55 mmol L^{-1} within 85 days, but the increase of total alkalinity was lower from day 61 on (Appendix, Figure 28)

Is the inhibition of sulphate reduction due to high temperatures reversible?

After 47 days, seawater media for sulphate reducing bacteria was added, to the incubations of 37 and 60 °C, to reestablish the initial dilution of the slurries (1:8, v:v). Then, these samples were incubated, at 13 °C for 46 days, to find out whether or not the inhibition of sulphate reduction due to high temperatures is reversible. However, no significant (Appendix, Table 13) increase of total alkalinity or hydrogen sulphide concentrations were detected after 46 days.

3.1.2 Radiotracer measurements

Sulphate reduction rates and AOM rates in the samples, determined by radiotracer measurements, were in a similar magnitude (Figure 23). This result shows that most of the sulphate reduction, in the analyzed sediments, is methane dependent. Additionally, the rates, determined by radiotracer measurements, show similar patterns like the rates determined by measuring total alkalinity and hydrogen sulphide over time. The rates were highest in the deepest horizon (T3), between 12 and 18 cm bsf. In this horizon, AOM rates ranged between 1.3 and 2.4 µmol CH_4 cm^{-3} d^{-1} and SR rates ranged between 1.1 and 1.4 µmol SO_4^{2-} cm^{-3} d^{-1}. The first horizon (T1) showed slightly lower AOM (between 0.9 and 1.1 µmol CH_4 cm^{-3} d^{-1}) and SR rates (between 0.6 and 1.3 µmol SO_4^{2-} cm^{-3} d^{-1}). The lowest activity of AOM (0.6 µmol CH_4 cm^{-3} d^{-1} in all replicates) and SR (between 0.5 and 0.8 µmol SO_4^{2-} cm^{-3} d^{-1}) were measured in the second horizon (T2) between 6-12 cm bsf. In some replicates AOM activity was higher than SR activity of the same horizon.

In both horizons, T1 and T3, one replicate showed no SR activity. These measurements are not considered in the following.

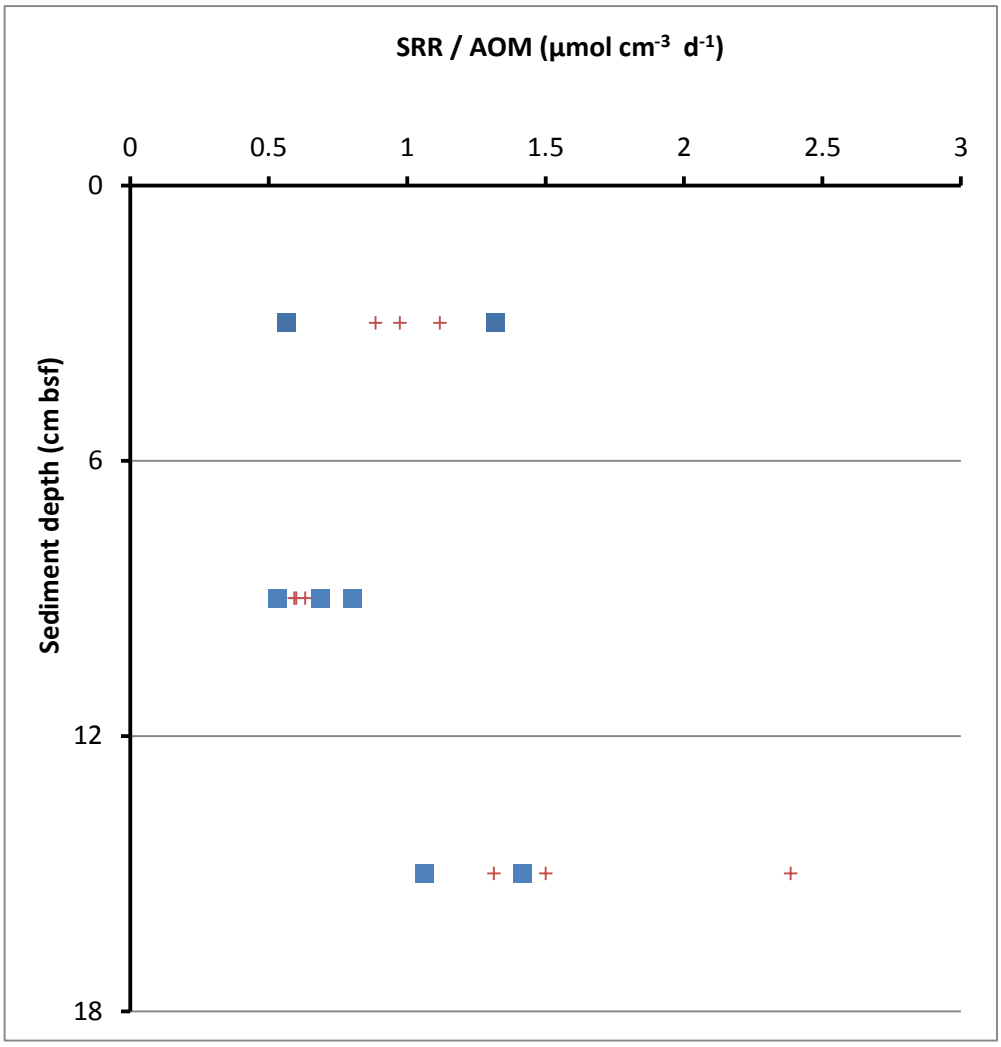

Figure 23: AOM (cross) and SR (squares) rates determined by radiotracer measurements in three horizons of the sediment core incubated at 13 °C (0-6; 6-12 and 12-18 cm bsf)

At 13 °C, AOM rates determined by radiotracer measurements were lower compared to rates determined by measuring sulphide (2.2 times lower) and alkalinity over time (3.3 times lower) (Table 5).

Table 5: Comparing AOM rates, determined for the same sediments, measuring sulphide and alkalinity over time or applying radiotracer measurements (13 °C).

		AOM (µmol CH_4 cm^{-3} d^{-1})		
Horizon	**Replicate**	**Radiotracer**	**Sulphide**	**Alkalinity**
T1	R1	0.97	2.38	3.4
	R2	1.12	2.27	3.0
	R3	0.89	2.43	3.5
T2	R1	0.60	1.47	2.4
	R2	0.59	1.44	2.4
	R3	0.63	1.40	2.2
T3	R1	2.39	3.12	4.4
	R2	1.50	3.40	4.7
	R3	1.31	2.93	4.4

3.2 Microbial community analyzes

3.2.1 CARD-FISH

The CARD-FISH method could not be successfully implemented for sediments at the blow-out. Despite of many trial runs, in which many steps from the basic CARD-FISH protocols (Pernthaler et al. 2002; Ishii et al. 2004) were adjusted or changed, no CARD-FISH signal was visible. Many steps were varied during the adjustment of the CARD-FISH method to blow-out sediment (Table 6).

The counting of cells on the sediments was not possible, due to high background fluorescence (sand grains, filter) and due to unclear view on the slides (striae). At the end of the trial runs, the view on the filter was clear but no CARD-FISH signal was detectable.

Table 6: Approaches to adapt the CARD-FISH protocol to sediments from the blow-out site

Keyword / Step	Intention	Evaluation / Variation	Result
Agarose embedding	Does agarose embedding influence CARD-FISH signal?	- No agarose embedding - Spraying agarose on filter - Dip filters shortly upside down in agarose	- No agarose: ≈ 1/4 cell loss / good view - Spraying: unevenly distributed => partly out of focus - Dipping: no cell loss, even surface, clear view => applied in the following
Dilution of samples	Evaluate (using DAPI): at what dilution is sedimet cover less than 70 % and cell density~20 cells per view	Dilutions from 1:500 =>1:3000	- Dilutions 1:2000: cell density = 10-20 cells /view - Sediment cover high but cells well visible when DAPI stained Dilutions applied in the following: 1:2000
All steps	Which steps causes the striae?	After each step=> one filter frozen for subsequent DAPI to see were the picture is not clear	All samples with striae => Wash more thoroughly!
Washing buffer	Improve view and decrease background fluorescence by using washing buffer	After hybridisation => wash filters in washing buffer (at 48 °C)	Successful: -Less background fluorescence / clear view on filter Applied in following steps: washing buffer after hybridisation
Blocking reagant	Get rid of the background fluorescence	Increase volume of Blocking reagant to 150 µL and extent subsequent incubation time to 45 minutes	Successful: -Slightly less background fluorescence Applied in following steps: more blocking reagant and longer incubation
Washing	Get rid of the background fluorescence	-Increase volumes of liquids and time of the washing during all washing steps. - Active washing (move filters around with forceps) - Several washing steps with fresh water after CARD	Successfull: - Less striae Applied in following steps: longer washing, more liquid, active washing
SEVERAL CARD-FISH RUNS WERE DONE AT THIS STAGE USING ONE ANME PROBE AFTER THE OTHER => BUT STILL NO CARD-FISH SIGNAL & HIGH BACKGROUND FLUORSCENCE => FROM HERE ON CONTINUED WITH PROBE EUB:338			
Dilution of samples, part II	Does the reduction of sediment cover reduce background fluorescence?	Sediment cover too high (when diluted 1:2000) => causes high background fluorescence =>detect CARD-FISH signal is difficult=>dilute up to 1:7000 (K. Knittel, personal communication) =>Dilutions between 1:6000 and 1:7000 were prepared	- Dilutions 1:7000: about 1-8 cells/view but background fluorescence low Dilutions applied in the following: 1:7000
Sedimentation of samples	Situation: - Either too much sediment cover and too few cells/filter or vice versa - Little furrows from sand grains on filters	Let working solution sit for 10 seconds before adding 1 mL of supernatant into filtration tower	Successfull: - Background fluorescence slightly decreased - No furrows from sand grains on the filter Applied in the following trail runs
NO CARD-FISH SIGNAL			
Keyword / Step	**Intention**	**Evaluation / Variation**	**Result**
Pre-hybridisation	CARD-FISH signal with Pre-hybridisation	-	No difference (also evaluated with other sediments were CARD-FISH was successful)
Hybridsation	Does the hybridisation time influence the outcome of CARD-FISH?	Hybridisation time increased from 2.5 up to 18 hours.	No difference (also evaluated with other sediments were CARD-FISH was successful)
[Tyramid]	Decrease tyramid concentration to decrease background fluorescence!	The following dilutions of tyramid were used: 1:300 / 1:1000 / 1:2000 / 1:3000 / 1:5000	Background fluorescence clearly decreased but still no CARD-FISH signals; Applied in the following: 1:2000 dilution of Tyramid.
Probes	Are the probes for Eubacteria not working?	Probes (already labelled with HRP), provided from Max-Planck Institute for Marine Microbiology were tested on sediment samples	No CARD-FISH signal
Fixation sediments	Went something wrong during fixation of samples?	After finishing rate measurements, 0.5 mL sediment slurry from incubations at 20 °C was fixed and analyzed as described in material & method section	No difference, compared to the initially fixed sediments
Pure culture	Is something wrong with the eubacteria probe?	Pure culture of *Desulfovibrio marinus* on filter. Trail runs also with MPI probe (see above)	No CARD-FISH signal
Inoculate sediments with pure cultures	No CARD-FISH signal due to sediment?	Compare outcome with pure culture CARD-FISH!	No CARD-FISH signal

3.2.2 Density of AOM consortia and total cell numbers

In all horizons of the blow-out core, cell aggregates that resemble AOM consortia were found (Figure 24). Sediments from the blow-out site were dominated by cells organized in these consortia, which represented between 93 and 83 % of the total cell number (Figure 25, Table 7). In contrast, no such cell aggregates were found in samples from the reference core.

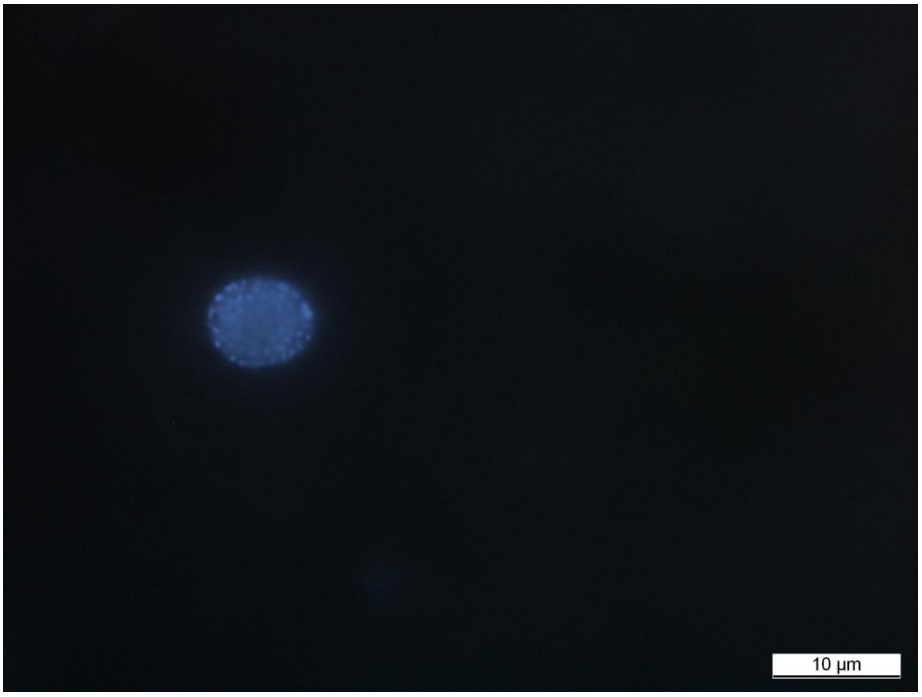

Figure 24: A DAPI stained aggregate of cells, which was counted as AOM consortia.

Total cell numbers at the blow-out site were highest in the deepest horizon T3, between 12-18 cm bsf ($6.75*10^9$ cells cm^{-3}) followed by horizon T2, between 0-6 cm bsf ($4.75*10^9$ cells cm^{-3}). Only half and one third of these total cell numbers respectively, were counted in the intermediate horizon T2, between 6-12 cm bsf ($2.31*10^9$ cells cm^{-3}).

The contribution of AOM cells to total cell numbers was large and relatively constant over depth. The percentage of AOM cells to the total cell numbers was 83 % (T2), 85 % (T1) and 93 % (T3) (Table 10).

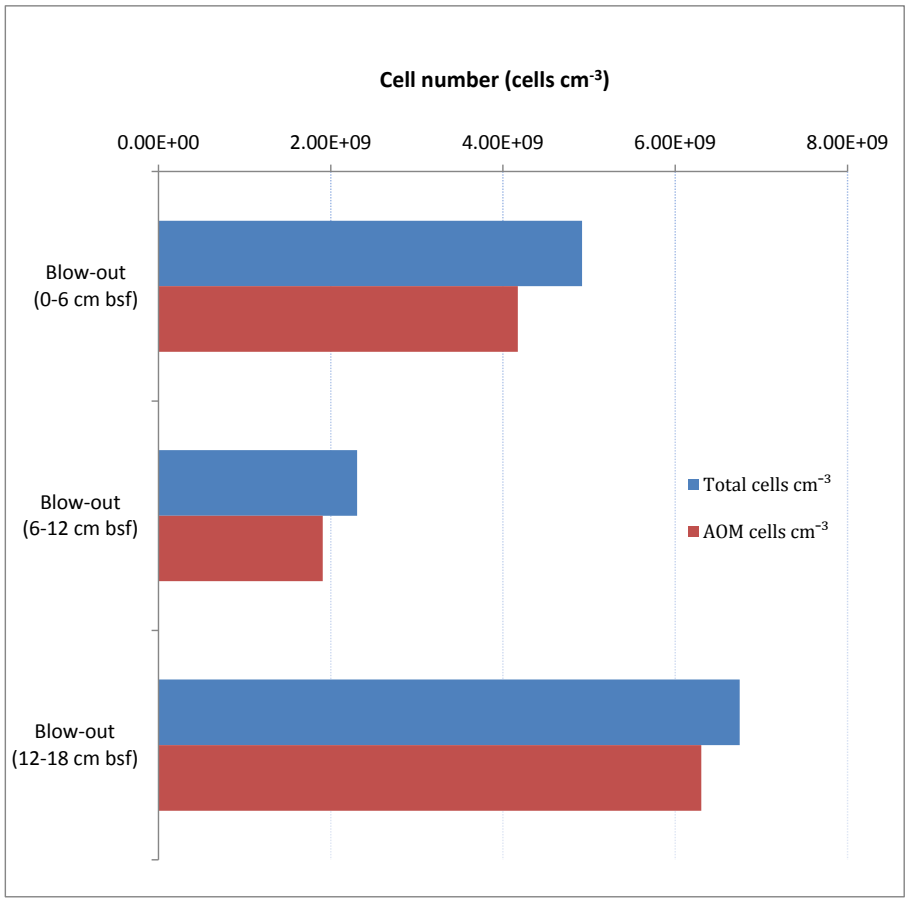

Figure 25: Total cell numbers and the percentage of cells, organized in consortia, in sediments from the blow-out site (determined by DAPI staining).

Mean diameters (n=25) of cell aggregates ranged between 2.9 µm (T1) and 3.9 µm (T3). The minimum diameter of a cell aggregate was 1 µm, the maximum diameter 8 µm. Correspondingly, the average number of cells per consortia was highest in the deepest horizon, T3 (493 cells/consortium). Compared to horizon T3, one third less cells per consortium were detected in the intermediate horizon T2 (314 cells/consortium) and half of the cells in the uppermost horizon T1 (203 cells/consortium). No significant difference between mean diameters of consortia, from the three depth horizons, was detected using a one-way ANOVA ($F=1.78$; df: 2; 39, $p>0.5$).

The highest consortia density was found in the first horizon T1 ($2.2*10^7$ aggregates cm^{-3}). In this horizon, consortia density was twice as high as in the deepest horizon T3 ($1.28*10^7$ aggregates cm^{-3}) and almost four times higher compared to the second horizon T2 ($6.07*10^6$ aggregates cm^{-3}). Integrating the aggregate counts over 18 cm bsf equals $2.5*10^{12}$ aggregates m^{-2}.

Total cell numbers at the blow-out site were about one order of magnitude higher compared to the reference site (Table 7).

Table 7: Comparison of total cell numbers and portion of cells organized in aggregates between sediments sampled at the blow-out site and at the reference site.

Site	Depth (cm bsf)	Total cell number (cells cm^{-3})	Number of cells not organized in aggregates (cells cm^{-3})	Cells organized in aggregates (%)	Aggregate density (aggregate cm^{-3})
	0-6	4.92×10^9	7.46×10^8	85	2.20×10^7
Blow-out	**6-12**	2.31×10^9	4.01×10^8	83	0.61×10^7
	12-18	6.75×10^9	4.46×10^8	93	1.28×10^7
	0-6	7.10×10^8	equals total cell number	0	0
Reference	**6-12**	3.91×10^8		0	0
	12-18	7.35×10^8		0	0

3.3 Mineralogy & Isotope analyzes

Samples from the blow-out site, showing signs of carbonate precipitation, were further analyzed for their isotopic compositions ($\delta^{13}C$ and $\delta^{18}O$) and their mineralogy. These samples are listed and described in Table 8.

Sample combinations BL8Crys/Trans/Bulk, BL1Res/Crys and T2Bulk/Crys (Crys=crystalline structure, Trans=transition crystalline/bulk sediment, Bulk=bulk sediment) respectively are each sequences from the outside to the interior of a sample (Table 8). Samples BL1 and BL8 (Block 1 and Block 8) were taken from cemented sediment that was sampled at the same site. BL8 samples originated from a crack in a cemented piece of white sediment. BL1 samples were extracted from the surface of cemented sediment. T2Crys was powder, produced from a white crystalline structure that was extracted from slurries of horizon T2. T2Crys was surrounded by reddish, sandy bulk sediment (T2Bulk). T2S was taken from spheroidal structures within a clam shell which was extracted from horizon T2.

Table 8: Summarized results from analyzes of mineralogy and isotopic composition.

ID	Description	Mineral1	%	Mineral2	%	Mineral3	%	Mineral4	%	Mineral5	%	$\delta^{18}O$	$\delta^{13}C$	Origin
BL8Crys	Pure crystalline structure /on top of crack	Brucite, $Mg(OH)_2$	52	Calcite, $CaCO_3$	27	Calcite magnesium, $MgCO_3$	17	-	-	-	-	-10.51	-13.55	Inside blow-out crater/ cemented sediment/ crack/ submersible JAGO/ Alkor cruise 290 in 2006
BL8Trans	Transition crystalline structure / bulk sediment	Brucite, $Mg(OH)_2$	55	Calcite, $CaCO_3$	35	-	-	-	-	-	-	-10.04	-15.56	
BL8Bulk	Pure bulk sediment	Vaterite, $CaCO_3$	34	Calcite, $CaCO_3$	23	Calcite magnesium, $MgCO_3$	22	Aragonite, $CaCO_3$	10	Brucite, $Mg(OH)_2$	7	-8.89	-13.44	
BL1Res	Residuals from cleaning of crust	-	-	-	-	-	-	-	-	-	-	-3.20	-7.28	Inside blow-out crater/ cemented sediment/ surface/ submersible JAGO/ Alkor cruise 290 in 2006
BL1Crys	Cleaned crystalline crust	Brucite, $Mg(OH)_2$	48	Aragonite, $CaCO_3$	38	Calcite, $CaCO_3$	7	Calcite magnesium, $MgCO_3$	6	-	-	3.6	-0.90	
T2Shell	Crystalline spheres inside clam shell	Aragonite, $CaCO_3$	80	-		-	-	-	-	-	-	4.37	1.49	Inside blow-out crater/ push corer by ROV/ Nordhoek Pathfinder cruise 2011 / Horizon T2 (6-12 cm bsf)
T2Crys	Crystal vein within sediment fragment	Aragonite, $CaCO_3$	82	Quartz, $Si(O)_2$	11	-	-	-	-	-	-	3.56	-0.916	
T2Bulk	Bulk sediment enclosing sample T2BCrys	-	-	-	-	-	-	-	-	-	-	3.95	-0.52	

The crystalline structure on the surface (BL8Crys) and material from the transition zone (BL8Trans) were composed mainly of brucite (52 and 55 %) and to a lesser extent of calcite (27 and 35 %). Additionally, BL8Crys contained magnesian calcite (17 %). Contrary, bulk sediment (BL8Bulk) from the same sample was dominated by different polymorphs of calcium carbonate. The bulk (BL8Bulk) consisted of vaterite (34 %), calcite (23 %), magnesian calcite (22 %), aragonite (10 %) and brucite (7 %). All BL8 samples showed negative $\delta^{13}C$ values (between -13.4 and -15.6) and negative $\delta^{18}O$ (between -8.9 and -10.5) values. The proportion of heavy isotopes (^{18}O and ^{13}C) was higher at the outside (BL8Crys: $\delta^{18}O$=-10.5, $\delta^{13}C$= -13.6) compared to the inside of the sample (BL8Bulk: $\delta^{18}O$=-8.9, $\delta^{13}C$=-13.4).

The pure crystalline crust from sample BL1Crys was, like BL8Crys and BL8Trans, dominated by brucite (48 %) and aragonite (38 %). Smaller percentages of calcite (7 %) and magnesian calcite (6 %) occurred in this crust as well.

The isotopic composition of sample BL1Crys was considerably different, compared to the other brucite dominated crystalline structures (BL8Crys and BL8Trans). The $\delta^{13}C$ value was slightly negative (-0.90 ‰) and the $\delta^{18}O$ clearly positive (3.60 ‰).

Material from sample BL1Res came from light brown thin layer that was milt off from top of the BL1Crys.

Isotopic analyzes were performed for this sample only. Both $\delta^{13}C$ and $\delta^{18}O$ values were negative (-7.28 and -3.20 ‰ respectively).

The carbonate vein, extracted from horizon T2 (T2Crys), consisted of aragonite mainly (82 %), with a small proportion of quartz (11 %). The values of $\delta^{13}C$ (-0.92 ‰) and $\delta^{18}O$ (3.56 ‰) of this crystalline structure were almost identical with those of BL1 (BL1Crys). The isotopic composition of bulk sediment (T2Bulk) was similar to T2Crys with clearly positive $\delta^{13}C$ (3.95 ‰) and slightly negative $\delta^{18}O$ (-0.52 ‰) values.

The material from the clam shells consisted mainly of aragonite (80 %). The deviation to 100 % is caused by the quantitative portion of 15 % pure Silicon mainly. The silicon originates from the sampling plate used during XRD. The $\delta^{13}C$ and $\delta^{18}O$ values were positive (1.49 and 4.37 ‰). The remaining deviation to 100 % is related to unidentified global amorphous stuff.

4 Discussion

4.1 AOM rates

Evaluation of potential rates

All depth horizons of the blow-out core, incubated at 4, 13 and 20 °C, showed high potential rates of methane-dependent sulphate reduction (between 1.4-3.4 µmol SO_4^{2-} cm^{-3} d^{-1}). Methane dependent sulphate reduction is equivalent to AOM activity. Potential AOM rates were similar to those obtained for established methane habitats in sediments at cold seep sites (Hydrate Ridge: Treude et al. 2003; Haakon Mosby Mud Volcano: Krüger et al. 2005, Gulf of Mexico: Joye et al. 2004) or in the Black Sea (Michaelis et al. 2002; Krüger et al. 2005; Treude et al. 2007; Table 9).

The blow-out site, investigated in this study, is located in a major area of shallow gas (Judd, Hovland 2007). In many areas of the North Sea methane rich fluids seep and gas, rich in methane, vents naturally into the water column (Rehder et al. 1998; Judd, Hovland 2007). AOM rates at the blow-out site were considerably higher than documented previously, at sites with natural methane seepage into shallow waters of the North Sea (Niemann et al. 2005; Wegener et al. 2008a; Table 9).

Table 9: Ranges of AOM rates in different marine environments. Ex-situ rates have been determined at in situ-temperature, but atmospheric pressure. Potential rates represent the maximum AOM capacity of the methane oxidizing community.

Sampling Site	Method	Range of AOM rates (µmol cm^{-3} d^{-1})	Integrated (mml m^{-2} d^{-1})	References
Bacteria mats Black Sea	ex-situ	1000- 10000	-	Treude et al. 2007
Hydrate Ridge, cold seep	ex-situ	200 - 5500	5 - 99	Treude et al. 2003 Boetius et al. 2001
Gulf of Mexico, cold seep	ex situ	100 - 500	1 - 13	Joye et al. 2004
Haakon Mosby, mud volcano	ex-situ	10 - 500	12 - 19	Niemann et al. 2006
Blow-out, North Sea	potential rate (long term, sulphide)	1400- 3400	435	This study
	potential rate (short-term, radiotracer)	600 - 2400	199	
Eckernförde Bay, continental shelf	potential rate	200- 900	-	Treude et al. 2005
	ex-situ	5 - 18	0.9 -1.5	
Methane Seeps, North Sea	potential rate	5 - 90	13	Wegener et al. 2008

Significant production of sulphide and total alkalinity was found in a few incubations without methane only. This is showing that the majority of sulfate reduction, in the investigated core from the blow-out site, is coupled to AOM and not to organoclastic sulphate reduction.

From in-vitro to in-situ

During the in-vitro experiments in this study, microorganisms were provided with excess nutrients, under relatively constant conditions (exceptions are sulphate, sulphide concentrations and total alkalinity). Thus, any inference from in-vitro to in-situ rates is difficult. However, some conclusions about in-situ rates will be discussed in the following.

In the view of relatively constant bottom-water temperatures at the blow-out site (about 7 °C), it can be assumed that in-situ rates are higher than the in-vitro rates measured at 4 °C. Since potential AOM rates doubled in-vitro from 4 to 13 °C. Additionally, dissolved methane concentrations in sediments from the blow-out site are higher than in the in-vitro incubations (Table 1). AOM rates generally increase with increasing methane concentration, if sulphate and other growth factors are available (Nauhaus et al. 2002).
Pore water profiles, from the pore water core show, that sulphate is not a limiting factor in sediments at blow-out site (minimum sulphate concentration at 18 cm bsf: 25 mmol L^{-1}, Figure 11). This theoretical assumption should be verified by in-situ AOM rate measurements using radiotracers.

Temperature dependence of AOM

AOM activity, in sediments from the blow-out site was clearly temperature dependent. The temperature optimum of AOM was between 13 and 20 °C in all horizons, indicating the presence of cold to intermediate temperature adapted microorganisms (psychrophilic to mesophilic). In this study, temperature optimum for AOM was above the relatively constant in-situ temperature at the blow out site (~7 °C). This finding is in accordance with in-vitro studies that showed a temperature optimum of AOM at 5-10 °C above in situ temperature (Krüger et al. 2005).

AOM activity has been reported from hydrothermal vents at water temperatures around 100 °C (Teske et al. 2002). However, no AOM activity was detected in sediment samples from the blow-out crater that were incubated at 60 °C. No AOM activity at 60 °C is indicating

sensitivity of the AOM organisms to higher temperatures. The inhibition of AOM due to increased temperature (60 °C) was not reversible. Neither an increase of sulphide concentration nor of total alkalinity was measured when these samples were incubated at 13 °C, over 46 days.

Sulphide concentrations in controls and samples incubated at 37 °C doubled within 48 days. In contrast, total alkalinity did not increase significantly. Perhaps, elevated temperatures enhanced the precipitation of carbonates. Thereby, bicarbonate is removed from the solutions and masks a potential increase of total alkalinity. On the other hand, it is possible that the increased temperature killed AOM microorganisms in the samples and the slight increase of sulphide was chemical rather than biological origin. The latter hypothesis is underlined by the finding that samples and controls, incubated at 37 °C, showed no activity, if incubated at 13°C.

It is very likely, that elevated temperatures (≥37 °C) cause an irreversible denaturation of proteins in the AOM organisms, including enzymes involved in AOM. This hypothesis could be confirmed in future observations by applying life/dead staining in sub-samples taken from Hungate tubes incubated as described in this thesis.

The minimum temperature for AOM was not in the range of the applied temperature incubations in this study and is below 4 °C.

AOM profile

AOM rates were highest in the deepest horizon (12-18 cm bsf), followed by the incubations of the upper (0-6 cm bsf) and the intermediate horizon (6-12 cm bsf). No clear trend of AOM activity with depth was identified which could be due to the large width of the measured horizons and the resulting poor vertical resolution of AOM rates. Additionally, a core extending 18 cm bsf would presumably show a clearer trend of AOM activity with depth.

Unexpectedly, the first horizon did not show the lowest AOM activity, despite the fact, that up to 1.5 cm of this horizon were oxidized. It is very likely, that some oxygen is transported into the highly permeable (low porosity) sandy sediments, directly via inflowing seawater or indirectly by diffusion from the oxygenated bottom waters. The presence of oxygen inhibits the strictly anaerobic bacteria and archaea, which points to very high AOM rates in the oxygen free part of the horizon between 0 and 5 cm bsf.

Inhibition of AOM

In the third horizon (12-18 cm bsf) sulphate reduction slowed down once reaching sulphide concentrations around 25 mmol L^{-1}, after 61 days. The initial sulphate concentration in the seawater medium was in the range of 28 mmol L^{-1} (Table 11). Taking into account that some sulphide has precipitated as iron sulphide, the inhibition of sulphate reduction in this horizon may be rather caused by depletion of the electron acceptor (sulphate) and not by end product accumulation. At cold seeps no SR activity was found at low sulphate concentrations (2 mmol L^{-1}) and elevated sulphide concentrations (26 mmol L^{-1}) (Treude et al. 2003). In horizons T1 and T2 sulphide production decreased slightly at hydrogen sulphide concentrations of 17 and 15 mmol L^{-1} respectively after 61 days (Appendix, Figure 27). In these horizons sufficient sulphate for AOM was available which leads to the assumption that the organisms are inhibited by the elevated sulphide concentrations.

It is likely that the toxicity of sulphide on sulphate reducing bacteria depends on the pH. The pH determines the chemical speciation of sulphide. At the pH values measured in the Hungate tubes (pH ≈ 8), about 90 % of the sulphide is present as HS^- which is less toxic than the undissociated form of sulphide (H_2S) (O'Flaherty et al. 1998; Moosa, Harrison 2006). In pure cultures of different sulphate reducing bacteria, 50 % growth inhibition was related to total sulphide concentrations (pH=8) between 15 and 44 mmol L^{-1}(O'Flaherty et al. 1998).

AOM, at least in the third horizon, is neither inhibited due to the long incubations time under laboratory conditions (61 days) nor by hydrogen sulphide concentrations of up to 25 mmol L^{-1}.

At 13 °C, AOM rates slowed down at sulphide concentrations between 15 and 25 mmol L^{-1} in all horizons.

Methods to determine potential AOM rates

In the monitoring experiments, the increase of total alkalinity over time was about 1.4 times higher compared to sulphide production. During AOM, the turnover of one methane molecule results in the formation of one molecule hydrogen sulphide and one molecule bicarbonate, causing a subsequent increase of total alkalinity by one unit. Thus, alkalinity and hydrogen sulphide concentrations should increase equally. The deviation from this theoretical assumption may possibly be caused by the precipitation of iron sulfides in the sediments, masking the gross turnover of sulphate.

In contrast, at higher temperatures, bicarbonate could be removed from the system by the precipitation of carbonates, which causes a decrease of total alkalinity by two units, via the turnover of two bicarbonate ions (Equation 7). This assumption is confirmed by the decrease of alkalinity over time in incubations at 60 °C. But also the increase of total alkalinity in the incubations at 4, 13 and 20 °C enhances the precipitation of carbonates which in turn decreases total alkalinity. This mechanism would result in an underestimation of AOM rates determined by measuring total alkalinity over time.

Equation 7

$$Ca^{2+} + 2HCO_3^- \ll=\gg CaCO_3(s) + CO_2 + H_2O$$

Theoretical, electron acceptors other than sulphate, which are energetically more feasible (e.g. nitrate, manganese or iron), may be used during AOM in anoxic sediments (Raghoebarsing et al. 2006; Caldwell et al. 2008). In this case AOM would not increase sulphide concentrations. This as well, would explain the steeper increase of total alkalinity compared to hydrogen sulphide. Nevertheless, sulphate is usually, by far, the dominant electron acceptor and plays quantitatively the most important role in marine sediments. Additionally, the seawater media for sulphate reducing bacteria does not contain any other potential electron acceptors than sulphate. If the strongly reduced slurries would contain electron acceptors such as nitrate, manganese or iron, they would exist in their reduced form only. Therefore these compounds cannot be considered as potential electron acceptors during AOM in the in-vitro experiments.

If the increase in hydrogen sulphide is measured directly, to determine of sulphate reduction rates, precipitation of iron sulphides may mask the gross turnover of sulphate. In opposite, all reduced sulfur species (such as iron sulphide) can be detected by applying radiotracer techniques, using ^{35}S-Sulphate to determine sulphate reduction rates (Kallmeyer et al. 2004). With this method the gross turnover of sulphate is measured.

Additionally, measuring rates of AOM with radiotracer techniques, using ^{14}C-methane, determines the gross turnover of methane. Methane turnover is not influenced by any of the reduced sulfur species that may form during AOM. Applying radiotracers should provide AOM measurements which are not influenced by iron sulphide or carbonate formations.

However, measuring total alkalinity and sulphide concentration over longer time scales has advantages as well. This method provides information about changes of AOM rates over time, which again provides information about the adaption, inhibition or growth of AOM microorganisms.

Rates determined by using radiotracers, monitoring total alkalinity or monitoring hydrogen sulphide were considerably different. At 13 °C, AOM rates determined by radiotracer measurements were lower compared to the rates determined by monitoring sulphide (2.2 times lower) or alkalinity over time (3.3 times lower, Table 3).Radiotracers were injected into the same sediment slurries that were pre-incubated in Hungate tubes, at 13 °C, for 85 days. AOM activity in these sediment slurries was already decreasing (Figure 27). Then seawater media was filled into the Hungate tubes. One week later radiotracer incubations started. Perhaps, some of the microorganisms had died or became inactive (end product inhibition) which would explain the lower AOM rates after 65 days.

Radiotracer measurements confirm two of the results from the in-vitro measurements of total alkalinity and hydrogen sulphide over time. First, most of the sulphate reduction is methane dependent. Second, the patterns of AOM in the horizons are identical, with the highest rates in the deepest horizon T3 (12-18 cm bsf), followed by uppermost horizon T1 (0-6 cm bsf) and the intermediate horizon T2 (6-12 cm bsf).

The blow-out as AOM habitat

Up to 15 cm bsf sulphate is supplied to AOM organisms in sufficient quantities at the blow-out site. Sulphate concentrations measured in the pore water core from the blow-out decreased from 27.4 (0-1 cm bsf) to 25.1 mmol L^{-1} (15 cm bsf) only (P. Linke, unpubl. data, Figure 11). Thus, despite high AOM rates and high sulphate consumption, the sediment is not sulphate depleted. High permeability of the sandy sediment enhances inflow of sulphate rich seawater into the sediment (Treude, Ziebis 2010). Additionally, the convection of sulphate rich seawater associated with gas discharge, may keep sulphate concentrations constant (Treude, Ziebis 2010).

The blow-out represents an El Dorado for AOM organisms. The depth profile in the blow-out sediment does neither resemble profiles at advective systems (cold seeps) nor at diffusive settings (at continental shelves or margins).

Similarly to cold seep habitats, but in contrast to diffusive settings in “normal” sediments, AOM is not limited by methane at the blow-out. Additionally, sulphate is supplied to the microorganisms over a zone that most likely expands beyond the sampling depth of 18 cm bsf. At this point, the geochemical settings at the blow-out differ from conditions at most cold seeps. Compared to the blow-out, AOM at cold seeps are often confined to a narrower zone, close to the sediment-water interface due to the upward flow of sulphate depleted fluids (Treude et al. 2003; de Beer et al. 2006). Additionally, sediments at cold seeps are often fine-grained and muddy (Treude et al. 2003; Joye et al. 2004; Niemann et al. 2006) which hampers the replenishment of sulphate.

It is likely, that methane and sulphate are supplied to anaerobic methanotrophs below the sampling depth of 18 cm bsf. And thus the AOM zone extends beyond 18 cm bsf in the sediment. For this reason, integrated potential AOM rates per square meter (Table 4) are presumably underestimated. Therefore, subjacent zones should be included in future investigations.

AOM organisms can metabolize methane in its dissolved form only. It was demonstrated during in vitro experiments that AOM rates increase with increasing dissolved methane concentrations (Nauhaus et al. 2002). In future experimental designs, incubations with identical dissolved methane concentration would be appropriate.
Regardless of temperature, the partial pressure of methane was equal in all incubations (1.1 atm). The solubility of methane in seawater is affected by temperature. Therefore, concentrations of dissolved methane in the incubations vary with different temperatures at constant partial pressure of methane in the samples (Table 1).

The reference core

Neither methane dependent nor organoclastic sulphate reduction was detected in sediments of the reference core.
However, the blow-out formed a 20 m deep crater. Thereby sediment layers got uncovered which had laid 20 m below the seafloor before. The blow-out core was taken within in this crater (section 2.1), about 20 m deeper below the sediment surface, compared to the reference core. It is therefore questionable if the reference core, that was taken 50 m away from the blow-out, is an appropriate reference core.

Perhaps, the blow-out event uncovered an AOM layer in 20 m depth which was already established due to methane seepage or diffusion into this zone. Therefore, a reference core with a length of at least 20 m, taken at a site not influenced by the blow-out event, would be more informative to find out whether or not the existing AOM community has evolved within 20 years in the blow-out crater. Nevertheless, it is questionable whether the sulphate supply 20 m bsf is sufficient to fuel AOM.

Measurements of methane concentrations in a pore water core from the reference site are underway. If methane is available at the reference site, possibly aerobic oxidation of methane takes place instead of AOM. But aerobic oxidation of methane cannot be detected by the applied methods. These analyzes can be carried out in future studies.

4.2 Microbial community analyzes

4.2.1 CARD-FISH: discussing the methodology

No results were obtained from CARD-FISH analyzes, despite of using standard CARD-FISH protocols, adjusted to marine sediments (modified from Pernthaler et al. 2002; Ishii et al. 2004) and a number of trials and approaches to adapt this method specifically to sediments from the blow-out site (Table 6). Finally, trial runs had to be stopped due to financial and time constrains. The various approaches that have been tested, narrow the causes of failure down to a few factors. They are: probes do not enter the cells or probes do not bind to the rRNA. Human failures cannot be excluded as well.

It is unlikely, that the type of sediment at blow-out was responsible for the failure since CARD-FISH protocols have already been conducted in samples from sandy sediments (Ishii et al. 2004).

The modification of the CARD-FISH method to sediments from the blow-out was done using probes that stain almost all types of eubacteria, except of some phyla, such as Planctomycetales and Verrucomicrobia (Amann et al. 1990). Sediments usually contain a large number of different eubacteria phyla, also at methane rich sites (Knittel et al. 2003). Therefore, cells which were targeted by the probes were most likely present in the blow-out sediment.

It can be excluded that chemicals were prepared wrong, since other scientists used the same chemicals during –successful- analyzes using the CARD-FISH method.

It was tried to reduce the chance of human failure by several ways. Firstly, other students, who already conducted CARD-FISH successfully, analyzed filters from the blow-out as well, in vain. Secondly, intended approaches and outcomes of CARD-FISH analyzes were discussed with other scientists and lab technicians. Thirdly, CARD-FISH was successfully applied by the author, in sediment samples from Eckernförde Bay. However, the latter trail run was done during an early stage of the establishment process using a probe for *Desulfovibrio* spp. (DSV probe 698; Manz et al. 1998).
Regardless of these efforts, it cannot be ruled out that errors occurred during the various establishment approaches and comprising CARD-FISH steps. Filters were not prepared in replicates. Therefore, the probability is higher to miss a successful functioning combination of the CARD-FISH steps due to human failure

Based on the unsuccessful trial runs with pure cultures of *Desulfovibrio marinus* it seemed most likely that the probes were spoiled. But applying additional probes, provided by the Max-Planck Institute for Marine Microbiology, did not show CARD-FISH signals either. In the next step, filters with cells from the pure culture of *Desulfovibrio marinus* should be analyzed using the EUB338 and the DSV698 probe (which is successfully applied in the laboratory at the moment). Comparing the outcomes should finally clarify if the problem is related to the applied EUB338 probe.

The permeabilization step was not modified during the establishment process, since the permeabilization of cells, using lysozyme, is well established for most bacterial cells. Applying lysozyme for permeabilization and the EUB338 probe during hybridization, resulted in detection rates between 51-100 % (mean: 83 %) of bacterial cells in sediments from the Wadden Sea (Pernthaler et al. 2002). Nevertheless, it has been recommended to adapt the permeabilization protocol to individual samples (Pernthaler et al. 2004). This approach could be pursued in the future.

Several steps helped to decrease the background fluorescent signal (Table 6). However, until the end of the CARD-FISH trials, background fluorescence from sand grains was visible. Therefore, it was throughout the experiments difficult to distinguish between stained cells and fluorescent particles. In future approaches, diluted samples (≈20 µL) could be pipetted directly on a glass slide into a circlet, drawn with a grease pencil. Then samples get imbedded in agarose, before continuing with the CARD-FISH method. This procedure may result in an additional reduction of background fluorescence (K. Knittel, pers. comm.).

In the next step, it is recommended to perform CARD-FISH trial runs with filters of pure cultures of *Desulfovibrio marinus* and with filters of sediments from the blow-out site inoculated with *Desulfovibrio marinus* cells using EUB338 and DSV698 probes. These trial runs should be carried out by another scientist or technician. Using this approach allows the elimination of several reasons for the unsuccessful CARD-FISH analyzes: scientists mistake, spoiled EUB338 probes and problems specifically related to blow-out sediment.

4.2.2 DAPI staining

The density of aggregates, which resemble AOM consortia, at the blow-out site was similar to established methane habitats at cold seep ecosystems and at natural gas seeps in the North Sea (Table 10).

The cell density mirrors the pattern of AOM activity in the three horizons. Highest cell density overlaps with highest AOM rate in the deepest horizon, T3 (12-18 cm bsf). In horizon T3, mean AOM rates (at 4, 13 and 20 °C) were on average about 1.3 times higher and cell density about 1.4 times compared to the first horizon. Lowest cell densities and AOM rates were found in the intermediate horizon, T2, (6-12 cm bsf). In this horizon, AOM rates were on average 1.9 times (at 4, 13 and 20 °C) and the cell density 2.9 times lower compared to the deepest horizon, T3, with the highest AOM activity.

As reported from other methane habitats, AOM organisms (i.e. cells organized in aggregates) clearly dominate microbial biomass in the sediment (Boetius et al. 2000; Knittel et al. 2003; Loesekann et al. 2007; Table 10).

Total cell numbers, in sediments from the blow-out crater, are one order of magnitude higher compared to sediments from the reference site (Table 10) and higher than total cell counts from intertidal sandy sediments in the North Sea without methane seepage (Llobet-

Brossa et al. 1998; Wieringa et al. 2000; Rusch et al. 2001). Differences in total cell numbers between reference and blow-out site are mainly caused by the large numbers of cells which are organized in aggregates at the blow-out site (Table 7). Higher microbial biomass in sediments with methane seepage, compared to sediments with no methane availability, has been documented from other sites before (Knittel et al. 2003; Wegener et al. 2008a).

Maximum aggregate density at the blow-out site was about fifteen times lower compared to the cold seep system at Hydrate Ridge (Treude et al. 2003). However, integrated aggregate density was three times lower only. This fact is attributed to the broad AOM zone in the blow-out sediments.

It is very likely, that the AOM zone extends beyond the sampling depth (18 cm bsf), because sulphate was not depleted and as methane is still available 18 cm bsf (Figure 11). Hence, in contrast to most other studies, the AOM zone was not fully analyzed during this study. Covering the whole AOM zone would result in higher integrated aggregate densities.

The average diameter of all consortia from the three depth horizons was 3.4 µm (min = 1 µm / max: 8 µm). Consortia with a considerably larger diameter have been found at Haakon Mosby mud volcano (50 µm, Loesekann et al. 2007) and at cold seeps in the Gulf of Mexico (25 µm, Orcutt et al. 2005).

AOM consortia with similar size distributions are reported from other, established methane habitats. The average diameter of consortia from Hydrate Ridge ranged, among different sampling sites, between 3.1 and 4.2 µm with maximum diameters between 10-12 µm (Knittel et al. 2003). The maximum diameter of AOM aggregates, at Tommeliten and Gullfaks methane seeps in the North Sea, was 10 µm (Wegener et al. 2008b).

The age of the AOM community at the blow-out site can be roughly estimated. Supposing doubling times for ANME between 4 and 7 months, (Nauhaus et al. 2007) and supposing in total $5.8*10^{15}$ AOM cells within sediments of the crater. The total number of AOM cells in the crater was calculated using a cell density of $2.5*10^{12}$ AOM cells m^{-2} (integrated over 18 cm bsf, Table 10) and a crater area of 72 m^2 (equals a crater radius of 5 m, Figure 9). The resulting ages of the AOM community range between 17 and 30 years using doubling times

of 4 and 7 months respectively (neglecting cell death, competition etc.). The calculated time span matches with the actual blow-out date in 1991.

The total AOM cell number in the crater is a very rough estimate. However, because of the characteristics of exponential growth, calculating the age of the consortia by using the AOM cell density of one square meter ($2.5*10^{12}$ AOM cells m^{-2}, Table 10) makes minor differences only. This calculation gives ages of the AOM community between 14 and 24 years, using doubling times of 4 and 7 months respectively.

This finding does not challenge the modeled, 70 year long lasting adaption of AOM communities to an onset of methane rich fluid flow (Dale et al. 2008). The scenario underlying this model is considerably different to the situation at the blow-out site. In the model simulations the AOM zone migrates upward due to the onset of slow fluid flow from deeper sediment layers. After 12 years, the methane rich fluid reaches the surface. After additional 13 years the AOM zone has established, from now on the model predicts a log growth phase. The fact that a highly active AOM community has established at the blow-out site within 21 years does not contradict the AOM model of Dale et. al. (2008). It is in agreement with the model, provided that methane and sulphate were constantly and sufficiently available over the past 21 years, i.e. that an AOM zone could establish soon after the blow-out event. A steady SMTZ zone throughout the crater, would offer ideal conditions for ANME and their syntrophic partners, which could result in a log growth phase.

The blow-out sediment represents a very dynamic methane habitat due to the very intense gas discharge. Therefore, it is difficult to reconstruct the establishment of today's AOM community at the blow-out site. The conditions at the blow-out site were, perhaps, inhospitable over years (for example due to sediment erosions) until the gas release diminished (Rehder et al. 1998) and the AOM community has established faster than expected. These assumptions are highly speculative and cannot be proved with the available information.

AOM consortia have distinct appearance which allows their quantification using unspecific DAPI staining (Boetius et al. 2000). However, ANME-1 and 3 cells may occur organized in consortia and as single cells. Additionally, preparation of filters (such as fixation or

sonication) may disrupt the cell aggregates into clusters of single cell. These single cells would not be counted as AOM organisms. Therefore, it is necessary to get the CARD-FISH method going for the blow-out sediments.

Table 10: Total cell counts and aggregate density at seeping and non-seeping marine habitats.

Side	Range Total cell number (cells cm^{-3})	Cells in aggregates (%)	Max aggregate density (aggregates cm^{-3})	Integrated aggregate density (aggregates m^{-2})	Reference
Blow-out, North Sea	23 - 68*10^8	85-93	2.2 *10^7	2.5*10^{12}	This study
Hydrate Ridge, cold seep	[x]50-960*10^8	[†x]79-94	31*10^7	7.9*10^{12}	[†]Boetius et al.2000 Treude et al. 2003 [x]Knittel et al. 2003
Eckernförde Bay, continental shelf	1.8*10^8	21-28	0.1x10^7	-	Treude et al. 2005
Haakon Mosby, mud volcano	2-102*10^8	[†]3-94	2.0*10^7	-	Niemann et al. 2006 [†]Lösekann et al. 2007
Methane seeps, North Sea	30-79*10^8	-	1.5*10^7	-	Wegener et al. 2008
Non seeping/ sandy sediments, North Sea	2-30*10^8	0	0	0	Llobet-Brossa et al. 1998 Wieringa et al. 2000 Rusch et al. 2001

4.3 Stable isotope composition of carbonates

No indications for a recent formation of methane derived carbonates were found in the isotope compositions ($\delta^{13}C$ and $\delta^{18}O$) of crystalline structures, extracted from material at the blow-out site. Numerical models have shown that carbonate layers of 1-2 cm may form, at high AOM rates (2270 µmol cm^{-2} y^{-1}), within 110 years (Luff et al. 2004). In vitro AOM rates at the blow-out ranged from 7810 to 15911 µmol cm^{-2} y^{-1} (at 4 and 13 °C respectively, determined by measuring sulphide over time). Considering these high AOM rates, formation of methane derived authigenic carbonate (MDAC) within 20 years is feasible, if AOM rates were constant over this time period. For this reason, material from the blow-out crater was microscopically inspected for the formation of carbonate crusts. Material resembling carbonate structures was further analyzed for its isotopic composition ($\delta^{13}C$ and $\delta^{18}O$) and mineralogy (XRD).

In general, methane derived authigenic carbonates (MDAC) have a wide range of mineralogical and isotopic compositions (Ritger et al. 1987; Bohrmann et al. 1998; Orphan et al. 2004; Judd, Hovland 2007 and Naehr et al. 2007). Aragonite, dolomite, magnesian calcite but also rare minerals like ikaite and glendonite have been related to AOM (Ritger et al. 1987; Greinert, Derkachev 2004).

In some samples from the blow-out aragonite and magnesian calcite were found. However, none of the analyzed samples showed isotopic signals that are indicative ($\delta^{13}C \leq -20$) for methane derived authigenic carbonates (Nelson, Smith 1996; Naehr et al. 2007). The theoretical $\delta^{13}C$ value of MDAC, at the blow-out, can be calculated by considering the $\delta^{13}C$ of the emitted methane ($\delta^{13}C = -70$), the isotopic fractionation during AOM (mean $10^3 \ln\alpha$ CH_4-CO_2 = between -2 and -14, Whiticar, Faber 1986; Alperin et al. 1988) and the isotopic fractionation during carbonate precipitation ($10^3 \ln\alpha$ CO_2-CH_4 = 11.6 at 7°C for calcite, Deines et al. 1974). Considering these parameters, the $\delta^{13}C$ values of calcite values would theoretically range between -60 and -74.

It is difficult to interpret the outcome of the isotope analyzes in this study. The $\delta^{18}O$ value comprises the isotope composition of all minerals in one sample (brucite, quartz and all kinds of carbonate minerals) since all these minerals contain oxygen. On the other hand, the $\delta^{13}C$ value summarizes the isotope composition of minerals that contain carbon only (in this study: the carbonate minerals). Keeping this information in mind, in the following, it is assumed that the $\delta^{18}O$ are valid for the carbonate structures.

In general, the isotopic signature of pure MDAC always shows negative $\delta^{13}C$ values, which range between -20 and -60 ‰ (Figure 5). The samples from residuals of block 1 (BL1res), and all samples from block 8 (BL8), which were taken with the ROV JAGO, inside the blow-out crater, clearly show negative $\delta^{13}C$ values (-7.3 to -17.6 ‰). This could indicate that minerals were, at least partly, derived from microbial oxidation of methane or sulphate reduction (Nelson, Smith 1996).

However, $\delta^{18}O$ values of MDAC should show positive values if they form in equilibrium under present-day (interglacial to glacial) conditions in bottom waters (e. g. Hovland et al. 1987; Bohrmann et al. 1998; Naehr et al. 2007). The depletion of ^{18}O isotopes in the analyzed samples clearly contradicts this assumption. Such low $\delta^{18}O$ values could be explained by the influence of meteoric water, high temperature during carbonate formation or carbonate diagenesis only (Sass et al. 1991; Nelson, Smith 1996). Meteoric water does not seep through sediments at the blow-out site, as indicated by the pore water profiles of chloride (P. Linke, unpubl. data, Figure 11). All other mechanisms that would explain strongly negative $\delta^{18}O$ exceed time scales of 20 years clearly.

The sediment layers 20 m bsf are about 40,000 years old, assuming constant sedimentation rates of 0.5 mm y^{-1} (de Haas et al. 1997). Other radiocarbon dating's from sediment cores in the central North Sea (Fladen Area, 122 m water depth and north of the Witch Ground basin, 150 m water depth) date sediments in 20 m depth back to 25,000 and 30,000 years (Sejrup et al. 1987b; Graham et al. 2010). This time period matches with the last glacial maximum (Peltier, Fairbanks 2006) when large parts of the North Sea were covered by an enormous ice sheet. During the last glacial maximum, parts of the central North Sea were dry or became dry when the ice masses receded (Sejrup et al. 1987a). Hence, sediments from the blow-out site were possibly influenced by meteoric waters during that or earlier glaciations which could partly explain the negative $\delta^{18}O$ values (Land 1989).
Calcite layers in Jurassic and Lower Cretaceous reservoir rocks sampled offshore Norway show isotopic compositions that resemble the one of BL8 (Saigal, Björlykke 1987). However, these calcite layers are located 1600 m bsf and have formed at elevated temperatures between 50-60 °C (Saigal, Björlykke 1987).

Additionally, crystalline structures of samples BL8Crys and BL1Crys were both dominated by brucite ($Mg(OH)_2$). Brucite does not contain carbon that could potentially derive from methane. This mineral is a product of geological processes like alteration of periclase (a metamorphic rock), contact metamorphism (Keith 1946) but is involved in the formation of chimneys at venting systems also (Martin, Russell 2007). The geological settings, which would allow brucite formation, occurred or would extend not only 20 but also 40,000 years. The origin of brucite cannot be settled with the available data.

All other samples show positive or slightly negative $\delta^{13}C$ values that clearly argue against MDAC.

The upward stream of gas or fluids is possibly too strong to allow the precipitation of carbonate minerals in sediments at the blow-out (Luff et al. 2004). At high fluid flow bicarbonate is transported through the sediment surface and into the water column which slows down the accumulation of bicarbonate. Additionally, the porous sediments and the associated exchange between pore and sea water may diminish authigenic carbonate formation due to bicarbonate removal. This is underlined by low total alkalinity in the pore

water core (0-15 cm bsf) which was sampled at the blow-out site (P.Linke, unpubl. data; Figure 11). At cold seeps total alkalinity can be up to one order of magnitude higher due to high AOM activity (Luff, Wallmann 2003; Boetius et al. 2009).

Perhaps, MDAC have already formed at the blow-out site in limited extent as thin layers or as dispersed carbonates within the sediment. Detecting and extracting such carbonate formations from sediments are difficult. In this study material sampled with a ROV and material extracted from the slurries was analyzed for carbonate formation. Dispersed carbonates were not detected in the slurries, maybe due to their small size. It would not be possible to extract very thin MDAC layers on the surface of the samples since the hand held rotary tool equipped with a diamond wheel would not allow this. Of course, extracting MDAC with a low purity would influence the results of the stable isotope analyzes. However, the visual observation of the samples under the light microscope did not reveal any heterogeneity of the extracted crystalline structures.

4.4 Conclusion & Outlook

Conclusion

The blow-out site is a dynamic and relatively young AOM habitat at the seafloor of the North Sea. Its date of origin is known due to the human cause of formation. Therefore, the blow-out represents a unique natural laboratory to study the adaption of AOM communities in a newly formed methane-seep.

Sediments in the blow-out crater harbor an extremely active AOM community. High methane turnover suggests that AOM communities are able to adapt, to a sudden onset of intense methane influx, at least within 20 years. At the blow-out site, AOM rates were in similar ranges, compared to established methane habitats, such as cold seep systems. Integrated potential AOM rates and AOM aggregate densities were among the highest ever observed, also due to a broad AOM zone. This is even more astonishing, considering that the AOM zone was, most likely, not fully covered by the 18 cm long push-core, which was analyzed in this study. Hence, a wider AOM zone and consequently even higher integrated AOM rates and AOM aggregated are assumed.

Structures, resembling carbonate minerals, were extracted from sediment samples originating from the blow-out site. Stable isotope analyzes of these structures showed no

indications for recent formation of methane derived authigenic carbonates. Most likely, intense gas flow flushes bicarbonate out of the porous, sandy sediments. Thereby, total alkalinity cannot increase and methane derived carbonate formation is hampered. This situation is in contrast to observations from other methane habitats, with less intense gas discharge, where formation of methane derived carbonates is a widespread phenomenon.

Specific staining of AOM cells using the CARD-FISH method was not successful, despite extensive efforts. AOM aggregates have been quantified solely, depending on their distinctive morphology, using non-specific fluorescence staining (DAPI). Therefore, AOM aggregate densities determined in this study should be perceived with caution.

Model simulations predict, that a steady state AOM biomass establishes within 60 years in response to an onset of methane influx (Dale et al. 2008). The existence of a highly active AOM community at the blow-out site is not necessarily in conflict with this estimate. Assuming a constant SMTZ at the blow-out site which would allow exponential growth since 20 years (Dale et al. 2008) and calculating AOM biomass using doubling times of ANME cells between 4 and 7 months (Nauhaus et al. 2007).

No AOM activity was detected in the reference core, leading to the assumption that the AOM community established at the blow-out site within 20 years. This conclusion should be drawn with care. Since the blow-out created a 20 m deep crater in the seabed, the blow-out core was sampled in sediment layers 20 m below the reference sediments. AOM organisms may be abundant 20 m bsf at the reference site as well. AOM in these depths may get fuelled by seeping methane from shallow gas reservoirs. Sulphate may be supplied by seawater which diffuses or convects through the permeable sandy sediments. Thus, the blow-out event may have uncovered an AOM zone which was already established before the blow-out took place. However, it is relatively unlikely that the depth of sulphate penetration reaches 20 m bsf in shallow, continental shelf sediments (Jørgensen et al. 1990).

At the moment, it is difficult to predict at what rate, time scale and extent methane clathrates in sediments will destabilize (Brook et al. 2008). In any case, a steady state AOM community could significantly reduce the methane emissions from melting gas hydrates. The

present study gives first indications that such AOM communities may establish within 20 years. Hence, the adaption time of AOM communities in response to an onset of methane discharge is relatively fast, at sites with sufficient sulphate supply. During ongoing releases of large volumes of methane, integrated rates of methane consumption by AOM are important, and limited by the supply of sulphate. At the blow-out site, the biological filter has a huge capacity to capture methane, due to a broad sulphate methane transition zone. If methane hydrates melt at other, less dynamic sites, with fine grained sediments, the situation could be different. In this case, high AOM rates would cause a depletion of sulphate, within the upper few centimeters below the seafloor. Hence, on longer time scales, rather sulphate supply than the adaption time of AOM communities would limit AOM to capture methane.

The studied blow-out site teaches, that AOM communities which may decrease methane efflux from sediments substantially, can establish within 20 years, at in-situ conditions. The question, whether or not, the AOM community has established within the last 20 years, cannot be answered finally. To gain certainness, it is necessary to analyze the sediment layers at reference sites 20 m bsf. It needs to be analyzed whether or not AOM activity is there as well.

Future issues

The present study raises more questions than it can answer. Probably, the most important future task is to find out, whether or not active AOM zones have established 20 m bsf at reference sites. This could clarify if the AOM community at the blow-out is older than 20 years. Detecting an active AOM zone 20 m below the seafloor would raise the question if AOM microorganisms exist, in this depth, in other areas of the North Sea as well. No AOM in this depth, would indicate, that the studied AOM community at the blow-out has established in sediments within the last 21 years. Of course, standard pore water parameters (such as methane, sulphate, sulphide, total alkalinity) should be measured in the “extended” 20 m long reference core, as well.

An additional task for future expeditions would be, to sample deeper sediment layers at the blow-out site as well. In contrast to most other studies, not the whole AOM zone was covered, by the 18 cm long push cores, which were analyzed in this study. It has to be kept in mind also, that the blow-out crater is a very heterogeneous environment due to the high

rates of gas discharge. AOM activity and its depth zonation are very likely subject to high spatial variation.

In addition to potential AOM rates, it's necessary to measure the ex-situ rates in a vertical resolution exceeding 5 cm horizons (1 cm intervals). Potential rates are the maximum AOM capacity of the AOM community at the blow-out site, measured under laboratory conditions. Ex situ rates are measured in undisturbed whole cores but at atmospheric pressure. Ex-situ rates are closer to the "real" situation in the sediments. A higher vertical resolution is necessary to shade light on depth zonation of AOM.

Furthermore, the search for methane derived carbonates should be intensified. Perhaps, carbonates have formed at AOM sites with lower gas discharge within the blow-out crater. A less dynamic site, would possibly allow an increase of total alkalinity which may result in authigenic carbonate formation. At such sites, samples should be retrieved and analyzed for carbonate formation. If methane derived carbonates are found, Uranium-Thorium dating should be applied to date these carbonates and hence the age of the AOM community.

It is inevitable to study the microbial community at the blow-out site using CARD-FISH to obtain reliable information about the density of AOM cells at the blow-out site.

On a broader perspective, it would be interesting to see how the results of this study can be extrapolated to other sites. It is mandatory to find out in what way methane will be emitted from melting methane hydrates due to global warming. This information is necessary to estimate AOM potential to prevent methane releases from sediments to the water column and atmosphere.

5 References

Internet:

URL 1: http://en.wikipedia.org/wiki/Methane, **01.08.2012**
URL 2: http://www.ipcc.ch/pdf/assessment-report/ar4/wg1/ar4-wg1-chapter2.pdf, **22.07.2012**
URL 3: http://xa.yimg.com/kq/groups/24627084/638885252/name/Brochure_Leica_Fluorescence_eng.pdf, **02.08.2012**
URL 4: http://www.geomar.de/de/forschen/fb2/fb2-mg/benthische-biogeochemie/geobiochemische-analytik/alkalinitaet, **20.10.2012**
URL 5: http://www.handbookofmineralogy.org/, **07.09.2012**

Literature:

Aloisi, Giovanni; Bouloubassi, Ioanna; Heijs, Sander K.; Pancost, Richard D.; Pierre, Catherine; Sinninghe Damsté, Jaap S. et al. (2002): CH4-consuming microorganisms and the formation of carbonate crusts at cold seeps. In *Earth and Planetary Science Letters* 203 (1), pp. 195–203.

Alperin, M. J.; Reeburgh, W. S.; Whiticar, M. J. (1988): Carbon and hydrogen isotope fractionation resulting from anaerobic methane oxidation. In *Global Biogeochem. Cycles* 2 (3), p. 279.

Amann, R. I.; Binder, B. J.; Olson, R. J.; Chrisholm, S. W.; Devereux, R.; Stahl, D. A. (1990): Combination of 16S Ribosomal-RNA-Targeted Oligonucleotide Probes With Flow-Cytometry for Analyzing mixed microbial-populations. In *Applied and Environmental Microbiology* 56 (6), pp. 1919–1925.

Amann, R. I.; Ludwig, W.; Schleifer, K. H. (1995): Phylogenetic identification and in situ detection of individual microbial cells without cultivation. In *Microbiol. Rev* 59 (1), pp. 143–169.

Beer, D. de; Sauter, E.; Niemann, H.; Kaul, N.; Foucher, J. P.; Witte, U. et al. (2006): In situ fluxes and zonation of microbial activity in surface sediments of the Hakon Mosby Mud Volcano. In *Limnology and Oceanography* 51 (3), pp. 1315–1331.

Biastoch, A.; Treude, T.; Rüpke, L. H.; Riebesell, U.; Roth, C.; Burwicz, E. B. et al. (2011): Rising Arctic Ocean temperatures cause gas hydrate destabilization and ocean acidification. In *Geophysical Research Letters* 38.

Bobrow, M. N.; Harris, T. D.; Shaughnessy, K. J.; Litt, G. J. (1989): Catalyzed reporter deposition, a novel method of signal amplification. Application to immunoassays. In *J. Immunol. Methods* 125 (1-2), pp. 279–285.

Boetius, Antje; Holler, Thomas; Knittel, Katrin; Felden, Janine; Wenzhöfer, Frank (2009): The Seabed as Natural Laboratory: Lessons From Uncultivated Methanotrophs. In Slava S. Epstein (Ed.): Microbiology Monographs. Berlin, Heidelberg: Springer Berlin Heidelberg, pp. 59–82.

Boetius, Antje; Ravenschlag, Katrin; Schubert, Carsten J.; Rickert, Dirk; Widdel, Friedrich; Gieseke, Armin et al. (2000): A marine microbial consortium apparently mediating anaerobic oxidation of methane. In *Nature* 407 (6804), pp. 623–626.

Boetius, Antje; Suess, Erwin (2004): Hydrate Ridge: a natural laboratory for the study of microbial life fueled by methane from near-surface gas hydrates. In *Chemical Geology* 205 (3-4), pp. 291–310.

Bohrmann, Gerhard; Greinert, Jens; Suess, Erwin; Torres, Marta (1998): Authigenic carbonates from the Cascadia subduction zone and their relation to gas hydrate stability. In *Geol* 26 (7), p. 647.

Brook, E.; Archer, D.; Dlugokencky, E.; Frolking, S.; Lawrence, D. (2008): Chapter 5: Potential for abrupt changes in atmospheric methane. In : Abrupt Climate Change. A report by the U.S. Climate Change Science Program; U.S. Geological Survey: Reston, vol. 2008, pp. 163–201.

Buffett, Bruce A. (2000): Clathrate Hydrates. In *Annu. Rev. Earth Planet. Sci* 28 (1), pp. 477–507.

Buffett, Bruce; Archer, David (2004): Global inventory of methane clathrate: sensitivity to changes in the deep ocean. In *Earth and Planetary Science Letters* 227 (3-4), pp. 185–199.

Bussmann, I.; Dando, P. R.; Niven, S. J.; Suess, E. (1999): Groundwater seepage in the marine environment:role for mass flux and bacterial activity. In *Mar. Ecol. Prog. Ser* 178, pp. 169–177.

Caldwell, Sara L.; Laidler, James R.; Brewer, Elizabeth A.; Eberly, Jed O.; Sandborgh, Sean C.; Colwell, Frederick S. (2008): Anaerobic Oxidation of Methane: Mechanisms, Bioenergetics, and the Ecology of Associated Microorganisms. In *Environ. Sci. Technol* 42 (18), pp. 6791–6799.

Cord-Ruwisch, R. (1985): A quick method for the determination of dissolved and precipitated sulfides in cultures of sulfate-reducing bacteria. In *J Microbiol Methods* (4), pp. 33–36.

Dale, A.W; van Cappellen, P.; Aguilera, D.R; Regnier, P. (2008): Methane efflux from marine sediments in passive and active margins: Estimations from bioenergetic reaction–transport simulations. In *Earth and Planetary Science Letters* 265 (3-4), pp. 329–344.

Deines, Peter; Langmuir, Donald; Harmon, Russell S. (1974): Stable carbon isotope ratios and the existence of a gas phase in the evolution of carbonate ground waters. In *Geochimica et Cosmochimica Acta* 38 (7), pp. 1147–1164.

Devereux, R.; Kane, M. D.; Winfrey, J.; Stahl, D. A. (1992): Genus-specific and group-specific hybridization probes for determinative and environmental studies of sulfate reducing bacteria. In *Systematic and applied microbiology* 15 (4), pp. 601–609.

Dickens, G. R.; Snyder, G. T. (2009): Interpreting upward methane flux from marine pore water profiles. In *Fire in the Ice* 9, pp. 7–10. Available online at http://www.owlnet.rice.edu/~gjh/Hydrate/Publications/MHNewswinter09.pdf.

Dickens, Gerald R.; O'Neil, James R.; Rea, David K.; Owen, Robert M. (1995): Dissociation of oceanic methane hydrate as a cause of the carbon isotope excursion at the end of the Paleocene. In *Paleoceanography* 10 (6), p. 965.

Fossing, Henrik; Jorgensen, BoBarker (1989): Measurement of bacterial sulfate reduction in sediments: Evaluation of a single-step chromium reduction method. In *Biogeochemistry* 8 (3).

Graham, Alastair G. C.; Lonegran, Lidia; Stoke, Martyn; S. (2010): Depositional environments and chronology of Late Weichselian glaciation and deglaciation in the central North Sea. In *Boreas*.

Greinert, J.; Derkachev, A. (2004): Glendonites and methane-derived Mg-calcites in the Sea of Okhotsk, Eastern Siberia: implications of a venting-related ikaite/glendonite formation. In *Marine Geology* 204 (1-2), pp. 129–144.

Haas, Henk de; Boer, Wim; van Weering, Tjeerd C.E (1997): Recent sedimentation and organic carbon burial in a shelf sea: the North Sea. In *Marine Geology* 144 (1-3), pp. 131–146.

Henrichs, S. M.; Reeburgh, W. S. (1987): Anaerobic mineralization of marine sediment organic matter – rates and the role of anaerobic processes in the oceanic carbon economy. In *Geomicrobiology Journal* (3-4), pp. 191–237.

Hovland, M.; Talbot; Qvale, H.; Olaussen, S.; Aasberg, L. (1987): Methane related carbonate cements in pockmarks of the North Sea. In *Journal of Sedimentary Petrology* 57 (5), pp. 881–892.

Hungate, R. E. (1950): The anaerobic mesophilic cellulolytic bacteria. In *Bacteriological Review* 14, pp. 0–49.

Ishii, Kousuke; Mußmann, Marc; MacGregor, Barbara J; Amann, Rudolf (2004): An improved fluorescence in situ hybridization protocol for the identification of bacteria and archaea in marine sediments. In *FEMS Microbiology Ecology* (50), pp. 203–212.

Ivanenkov, V.N; Lyakhin, Y. (1978): Determination of total alkalinity in seawaer. In : Methods of hydrochemical investigations in the oceans, pp. 110–114.

Iversen, N.; Blackburn, T.H (1981): Seasonal Rates of Methane Oxidation in Anoxic Marine Sediments. In *Applied and Environmental Microbiology* 41 (6), pp. 1295–1300.

Iversen, N.; Jorgensen, B. B. (1985): Anaerobic methane oxidation rates at the sulfate methane transition in marine sediments from Kattegat and Skagerrak (Denmark). In *Limnology and Oceanography* 30 (5), pp. 944–955.

Jørgensen, B. B. (1978): A comparison of methods for the quantification of bacterial sulfate reduction in coastal marine sediments. In *Geomicrobiology Journal* 1 (1), pp. 11–27.

Jørgensen, B. B.; Bang, M.; Blackburn, T. H. (1990): Anaerobic mineralization in marine sediments from the Baltic Sea-North Sea transition. In *Mar. Ecol. Prog. Ser* 59, pp. 39–54.

Jørgensen, B. B.; Fenchel, T. (1974): The sulfur cycle of a marine sediment model system. In *Mar. Biol* 24 (3), pp. 189–201.

Jørgensen, Bo Barker (1982): Mineralization of organic matter in the sea bed—the role of sulphate reduction. In *Nature* 296 (5858), pp. 643–645.

Joye, Samantha B.; Boetius, Antje; Orcutt, Beth N.; Montoya, Joseph P.; Schulz, Heide N.; Erickson, Matthew J.; Lugo, Samantha K. (2004): The anaerobic oxidation of methane and sulfate reduction in sediments from Gulf of Mexico cold seeps. In *Chemical Geology* 205 (3-4), pp. 219–238.

Judd, A. G.; Hovland, M. (2007): Seabed fluid flow. The impact on geology, biology and the marine environment. Cambridge: Cambridge University Press.

Kallmeyer, J.; Ferdelman, T. G.; Weber, A.; Fossing, H.; Jorgensen, B. B. (2004): Evaluation of a cold chromium distillation procedure for recovering very small amounts of radiolabeled sulfide related to sulfate reduction measurements. In *Limnol. Oceangr. Methods* 2, pp. 171–180.

Keith, M. L. (1946): Brucite deposits in the Rutherglen District, Ontairo. In *Geol Soc America Bull* 57 (10), p. 967.

Kennett, J. P.; Stott, L. D. (1991): Abrupt deep-sea warming, palaeoceanographic changes and benthic extinctions at the end of the Palaeocene. In *Nature* 353 (6341), pp. 225–229.

Klauda, J. B.; Sandler, S. I. (2005): Global distribution of methane hydrate in ocean sediment. In *Energy Fuels* 19, pp. 459–470.

Knittel, K.; Boetius, A. (2009): Anaerobic Oxidation of Methane: Progress with an Unknown Process. In *Annu. Rev. Microbiol* 63 (1), pp. 311–334.

Knittel, K.; Losekann, T.; Boetius, A.; Kort, R.; Amann, R. (2005): Diversity and distribution of methanotrophic archaea at cold seeps. In *Applied and Environmental Microbiology* 71 (1), pp. 467–479.

Knittel, Katrin; Boetius, Antje; Lemke, Andreas; Eilers, Heike; Lochte, Karin; Pfannkuche, Olaf et al. (2003): Activity, Distribution, and Diversity of Sulfate Reducers and Other Bacteria in Sediments above Gas Hydrate (Cascadia Margin, Oregon). In *Geomicrobiology Journal* 20 (4), pp. 269–294.

Krey, V.; Canadell, J. G.; Nakicenovic, N.; Abe, Y.; Andruleit, H.; Archer, D. et al. (2009): Gas hydrates: entrance to a methane age or climate threat? In *Environ. Res. Lett.* 4 (3).

Krüger, M.; Treude, T.; Wolters, H.; Nauhaus, K.; Boetius, A. (2005): Microbial methane turnover in different marine habitats. In *Palaeogeography, Palaeoclimatology, Palaeoecology* 227 (1-3), pp. 6–17.

Kulm, L. D.; Suess, E.; MOORE, J. C.; Carson, B.; LEWIS, B. T.; RITGER, S. D. et al. (1986): Oregon Subduction Zone: Venting, Fauna, and Carbonates. In *Science* 231 (4738), pp. 561–566.

Kvenvolden, Keith A. (1993): Gas hydrates—geological perspective and global change. In *Rev. Geophys* 31 (2), p. 173.

Land, Lynton S. (1989): The carbon and oxygen isotopic chemistry of surficial holocene shallow marine carbonate sediment and quaternary limestone and dolomite. In : Handbook of Environmental Isotope Geochemistry, 3 The Marine Environment, pp. 191–211.

Linke, P.; Sommer, S.; Schmidt, M.; Türk, M.; Bodenbinder, A.; Wefers, P. et al. (2011): ECO_2: Sub-seabed CO_2 storage storage: Impact on marine ecosystems - Cruise Report Alkor 374 (51): December 2011. In *Reports from IFM-GEOMAR* .

Llobet-Brossa, E.; Rossello-Mora, R.; Amann, R. (1998): Microbial community composition of Wadden Sea sediments as revealed by fluorescence in situ hybridization. In *Applied and Environmental Microbiology* 64 (7), pp. 2691–2696.

Loesekann, Tina; Knittel, Katrin; Nadalig, Thierry; Fuchs, Bernhard; Niemann, Helge; Boetius, Antje; Amann, Rudolf (2007): Diversity and abundance of aerobic and anaerobic methane oxidizers at the Haakon Mosby mud volcano, Barents Sea. In *Applied and Environmental Microbiology* 73 (10), pp. 3348–3362.

Luff, Roger; Wallmann, Klaus (2003): Fluid flow, methane fluxes, carbonate precipitation and biogeochemical turnover in gas hydrate-bearing sediments at Hydrate Ridge, Cascadia Margin: numerical modeling and mass balances. In *Geochimica et Cosmochimica Acta* 67 (18), pp. 3403–3421.

Luff, Roger; Wallmann, Klaus; Aloisi, Giovanni (2004): Numerical modeling of carbonate crust formation at cold vent sites: significance for fluid and methane budgets and chemosynthetic biological communities. In *Earth and Planetary Science Letters* 221 (1-4), pp. 337–353.

Magalhães, Vitor H.; Pinheiro, Luis M.; Ivanov, Michael K.; Kozlova, Elena; Blinova, Valentina; Kolganova, J. et al. (2012): Formation processes of methane-derived authigenic carbonates from the Gulf of Cadiz. In *Sedimentary Geology* 243-244, pp. 155–168.

Manz, Werner; Eisenbrecher, Michael; Neu, Thomas R.; Szewzyk, Ulrich (1998): Abundance and spatial organization of Gram-negative sulfate-reducing bacteria in activated sludge investigated by in situ probing with specific 16S rRNA targeted oligonucleotides. In *FEMS Microbiology Ecology* 25 (1), pp. 43–61.

Martin, W.; Russell, M. J. (2007): On the origin of biochemistry at an alkaline hydrothermal vent. In *Philosophical Transactions of the Royal Society B: Biological Sciences* 362 (1486), pp. 1887–1926.

Michaelis, W.; Seifert, R.; Nauhaus, K.; Treude, T.; Thiel, V.; Blumenberg, M. et al. (2002): Microbial reefs in the Black Sea fueled by anaerobic oxidation of methane. In *Science* 297 (5583), pp. 1013–1015.

Moosa, S.; Harrison, S.T.L (2006): Product inhibition by sulphide species on biological sulphate reduction for the treatment of acid mine drainage. In *Hydrometallurgy* 83 (1-4), pp. 214–222.

Naehr, Thomas H.; Eichhubl, Peter; Orphan, Victoria J.; Hovland, Martin; Paull, Charles K.; Ussler, William et al. (2007): Authigenic carbonate formation at hydrocarbon seeps in continental margin sediments: A comparative study. In *Deep Sea Research Part II: Topical Studies in Oceanography* 54 (11-13), pp. 1268–1291.

Nauhaus, K.; Boetius, A.; Kruger, M.; Widdel, F. (2002): In vitro demonstration of anaerobic oxidation of methane coupled to sulphate reduction in sediment from a marine gas hydrate area. In *Environ Microbiol* 4 (5), pp. 296–305.

Nauhaus, Katja; Albrecht, Melanie; Elvert, Marcus; Boetius, Antje; Widdel, Friedrich (2007): In vitro cell growth of marine archaeal-bacterial consortia during anaerobic oxidation of methane with sulfate. In *Environ Microbiol* 9 (1), pp. 187–196.

Nelson, C. S.; Smith, A. M. (1996): Stable oxygen and carbon isotope compositional fields for skeletal and diagenetic components in New Zealand cenozoic nontropical carbonate sediments and limestones: A synthesis and review. In *New Zealand Journal of Geology and Geophysics* 39 (1), pp. 93–107.

Niemann, H.; Elvert, M.; Hovland, M.; Orcutt, B.; Judd, A.; Suck, I. et al. (2005): Methane emission and consumption at a North Sea gas seep (Tommeliten area). In *BIOGEOSCIENCES* 2 (4), pp. 335–351.

Niemann, H.; Fischer, D.; Graffe, D.; Knittel, K.; Montiel, A.; Heilmayer, O. et al. (2009): Biogeochemistry of a low-activity cold seep in the Larsen B area, western Weddell Sea, Antarctica. In *BIOGEOSCIENCES* 6 (11), pp. 2383–2395.

Niemann, Helge; Lösekann, Tina; Beer, Dirk de; Elvert, Marcus; Nadalig, Thierry; Knittel, Katrin et al. (2006): Novel microbial communities of the Haakon Mosby mud volcano and their role as a methane sink. In *Nature* 443 (7113), pp. 854–858.

O'Flaherty, Vincent; Mahony, Thérèse; O'Kennedy, Ronan; Colleran, Emer (1998): Effect of pH on growth kinetics and sulphide toxicity thresholds of a range of methanogenic, syntrophic and sulphate-reducing bacteria. In *Process Biochemistry* 33 (5), pp. 555–569.

Orcutt, Beth; Boetius, Antje; Elvert, Marcus; Samarkin, Vladimir; Joye, Samantha B. (2005): Molecular biogeochemistry of sulfate reduction, methanogenesis and the anaerobic oxidation of methane at Gulf of Mexico cold seeps. In *Geochimica et Cosmochimica Acta* 69 (17), pp. 4267–4281.

Orphan, V.J; Ussler, W.; Naehr, T.H; House, C.H; Hinrichs, K.-U; Paull, C.K (2004): Geological, geochemical, and microbiological heterogeneity of the seafloor around methane vents in the Eel River Basin, offshore California. In *Chemical Geology* 205 (3-4), pp. 265–289.

Peckmann, J.; Thiel, V.; Michaelis, W.; Clari, P.; Gaillard, C.; Martire, L.; Reitner, J. (1999): Cold seep deposits of Beauvoisin (Oxfordian; southeastern France) and Marmorito (Miocene; northern Italy): microbially induced authigenic carbonates. In *International Journal of Earth Sciences* 88 (1), pp. 60–75.

Peltier, W. R.; Fairbanks, R. G. (2006): Global glacial ice volume and Last Glacial Maximum duration from an extended Barbados sea level record. In *QUATERNARY SCIENCE REVIEWS* 25 (23-24), pp. 3322–3337.

Pernthaler, A.; Pernthaler, J.; Amann, R. (2002): Fluorescence In Situ Hybridization and Catalyzed Reporter Deposition for the Identification of Marine Bacteria. In *Applied and Environmental Microbiology* 68 (6), pp. 3094–3101.

Pernthaler, A.; Pernthaler, J.; Amann, R. (2004): Sensitive multi-color fluorescence in situ hybridisation for the identification of environmental microorganisms. In *Molecular Microbial Ecology Manual* (3.11), pp. 711–726.

Pfannkuche, O. (2006): Preliminary Alkor Cruise 259: 10. – 22. 06. 2005.

Pfannkuche, O.; Bannert, B.; Hissmann, K.; Kriwanek, S.; Linke, P.; Makarow, D. et al. (2006): Gas seeps in the central and northern North Sea - Cruise Report Alkor 290: 10. 10 – 01. 11. 2006. In *Reports from IFM-GEOMAR, Kiel*.

Phrampus, Benjamin J.; Hornbach, Matthew J. (2012): Recent changes to the Gulf Stream causing widespread gas hydrate destabilization. In *Nature* 490 (7421), pp. 527–530.

Pierre, Catherine; Blanc-Valleron, Marie-Madeleine; Demange, Jérôme; Boudouma, Omar; Foucher, Jean-Paul; Pape, Thomas et al. (2012): Authigenic carbonates from active methane seeps offshore southwest Africa. In *Geo-Mar Lett*.

Porter, K. G.; Feig, Y. S. (1980): THE USE OF DAPI FOR IDENTIFYING AND COUNTING AQUATIC MICROFLORA. In *LIMNOLOGY AND OCEANOGRAPHY* 25 (5), pp. 943–948.

Raghoebarsing, Ashna A.; Pol, Arjan; van de Pas-Schoonen, Katinka T.; Smolders, Alfons J. P.; Ettwig, Katharina F.; Rijpstra, W. Irene C. et al. (2006): A microbial consortium couples anaerobic methane oxidation to denitrification. In *Nature* 440 (7086), pp. 918–921.

Ravenschlag, K.; Sahm, K.; Knoblauch, C.; Jørgensen, B. B.; Amann, R. (2000): Community structure, cellular rRNA content, and activity of sulfate-reducing bacteria in marine arctic sediments. In *Appl. Environ. Microbiol* 66 (8), pp. 3592–3602.

Reeburgh, W. S. (2007): Oceanic Methane Biogeochemistry. In *Chem. Rev.* 107 (2), pp. 486–513.

Rehder, G.; Keir, R. S.; Suess, E.; Pohlmann, T. (1998): The Multiple Sources and Patterns of Methane in North Sea Waters. In *Aquatic Geochemistry* 4 (3/4), pp. 403–427.

Ritger, S.; Carson, B.; Suess, E. (1987): METHANE-DERIVED AUTHIGENIC CARBONATES FORMED BY SUBDUCTION INDUCED PORE-WATER EXPULSION ALONG THE OREGON WASHINGTON MARGIN. In *GEOLOGICAL SOCIETY OF AMERICA BULLETIN* 98 (2), pp. 147–156.

Rusch, A.; Forster, S.; Huettel, M. (2001): Bacteria, diatoms and detritus in an intertidal sandflat subject to advective transport across the water-sediment interface. In *Biogeochemistry* 55 (1), pp. 1–27.

Saigal, G. C.; Björlykke, K. (1987): Carbonate cements in clastic reservoir rocks from offshore Norway-relationsships between isotopic composition, textural evelopment and burial depth. In *Diagenesis of Sedimentary Sequences* (36), pp. 313–324.

Sass, Eytan; Bein, Amos; Almogi-Labin, Ahuva (1991): Oxygen-isotope composition of diagenetic calcite in organic-rich rocks: Evidence for 18O depletion in marine anaerobic pore water. In *Geol* 19 (8), p. 839.

Schönfeld, Joachim; Alve, Elisabeth; Geslin, Emmanuelle; Jorissen, Frans; Korsun, Sergei; Spezzaferri, Silvia (2012): The FOBIMO (FOraminiferal BIo-MOnitoring) initiative—Towards a standardised protocol for soft-bottom benthic foraminiferal monitoring studies. In *Marine Micropaleontology* 94-95, pp. 1–13.

Schubert, Carsten J.; Coolen, Marco J. L.; Neretin, Lev N.; Schippers, Axel; Abbas, Ben; Durisch-Kaiser, Edith et al. (2006): Aerobic and anaerobic methanotrophs in the Black Sea water column. In *Environ Microbiol* 8 (10), pp. 1844–1856.

Schulz, Horst D.; Zabel, Matthias (2006): Marine geochemistry. 2nd ed. Berlin ;, New York: Springer.

Sejrup, H. P.; Aarseth, I.; Ellingsen, k. L.; Reither, E.; Jansen, E. (1987a): Quaternary stratigraphy of the Fladen area, central North Sea: a multidiscipliary study. In *Journal of Quaternary Science* (2), pp. 35–58.

Sejrup, H. P.; Aarseth, I.; Ellingsen, k. L.; Reither, E.; Jansen, E. (1987b): Quaternary stratigraphy of the Fladen area, central North Sea: a multidisciplinary study. In *Journal of Quaternary Science* (2), pp. 35–58.

Stakes, Debra S.; Orange, Daniel; Paduan, Jennifer B.; Salamy, Karen A.; Maher, Norman (1999): Cold-seeps and authigenic carbonate formation in Monterey Bay, California. In *Marine Geology* 159 (1-4), pp. 93–109.

Teske, A.; Hinrichs, K.-U; Edgcomb, V.; Vera Gomez, A. de; Kysela, D.; Sylva, S. P. et al. (2002): Microbial Diversity of Hydrothermal Sediments in the Guaymas Basin: Evidence for Anaerobic Methanotrophic Communities. In *Applied and Environmental Microbiology* 68 (4), pp. 1994–2007.

Tishchenko, P.; Hensen, Ch.; Wallmann, K.; Wong, C. S. (2005): Calculation of the stability and solubility of methane hydrate in seawater. In *Chemical Geology* 219 (1-4), pp. 37–52.

Treude, T.; Boetius, A.; Knittel, K.; Wallmann, K.; Barker Jørgensen, B. (2003): Anaerobic oxidation of methane above gas hydrates at Hydrate Ridge, NE Pacific Ocean. In *Mar. Ecol. Prog. Ser.* 264, pp. 1–14.

Treude, T.; Knittel, K.; Blumenberg, M.; Seifert, R.; Boetius, A. (2005a): Subsurface microbial methanotrophic mats in the Black Sea. In *APPLIED AND ENVIRONMENTAL MICROBIOLOGY* 71 (10), pp. 6375–6378.

Treude, T.; Kruger, M.; Boetius, A.; Jorgensen, B. B. (2005b): Environmental control on anaerobic oxidation of methane in the gassy sediments of Eckernforde Bay (German Baltic). In *LIMNOLOGY AND OCEANOGRAPHY* 50 (6), pp. 1771–1786.

Treude, T.; Orphan, V.; Knittel, K.; Gieseke, A.; House, C. H.; Boetius, A. (2007): Consumption of Methane and CO2 by Methanotrophic Microbial Mats from Gas Seeps of the Anoxic Black Sea. In *Applied and Environmental Microbiology* 73 (7), pp. 2271–2283.

Treude, T.; Ziebis, W. (2010): Methane oxidation in permeable sediments at hydrocarbon seeps in the Santa Barbara Channel, California. In *Biogeosciences* 7 (10), pp. 3095–3108.

Urey, H. C. (1947): Chemical properties of isotopic compounds. In *Chimia (Aarau)* 1 (4), p. 90.

Valentine, David L.; Blanton, Douglas C.; Reeburgh, William S.; Kastner, Miriam (2001): Water column methane oxidation adjacent to an area of active hydrate dissociation, Eel river Basin. In *Geochimica et Cosmochimica Acta* 65 (16), pp. 2633–2640.

Vogt, P. R.; Cherkashev, G.; Ginsburg, G.; Ivanov, G.; Milkov, A.; Crane, K. et al. (1997): Haakon Mosby Mud Volcano provides unusual example of venting. In *Eos Trans. AGU* 78 (48), p. 549.

Wefer, Gerold (2003): Ocean margin systems. With 31 tables. Berlin [u.a.]: Springer.

Wegener, G.; Boetius, A. (2009): An experimental study on short-term changes in the anaerobic oxidation of methane in response to varying methane and sulfate fluxes. In *Biogeosciences* 6 (5), pp. 867–876.

Wegener, G.; Shovitri, M.; Knittel, K.; Niemann, H.; Hovland, M.; Boetius, A. (2008a): Biogeochemical processes and microbial diversity of the Gullfaks and Tommeliten methane seeps (Northern North Sea). In *BIOGEOSCIENCES* 5 (4), pp. 1127–1144.

Wegener, G.; Shovitri, M.; Knittel, K.; Niemann, H.; Hovland, M.; Boetius, A. (2008b): Biogeochemical processes and microbial diversity of the Gullfaks and Tommeliten methane seeps (Northern North Sea). In *Biogeosciences Discuss* 5 (1), pp. 971–1015.

Whiticar, M.J; Faber, E.; Schoell, M. (1986): Biogenic methane formation in marine and freshwater environments: CO2 reduction vs. acetate fermentation—Isotope evidence. In *Geochimica et Cosmochimica Acta* 50 (5), pp. 693–709.

Whiticar, Michael J.; Faber, Eckhard (1986): Methane oxidation in sediment and water column environments—Isotope evidence. In *Organic Geochemistry* 10 (4-6), pp. 759–768.

Widdel, F.; Bak, F. (1992): Gram-negative mesophilic sulfate-reducing bacteria. In *The Prokaryotes* (IV), pp. 3352–3378.

Wieringa, Elze B. A.; Overmann, Jorg; Cypionka, Heribert (2000): Detection of abundant sulphate-reducing bacteria in marine oxic sediment layers by a combined cultivation and molecular approach. In *Environ Microbiol* 2 (4), pp. 417–427.

Yamamoto, Sachio; Alcauskas, James B.; Crozier, Thomas E. (1976): Solubility of methane in distilled water and seawater. In *J. Chem. Eng. Data* 21 (1), pp. 78–80.

6 Appendix

A.1. Measuring turnover rates

Copper Sulphate Solution ($CuSO_4^{2-}$)

1.25 g $CuSO_4^{2-}$ x 5 H_2O was dissolved in ultrapure H_20. 6.51 mL HCl (26 %) was added and the solution filled up to a total volume of 1 L with ultrapure water.

Indicator solution for determining total alkalinity

32 mg Methyl Red were mixed with 1.19 mL sodium hydroxide solution (0.1 M) and dissolved in 80 mL ethanol (96 %). 10 mg of Methylene Blue were dissolved in 10 mL ethanol (96 %). 4.8 mL of the Methylene Blue solution were then mixed with 80 mL of the Methyl Red solution to obtain the final indicator solution.

Sea water medium (PSU: 35) for sulphate reducing bacteria (SRB-medium)

The SRB-medium was prepared according to (Widdel, Bak 1992) in glass bottles equipped with a magnetic stir bar and septum stopper. Hereby 1 mL Resazurin solution was added to 1000 mL sea water solution and autoclaved (refer to Table 11 for the compositions of all reagents). Resazurin causes a pink staining of the solution in the presence of oxygen. After autoclaving the medium was cooled down to 84 °C, put on ice and flushed with N_2 (5 minutes, 0.2 bar). After 10 minutes the flushing was continued with a N_2/CO_2 (80:20) gas solution (15 minutes, 0.2 bar). Under continuous stirring and N_2/CO_2 flushing 30 mL bicarbonate solution, 50 mL NH_4Cl/ KH_2PO_4 solution, 1 mL vitamin-solution, 1 mL thiamine-solution, 1 mL cyanocobalamin, 1 mL riboflavin-solution, 1 mL selenite/wolframite solution, 1 mL trace element solution and 1 mL sulphide solution were added to the medium with syringes through a PES filter (0.2 µm, Whatman). Flushing with N_2/CO_2 was continued until the solution was clear and thus depleted in oxygen. The pH was set to 7.5 with HCl or Na_2CO_3 solution respectively. The medium has been stored at 4°C for further use.

Sulphide Standards

Standards for the calibration curve (Figure 26) were prepared by adding appropriate volumes of 20 mM sodium sulphide solution (Na_2Sx9H_2O, MW: 240.18 g) in anoxic ultra pure water.

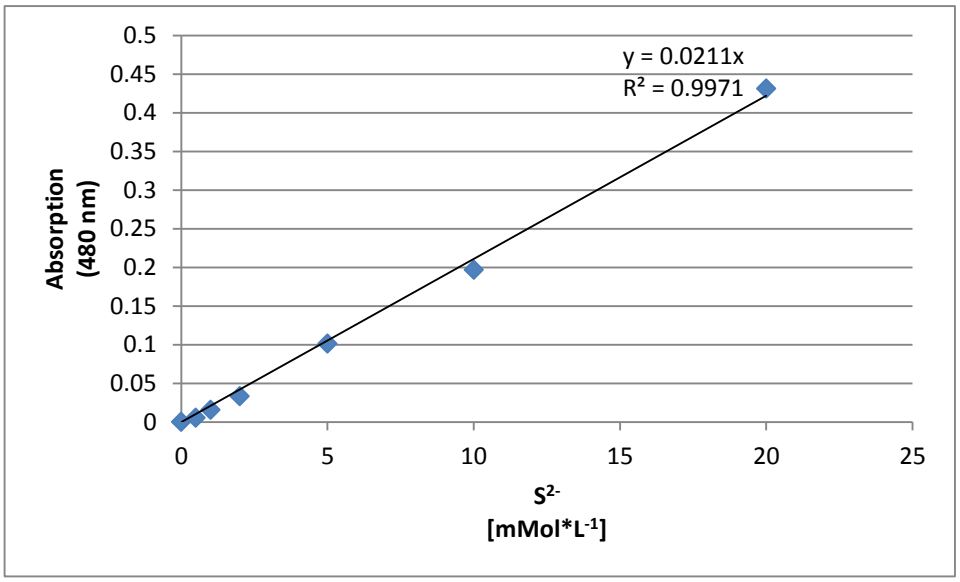

Figure 26: Calibration curve for the photometric determination of sulphide concentrations.

Table 11: Ingredients of the sea water medium for sulphate reducing bacteria.

Reagant	Ingredient 1	Ingredient 2	Ingredient 3	Ingredient 4	Ingredient 5	Ingredient 6	Ingredient 7	Ingredient 8	Ingredient 9	Ingredient 10	Preparation
Vitamine-solution (100mL)	MQ (100mL)	Na_2HPO_4 (0.356g, MW; 177.99g)	NaH_2PO_4 (0.27g , MW; 156.01g)	4-Aminobenzoat (4mg, MW: 137.14g)	D-(+)-Biotin (1mg, MW: 244.31g)	Nicotinacid (10mg, MW: 123.11g)	Calcium-D-(+)-panthonthenat (5mg, MW: 476.53g)	Pyridoxamine-dihydrochlorid (15mg, MW: 241.11g)	Lipon acid (1.5mg, MW: 206.33g)		Prepare buffer with ingredients 1+2+3 adjust ph=7, solve other ingredients, filter (sterile) into Eppendorf tubes, store 1 mL aliquotes at -20 °C.
Thiamine (B1) solution (100mL)	25 mM Na Buffer, pH 3.4 (0.345g NaH_2PO_4)	Thiamine (10mg, MW: 337.27g)									Solve ingredients, filter (sterile) into Eppendorf tubes, store 1mL aliquotes at -20°C.
Cyanocobalamin -solution (100mL)	MQ (100mL)	Cyanocobalamin (5mg MW: 1355.37g)									Solve ingredients, filter (sterile) into Eppendorf tubes, store 1 mL aliquotes at -20 °C.
Riboflavin-solution (100mL)	20 mM Acetic acid (100mL)	Riboflavin (5mg, MW: 367.37g)									Solve ingredients, filter (sterile) into Eppendorf tubes, store 1 mL aliquotes at -20°C.
Selenite/Wolframite (1000mL)	MQ (1000mL)	NaOH (400mg, MW: 40g)	$Na_2WO_4*2H_20$ (8mg, MW: 329.86g)	Na_2SeO_3 (6mg, MW:172.94g)							Solve ingredients, filter (sterile) into autoclaved glass bottle, store at 4 °C.
Trace elements (1000mL)	MQ (1000mL)	HCl, 37 % (12.5 mL)	$FeSO_4*7H_20$ (2100mg, MW: 287.02g)	H_3BO_3 (30mg, MW: 61.84g)	I_2*4H_2O (100mg, MW: 325.87g)	$CoCl_2*6H_2O$ (190mg, MW: 237.9g)	$NiCl_2*6H_2O$ (24mg, MW: 237.70g)	$CuCl_2*2H_2O$ (2mg, MW:170.48g)	$ZnSO_4*7H_20$ (144mg, MW: 287.54g)	$Na_2MoO_4*2H_2O$ (36mg, MW: 241.95g)	Solve ingredients, filter (sterile) into autoclaved glass bottle, store at 4°C.
Bicarbonate solution (1000mL)	MQ (1000mL)	$NaHCO_3$ (84g, MW: 84.01g)									Solve ingredients , flush with CO_2 (5min), autoclave, store 30mL aliqoutes at RT.
NH_4Cl/ KH_2PO_4 solution (1000mL)	MQ (1000mL)	NH_4Cl (5g, MW: 53,49g)	KH_2PO_4 (4g, MW:136.09g)								Solve ingredients, flush with N_2 (5 min), autoclave, store 50 mL aliquotes at RT.
6.5 % HCl solution (100mL)	25 % HCl solution (26mL)	MQ (74mL)									Fill into autoclave glass bottle, store at RT
Na_2CO_3 solution,1 M (100mL)	MQ (100mL)	Na_2CO_3 (10,6mg, MW: 105.99g)									Solve ingredient, fill into autoclaved glass bottle, store at RT.
Sulphide solution, 1M (100mL)	MQ (100mL)	Na_2S*9H_20 (24g, MW: 240.18g)									Solve ingredient in autoclaved glass bottle, flush with N_2 (5min), store at 4°C.
Resazurin (100mL)	MQ (100mL)	Resazurin (100mg, MW: 251.18g)									Fill in glass bottle, autoclave, store at RT.
Saltwater solution (920mL)	MQ (920mL)	KBr (90g, MW: 119.01g)	KCl (0.6g, MW: 74.56g)	$CaCl_2*2H_2O$ (1.47g, MW: 147.02g)	$MgCl_2*6H_2O$ (5.67g, MW: 203.3g)	$MgSO_4*7H_2O$ (6.8g, MW: 246.48g)	NaCl (26,37g, MW: 58.44g)				Store at RT.

Table 12: Output from linear regression analyzes of data derived from the increase/decrease of alkalinity or sulphide respectively over time. Significant linear regressions models are highlighted yellow. Stars indicate significance level: (*) for 0.05, (**) for 0.01, and (***) for 0.001. From top to bottom: horizons T1, T2 and T3.

Alkalinity

Temperature / Replicate #	Control		Sample	
	F	n	F	n
4°C/1	27.5***	10	660.1***	10
4°C/2	8.4*	11	159.1***	8
4°C/3	5.8*	12	193.7***	8
13°C/1	0.0	13	266.6***	11
13°C/2	37.4***	14	713.9***	11
13°C/3	0.6	14	386.1***	10
20°C/1	71.2***	12	366.9***	6
20°C/2	0.9	14	290.2***	13
20°C/3	4.0	14	270.1***	11
37°C/1	0.8	12	5.177	11
37°C/2	0.5	12	1.441	11
37°C/3	1.4	12	4.993	11
60°C/1	62.1***	11	44.2***	11
60°C/2	45.4***	10	67.9***	12
60°C/3	114.8***	11	44.2***	11

Temperature / Replicate #	Control		Sample	
	F	n	F	n
4°C/1	0.1	12	660.1***	10
4°C/2	0.0	12	159.1***	8
4°C/3	1.5	12	193.7***	8
13°C/1	0.8	12	266.6***	11
13°C/2	3.5	14	713.9***	11
13°C/3	5.2	14	386.1***	10
20°C/1	6.2*	14	366.9***	6
20°C/2	0.1	14	290.2***	13
20°C/3	12.8**	13	270.1***	11
37°C/1	2.0	12	5.2	11
37°C/2	2.6	12	1.4	11
37°C/3	0.1	12	5.0	11
60°C/1	48.5***	10	44.2***	11
60°C/2	47.7***	11	67.9***	12
60°C/3	87.9***	12	44.2***	11

Temperature / Replicate #	Control		Sample	
	F	n	F	n
4°C/1	9.385*	11	337.3***	11
4°C/2	4.0	11	214.3***	9
4°C/3	1.1	9	156.4***	10
13°C/1	4.4	13	657.0***	11
13°C/2	4.4	12	1191.0***	12
13°C/3	0.2	13	1816.0***	12
20°C/1	0.2	14	228***	10
20°C/2	3.2	13	204.1***	12
20°C/3	1.7	13	301.4***	10
37°C/1	10.1*	10	40.62***	10
37°C/2	0.7	10	8.558	4
37°C/3	0.0	12	48.89***	10
60°C/1	28.5***	10	174.9***	10
60°C/2	138.2***	10	109.1***	10
60°C/3	74.7***	9	120***	8

Sulphide

Temperature / Replicate #	Control		Sample	
	F	n	F	n
4°C/1	5.5*	12	941.5***	10
4°C/2	0.0	12	997.6***	8
4°C/3	1.6	12	175.2***	9
13°C/1	0.1	14	185.0***	9
13°C/2	5.1*	14	363.5***	10
13°C/3	0.0	14	184.7***	8
20°C/1	3.8	14	349.4***	11
20°C/2	7.6*	14	152.8***	8
20°C/3	11.45**	14	362.3***	8
37°C/1	4.7	12	76.9***	10
37°C/2	30.4***	12	56.5***	11
37°C/3	24.08***	12	11.2**	11
60°C/1	0.6	10	2.9	12
60°C/2	0.7	11	1.7	12
60°C/3	0.6	11	5.6*	12

Temperature / Replicate #	Control		Sample	
	F	n	F	n
4°C/1	0.0	12	776.1***	10
4°C/2	1.7	12	577.9***	8
4°C/3	2.7	12	531.6***	8
13°C/1	1.1	14	471.1***	12
13°C/2	4.1	14	569.4***	11
13°C/3	0.7	14	626.1***	12
20°C/1	16.0**	14	1156***	12
20°C/2	28.98***	14	1217.0***	11
20°C/3	23.79***	14	1731.0***	11
37°C/1	23.84***	12	21.6**	10
37°C/2	10.64**	12	10.29*	11
37°C/3	10.03*	12	5.6*	11
60°C/1	0.9	12	0.5	11
60°C/2	0.9	11	0.3	10
60°C/3	3.0	12	0.3	10

Temperature / Replicate #	Control		Sample	
	F	n	F	n
4°C/1	0.0	11	447.1***	9
4°C/2	0.0	11	182.5***	10
4°C/3	5.1	11	176.5***	10
13°C/1	17.7**	14	454.8***	12
13°C/2	15.0**	14	491.1***	12
13°C/3	36.76***	14	1393.0***	10
20°C/1	4.1	14	794.3***	13
20°C/2	16.6**	14	737.2***	11
20°C/3	16.9**	14	472.2***	10
37°C/1	18.8**	12	110.5***	10
37°C/2	6.1*	12	255.7***	9
37°C/3	6.6*	12	37.0***	11
60°C/1	0.3	12	0.07	9
60°C/2	0.0	12	0.53	11
60°C/3	0.6	12	1.22	9

Table 13: Output from linear regression analyzes. Data derived from the increase/decrease of alkalinity or sulphide respectively over time from reversibility experiments. Yellow highlighted samples indicate significant linear regression model (p≤5 %).

Alkalinity

Horizon /Temperature / Replicate #	Control		Sample	
	F	n	F	n
T1/37/R1	0.6	4	0.4	4
T1/37/R2	2.9	4	0.9	4
T1/37/R3	0.5	4	1.3	4
T2/37/R1	1.2	4	0.2	4
T2/37/R2	2.4	4	0.5	4
T2/37/R3	0.0	4	0.4	4
T3/37/R1	17.6	4	3.2	4
T3/37/R2	1.7	4	2.9	4
T3/37/R3	2.3	4	0.1	4
T1/60/R1	5.2	4	7.6*	4
T1/60/R2	2.3	4	0.1	4
T1/60/R3	0.5	4	0.8	4
T2/60/R1	4.5	4	1.6	4
T2/60/R2	0.1	4	11.4	4
T2/60/R3	2.9	4	2.3	4
T3/60/R1	0.0	4	1.1	4
T3/60/R2	0.1	4	3.0	4
T3/60/R3	3.2	4	17.5	4

Sulphide

Horizon /Temperature / Replicate #	Control		Sample	
	F	n	F	n
T1/37/R1	0.1	4	0.00	4
T1/37/R2	0.0	4	0.01	4
T1/37/R3	0.9	4	0.00	4
T2/37/R1	0.4	4	0.05	4
T2/37/R2	0.0	4	0.02	4
T2/37/R3	0.0	4	0.89	4
T3/37/R1	2.2	4	0.67	4
T3/37/R2	6.3	4	0.00	4
T3/37/R3	0.3	4	0.01	4
T1/60/R1	2.1	4	0.01	4
T1/60/R2	0.1	4	0.08	4
T1/60/R3	0.0	4	0.53	4
T2/60/R1	0.0	4	0.46	4
T2/60/R2	0.0	4	1.36	4
T2/60/R3	0.0	4	0.14	4
T3/60/R1	0.5	4	2.81	4
T3/60/R2	0.6	4	1.74	4
T3/60/R3	0.2	4	0.69	4

A.2. Radiotracer measurements

Table 14: Dilution factors of samples for measuring AOM and SR rates using radiotracers.

	Final dilution (1:x)	
ID	SRR	AOM
T1R1	18.5	10.0
T1R2	10.0	10.0
T1R3	10.0	10.0
T2R1	10.0	10.0
T2R2	10.0	10.0
T2R3	10.0	10.0
T3R1	10.3	10.3
T3R2	11.0	11.0
T3R3	11.1	11.1

A.3. Reagents for Card-Fish

All reagents that were prepared are listed below (Table 15). Here is a list of the ready for use chemicals:

- **Agarose**, MetaPhor
- **Blocking reagent**, Invitrogen
- **Citifluor,** Citifluor, London, UK
- **DAPI**, dilactate, Roth
- **Dextran sulfate sodium salt**, Sigma
- **Ethanol 96 %** absolute pure, AppliChem
- **Formamid** (ultra pure)., Merck
- **Hydrogen peroxide, H_2O_2**, (30 %), Sigma
- **Lysozyme** ,from chicken egg, white, Fluka 62970-5G-F
- **Methanol** p.a., AppliChem
- **Proteinase K** (0.01 mol L^{-1} = 20 mg L^{-1}), Merck 1.07393.0010, 10 mL
- **Sodium dodecyl sulphate, SDS** (p.a.), VWR
- **Tris hydrochloride, Tris HCl** (Buffer grade), AppliChem
- **Vectashield**, Vector Lab., Burlingame, USA
- **Ethylenediaminetetraacetic acid, EDTA (**ultra pure), Fluka

Table 15: Reagents for Card-FISH

Reagant	Ingredient 1	Ingredient 2	Ingredient 3	Ingredient 4	Ingredient 5	Ingredient 6	Preparation
0.5 M EDTA, pH=7.3	MQ (500 mL)	EDTA (73.06 g, MW: 292.24 g)					Adjust pH with NaOH pellets, autoclave, store at RT.
1 M Tris-HCl, pH=7.3	MQ (1000 mL)	Tris-HCl (157.60 g, MW=121.14 g)					Adjust pH with NaOH pellets, autoclave, store at RT.
10x Phosphate Buffered Saline (PBS)	MQ (1000 mL)	NaCl, (80 g, MW: 58.44 g)	KCl (2 g, MW: 74.55 g)	Na_2HPO_4 (14.1 g, MW:141.96 g)	KH_2PO_4 (2.7 g, MW: 136.09 g)		Dissolve ingredients, adjust to ph=7.3, autoclave, store 50 mL aliqouts at -20°C.
1xPBS	MQ (900 mL)	10xPBS (100 mL)					Sterile filter before use, store 50 mL aliqoutes at - 20°C.
1xPBS/EtOH (1:1)	1xPBS (25 mL)	EtOH, 96 % (25 mL)					Store at RT, use undenaturated EtOH.
2xSSC, pH= 7	MQ (1000 mL)	NaCl, 300 mM (17.5 g, MW: 58.44 g)	NaCitrat*2xH_2O (10.03 g, MW: 294.1 g)				Store at RT
4% Formalin in 1% PBS	37% Formalin (108.1 mL)	1xPBS (891.9 mL)					Store at 4°C.
Achromopeptidase buffer	MQ (1 mL)	Achromopeptidase (3 g, 1000 U/mL)					Store 50 µL aliqoutes at -20°C.
Agarose 0.2%, w:v	MQ (200 mL)	low melting agarose (0.4 g)					Boil and let cool to 40°C before embedding filters.
Blocking reagant in 1xPBS	1xPBS (10 mL)	Blocking Reagant (100 mg)					Blocking buffer from *Tyramide Signal Amplification Kit* Invitrogen, Store in 1 mL aliqoutes at -20 °C.
DAPI (1µg/mL)							
H_2O_2 (3 % / 0.5% / 0.0015%)	MQ (270 / 295 / 299.1 µL)	30 % H_2O_2 (30 / 5 / 0.9 µL)					Prepare H_2O_2 solutions fresh from stock .
Hybridisation buffer	MQ (0-14 mL)	Formamide, 70 % (2 / 14 mL)	NaCl solution, 5 M (3.6 mL)	Blocking reagant (2 mL)	SDS, 10% (20 µL)	Dextran sulphate (2 g)	Prepare buffer with 10 and 70% formamide, mix designated concentration , vortex, finally add dextran sulphate and solve (40-60°C), store at - 20 °C
Lysozyme (5 mg /mL)	MQ (4 mL)	EDTA, 0.5 M (0.5 mL)	1 M Tris-HCl, pH=7.3 (0.5 mL)	Lysozyme (50 mg, 20000 U/µL)			Prepare fresh.
Methanol / H_2O_2 solultion (0.15 %)	Methanol (10 mL)	H_2O_2,30 % (50 µL)					
NaCl solution, 5 M	MQ (500 mL)	NaCl (146.1 g,MW: 58.44 g)					Dissolve salt, autoclave, store at room temperature (RT).
Proteinase K solution (7.6 µg/mL)	MQ (7 mL)	EDTA, 0.5 M (1 mL)	1 M Tris-HCl, pH=7.3 (1 mL)	NaCl solution, 5 M (1 mL)	Proteinase K (7.5 µL, 20 mg/L)		Prepare fresh.
Sodium Dodecyl Sulphate (SDS), 10 %	Autoclaved MQ (100 mL)	SDS (10 g, MW: 288,38 g)					Sterile filter before use, dilute to designated concetration with Milli-Q, store at RT.
Streptavidin-Horseradishperoxidase (Streptavidin-HRP)	Blocking reagant in 1xPBS (297 µL)	Streptavidin-HRP, 1:1000 (3 µL)					Prepare fresh.
Tyramide Solution	Amplification buffer (300 µL)	H_2O_2, 0.5% (1 µL)	Fluorescent labeled Tyramide (3 µL)				Amplification buffer from *Tyramide Signal Amplification Kit* Invitrogen, prepare fresh.
Washing buffer	MQ (44.45 -48.65 mL)	NaCl, 1 M (40-4500 µL)	Tris- HCl, 1 M 1 mL	EDTA, 0.5 M 0.5 mL	SDS, 10% (50 µL)		Mix buffer according to formamid concentration during hybridization (sum: NaCl + water = 49 mL) Formamid: 20/ 40/ 50/ 60 % use 2150/460/180/40 µL NaCl solution)

A.4. Monitoring hydrogen sulphide and total alkalinity– graphs

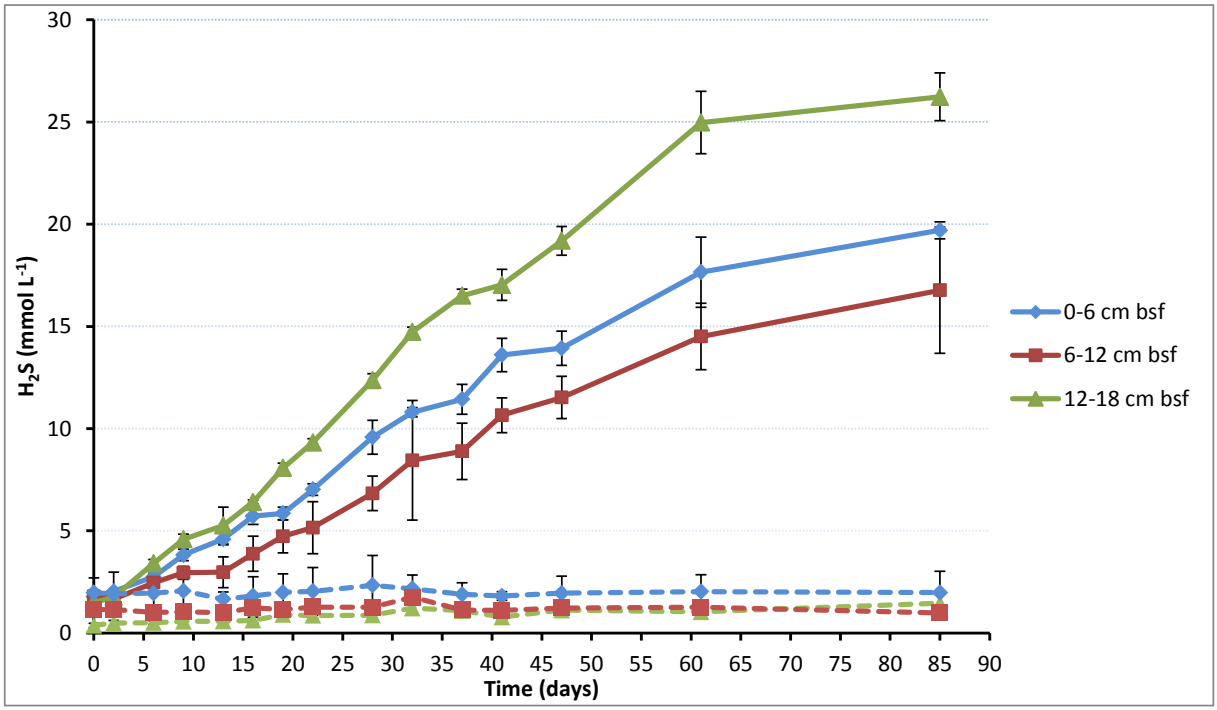

Figure 27: Mean hydrogen sulphide concentrations (n=3, bars indicate 95 % confidence intervals) measured in three depth horizons over 85 days. Samples with methane headspace (solid lines) and controls with nitrogen headspace (dashed lines) were incubated at 13 °C.

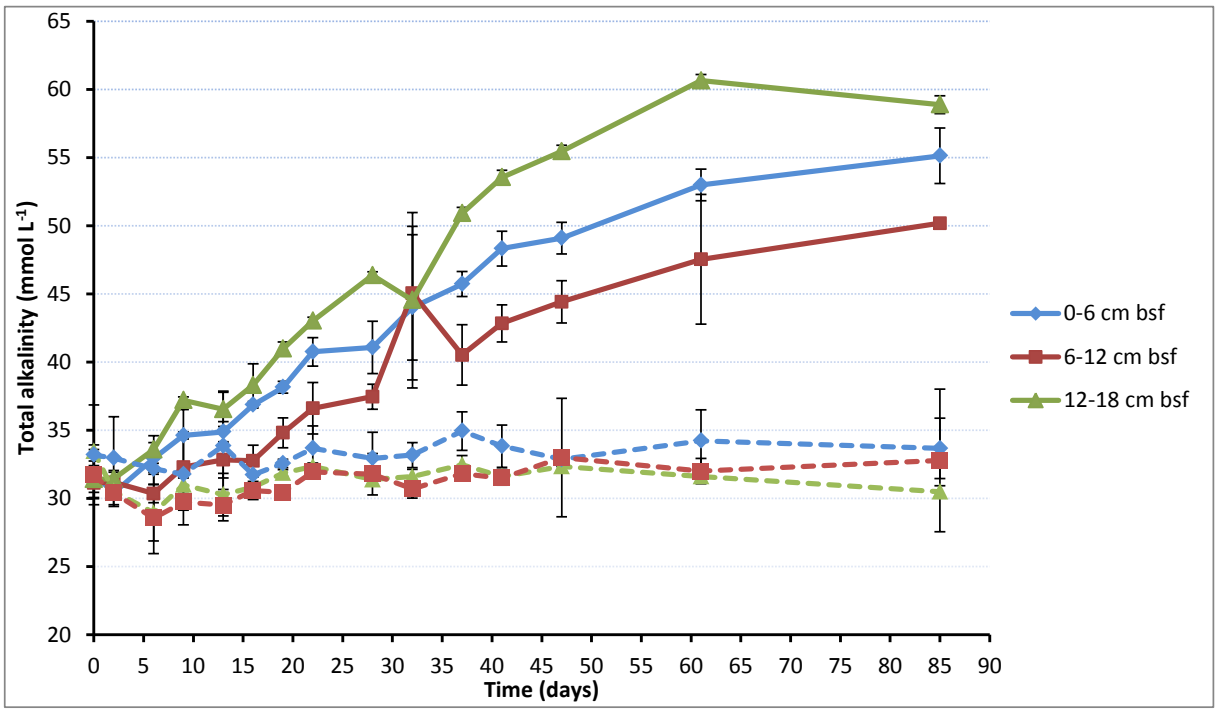

Figure 28: Mean total alkalinity (n=3, bars indicate 95 % confidence intervals) measured in three depth horizons over 85 days. Samples with methane headspace (solid lines) and controls with nitrogen headspace (dashed lines) were incubated at 13 °C.

A.5. Other

Table 16: Wet/dry weights, densities and porosity of the analyzed sediments.

Core ID	Horizon (cm bsf)	Sed wet weight of 3 mL sediment (g)	Density (g mL^{-1})	Sed dry weight of 3 mL sediment (g)	Porosity
Blow-out	0-5	5.0165	1.67	3.56	0.29
Blow-out	6-11	5.6144	1.87	4.17	0.26
Blow-out	12-18	5.1493	1.72	3.67	0.29
Reference MUC	0-6	5.6325	1.88	4.37	0.22
Reference PC	0-6	4.3585	1.45	3.36	0.23
Reference PC	6-12	5.6237	1.87	4.39	0.22
Reference PC	12-18	5.6339	1.88	4.53	0.20

Acknowledgements

Many people supported me during all kinds of practical and theoretical work and during the writing process.

First of all, I would like to express my gratitude to my research supervisor Prof. Dr. Tina Treude for giving me the opportunity to undertake my master's thesis in her working group. I appreciated her enthusiasm, support and encouragements.

Thank you, Prof. Dr. Bölter for being an exemplary second reviewer. I benefited from your support and discussions with you. Additionally, I have greatly benefited from IPÖ lab facilities and support of IPÖ staff.

I am very grateful to Dr. Stefan Krause who introduced me into the world of anoxic sediment handling and other laboratory methods. Thanks for all your support and advice.

I would also like to thank the project initiator Dr. Peter Linke for providing the main ingredients of my thesis: the sediment cores. Additional, he and Dr. Matthias Häckel made data available to me from the sampling stations.

I am also thankful to Dr. Volker Liebetrau for the support and very valuable discussions about geological aspects of my thesis.

Many thanks go out to Jutta Heinze and Dr. Nico Augustin for helping me with the XRD analyzes and XRD spectra evaluation.

Thank you Dr. Joachim Schönfeld, for helping me during the core slicing and interesting hints on various topics related to marine sediments.

Additionally, I am grateful to all other members of the working group: Dr. Vicky Bertics, Julia Farkas, Jessica Gier, Katja Laufer, Kerstin Kretschmer, Marion Liebetrau, Sonakshi Mishra Gabi Schüssler, Johanna Schweers, Philipp Steeb and Peggy Wefers. Many thanks for your support, advice and all the fruitful discussions.

I am grateful to Nada and my father for helpful comments on the manuscript and numerous other support.

Finally I would like to thank my family for supporting me throughout my studies.

Declaration of Authorship

I certify that the work presented here is, to the best of my knowledge and belief, original and the result of my own investigations, except as acknowledged. It has not been submitted, either in part or whole, for a degree at this or any other University.

I agree to include this thesis in the libraries of Helmholtz Centre for Ocean Research Kiel GEOMAR and of the University of Kiel.

Kiel, November 12, 2012 _____